

Fall 2006

Group 12 and group 13 metal complexes of cross-bridged tetraamine macrocycles

Wei-Chih Lee

University of New Hampshire, Durham

Follow this and additional works at: <https://scholars.unh.edu/thesis>

Recommended Citation

Lee, Wei-Chih, "Group 12 and group 13 metal complexes of cross-bridged tetraamine macrocycles" (2006). *Master's Theses and Capstones*. 205.

<https://scholars.unh.edu/thesis/205>

This Thesis is brought to you for free and open access by the Student Scholarship at University of New Hampshire Scholars' Repository. It has been accepted for inclusion in Master's Theses and Capstones by an authorized administrator of University of New Hampshire Scholars' Repository. For more information, please contact nicole.hentz@unh.edu.

NOTE TO USERS

Page(s) not included in the original manuscript and are unavailable from the author or university. The manuscript was scanned as received.

51

This reproduction is the best copy available.

UMI[®]

**GROUP 12 AND GROUP 13 METAL COMPLEXES OF CROSS-BRIDGED
TETRAAMINE MACROCYCLES**

BY

WEI-CHIH LEE

B.S., National Cheng Kung University, 2000

THESIS

Submitted to the University of New Hampshire

In Partial Fulfillment of

the Requirements for the Degree of

Master of Science

in

Chemistry

September, 2006

UMI Number: 1437634

INFORMATION TO USERS

The quality of this reproduction is dependent upon the quality of the copy submitted. Broken or indistinct print, colored or poor quality illustrations and photographs, print bleed-through, substandard margins, and improper alignment can adversely affect reproduction.

In the unlikely event that the author did not send a complete manuscript and there are missing pages, these will be noted. Also, if unauthorized copyright material had to be removed, a note will indicate the deletion.

UMI[®]

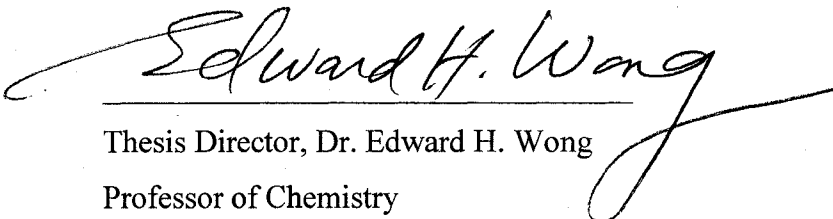
UMI Microform 1437634

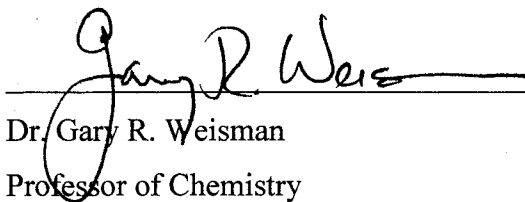
Copyright 2006 by ProQuest Information and Learning Company.

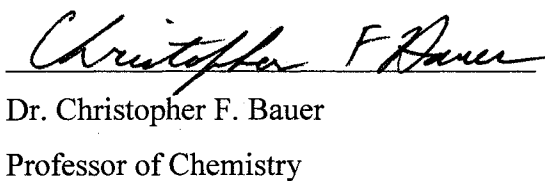
All rights reserved. This microform edition is protected against unauthorized copying under Title 17, United States Code.

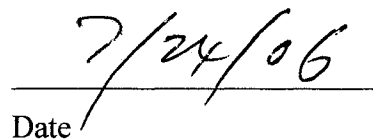
ProQuest Information and Learning Company
300 North Zeeb Road
P.O. Box 1346
Ann Arbor, MI 48106-1346

This thesis has been examined and approved.


Thesis Director, Dr. Edward H. Wong
Professor of Chemistry


Dr. Gary R. Weisman
Professor of Chemistry


Dr. Christopher F. Bauer
Professor of Chemistry


Date

DEDICATION

This thesis work is dedicated to my loving family for their continued support.

ACKNOWLEDGMENT

I would first like to thank my advisor Prof. Edward Wong for his inspirational instruction and guidance during my pursuit of the master degree. In addition to his excellent teaching, Prof. Edward Wong is always very patient and taught me some valuable life lessons. All of which I am forever indebted to him for. I would also like to thank my co-advisor Prof. Gary Weisman for his professional guidance to this research.

There are several faculty members who I am very grateful to have had the privilege of learning from at UNH. Dr. Charles Zercher, Dr. Roy Planalp, Dr. Glen Miller demonstrated an incredible enthusiasm for chemistry and teaching. I am very appreciative for their support and guidance.

I was very fortunate to have had many great friendships during my time at UNH. I would like to thank all Chinese graduate students in the department, especially Weimin Lin and Jingwei Li, and members in the Weisman and Wong group for all of the good times.

There are many people in the chemistry department that I am forever indebted to for their support, guidance and teaching during my time at UNH. I would like to thank Cindi Rohwer and Peg Torch for their helps. I would like to thank Kathy Gallagher for her great help with the NMR instrument.

TABLE OF CONTENTS

DEDICATION.....	iii
ACKNOWLEDGMENT.....	iv
TABLE OF CONTENTS.....	v
LIST OF FIGURES	viii
LIST OF TABLES.....	xiii
LIST OF SCHEMES.....	xiv
ABSTRACT.....	xv
CHAPTER I . INTRODUCTION.....	1
1.1 Background.....	1
1.2 Gallium(III) and Indium(III) Chemistry	3
1.2.1 Gallium(III) and Indium(III) Radionuclides.....	3
1.2.2 Properties of Trivalent Gallium and Indium Cations in Aqueous Solution.....	3
1.3 Bifunctional Chelators (BFCs)	5
1.4 Coordination Chemistry of Gallium and Indium Complexes of Cyclen, Cyclam and Their Derivatives	6

1.5 Gallium and Indium Coordination Chemistry of Cross-Bridged Tetraazamacrocyclic Ligands.....	10
1.6 Research Goals.....	15
CHAPTER II . GALLIUM (III) AND INDIUM (III) COMPLEXES OF CROSS- BRIDGED TETRAAZAMACROCYLIC LIGANDS	16
2.1 Introduction.....	16
2.2 Synthesis and Characterization.....	17
2.2.1 Synthesis of the In(III) Complex of H ₂ -CB-DO2A · nTFA	17
2.2.2 Attempted H ₂ -CB-TE2A.nTFA Complexation of Ga(III) and In(III).....	24
Indirect Routes	27
2.2.3 Attempted In(III) Complexation with ^t Bu ₂ -CB-TE2A	27
2.2.4 Arming (Alkylation) of [InBr ₂ -CB-Cyclam]Br	29
2.2.5 Synthesis of “[In-CB-TE2A]Br”.....	34
2.2.6 Attempted Synthesis of the Gallium (III) Complex of CB-TE2A (Attempted Alkylation of [GaBr ₂ -CB-Cyclam]Br).....	38
2.2.7 Attempted In(III) Complexation of Dibenzo Annelated Cross-Bridged Cyclam	42
2.3 Synthesis of Hg-CB-DO2A	45

2.4 Summary and Conclusions	48
CHAPTER III. KINETIC INERTNESS STUDIES OF DIAMAGNETIC METAL	
COMPLEXES OF CROSS-BRIDGED LIGANDS	50
3.1 Introduction.....	50
3.2 Results and Discussion	51
3.2.1 Relative Kinetic Inertness of Ga(III) and In(III) Complexes.....	51
3.2.2 Relative Kinetic Inertness of Zn(II), Cd(II) and Hg(II) Complexes.....	61
3.2.3 NH/ND Exchange for Ga(III) and In(III) Cross-Bridged Complexes.....	67
3.3 Summary and Discussion.....	71
3.4 Conclusions and Future Work	74
3.5 Experimental Section for Kinetic Studies.....	76
CHAPTER IV. EXPERIMENTAL SECTION.....	77
LIST OF REFERENCES.....	82
APPENDIX SPECTRA	87

LIST OF FIGURES

<u>Figure</u>	<u>Page</u>
Figure 1.1 A targeted metallo-radiopharmaceutical.	1
Figure 1.2 Structure of Somatostatin and its analog, Octreotide.	2
Figure 1.3 Structure of ^{111}In -DTPA-Octreotide.	2
Figure 1.4 Hydrolysis of the hydrated Ga^{3+} cation.	4
Figure 1.5 Hydrolysis of the hydrated Ga^{3+} cation.	4
Figure 1.6 Some Common Bifunctional Chelators (BFCs).	6
Figure 1.7 Possible coordination modes of trans- (top) and cis- (bottom) isomers for cyclam.	7
Figure 1.8 ORTEP plot of the crystal structure of $[\text{Ga-DOTA-d-PhenH}_2]$.	8
Figure 1.9 ORTEP drawing of In(DOTA-AA) .	9
Figure 1.10 Comparison of the coordination geometry of In(DOTA-AA) in its solid state (left) and in solution (right).	9
Figure 1.11 General structures of cross-bridged ligands.	10
Figure 1.12 Metal complexation of cross-bridged ligands with all four nitrogen donor electron pairs convergent upon a molecular cleft	11
Figure 1.13 (a) Cis- V configuration for the metal complexes of cross-bridged ligands (left); (b) generic structure of a metal complex of a two pendant-armed cross-bridged ligand (right).	11
Figure 1.14 X-ray structure of $[\text{Ga-CB-DO2A}]\text{NO}_3$.	13
Figure 1.15 X-ray structure of $[\text{InBr}_2\text{-CB-Cylen}]\text{Br}$.	14
Figure 1.16 NH/ND exchange process in D_2O or CD_3OD .	15
Figure 2.1 Cross-bridged ligands studied in Ga(III) and In(III) complexations.	16

Figure 2.2 ^1H NMR spectra comparison (a) crude product in CD_3OD (top); (b) $[\text{In-CB-DO2A} \cdot \text{NaOAc}]\text{BPh}_4$ in CD_3CN (bottom).	18
Figure 2.3 FAB (positive mode) mass spectrum of $[\text{In-CB-DO2A} \cdot \text{NaOAc}]\text{BPh}_4$.	19
Figure 2.4 IR spectrum of $[\text{In-CB-DO2A} \cdot \text{NaOAc}]\text{BPh}_4$.	20
Figure 2.5 Possible structures of $[\text{In-CB-DO2A} \cdot \text{NaOAc}]\text{BPh}_4$.	20
Figure 2.6 ^1H NMR spectrum of $[\text{In-CB-DO2A}]^+$.	21
Figure 2.7 $^{13}\text{C}\{^1\text{H}\}$ NMR spectra comparison (a) “ $[\text{In-CB-DO2A}]\text{Cl}$ ” in D_2O (top); (b) $[\text{In-CB-DO2A} \cdot \text{NaOAc}]\text{BPh}_4$ in CD_3CN (bottom).	21
Figure 2.8 2D [^1H , ^{13}C] HMQC spectrum of “ $[\text{In-CB-DO2A}]\text{Cl}$ ”.	22
Figure 2.9 IR spectrum of “ $[\text{In-CB-DO2A}]\text{Cl}$ ”.	23
Figure 2.10 ESI-MS (positive mode) spectrum of “ $[\text{In-CB-DO2A}]\text{Cl}$ ”.	23
Figure 2.11 ESI-MS spectrum of crude product of attempted complexation in EtOH.	26
Figure 2.12 $^{13}\text{C}\{^1\text{H}\}$ NMR spectrum of crude product of attempted complexation in EtOH.	27
Figure 2.13 IR spectrum of precipitated product of attempted In(III) complexation of $^t\text{Bu}_2\text{-CB-TE2A}$.	28
Figure 2.14 $^{13}\text{C}\{^1\text{H}\}$ NMR spectra comparison (a) precipitated product in D_2O (top); (b) protonated $\text{H}_2\text{-CB-TE2A} \cdot n\text{TFA}$ in CD_3CN (bottom).	28
Figure 2.15 ^1H NMR spectrum of $[\text{InBr}_2\text{-Et}_2\text{-CB-TE2A}]\text{Br}$ in CD_3CN .	31
Figure 2.16 $^{13}\text{C}\{^1\text{H}\}$ NMR spectrum of $[\text{InBr}_2\text{-Et}_2\text{-CB-TE2A}]\text{Br}$ in CD_3CN .	31
Figure 2.17 2D [^1H , ^{13}C] HMQC spectrum of $[\text{InBr}_2\text{-Et}_2\text{-CB-TE2A}]\text{Br}$.	31
Figure 2.18 ESI-MS (positive mode) spectrum of $[\text{InBr}_2\text{-Et}_2\text{-CB-TE2A}]\text{Br}$.	32
Figure 2.19 IR spectrum of $[\text{InBr}_2\text{-Et}_2\text{-CB-TE2A}]\text{Br} \cdot \text{H}_2\text{O}$.	33
Figure 2.20 ORTEP drawing of $[\text{InBr}_2\text{-Et}_2\text{-CB-TE2A}]\text{Br} \cdot \text{H}_2\text{O}$ (ellipsoids are at 50% probability).	33

Figure 2.21 ESI-MS (positive mode) spectrum of [InBr ₂ -CB-TE2A]Br.	35
Figure 2.22 IR spectrum of [In-CB-TE2A]Br.	35
Figure 2.23 ¹ H NMR spectrum of [In-CB-TE2A]Br in D ₂ O.	36
Figure 2.24 Variable temperature ¹³ C{ ¹ H} NMR spectra of [In-CB-TE2A]Br at (a) 25 °C in D ₂ O (top); (b) 85 °C in D ₂ O (middle); (c) -80 °C in CD ₃ OD (bottom).	36
Figure 2.25 A possible dynamic enantionmerization process of [In-CB-TE2A] ⁺ .	37
Figure 2.26 ESI-MS (positive mode) spectrum of the supernatant for the preparation of [GaBr ₂ -Et ₂ -CB-TE2A] ⁺ .	39
Figure 2.27 Proposed products based on the ESI-MS spectrum.	40
Figure 2.28 ¹ H NMR spectra of NH/ND exchange of [GaBr ₂ -CB-Cyclam]Br in D ₂ O: (a) complex only (top); (b) complex + 6 eqv. sodium carbonate (middle); (c) complex + 20 eqv. sodium acetate (bottom).	41
Figure 2.29 (a) ¹ H NMR spectrum of protonated dibenzo annelated dimethyl CB-Cyclam in D ₂ O.	43
Figure 2.29 (b) ¹ H NMR spectrum of protonated dibenzo annelated dimethyl CB-Cyclam in CD ₃ CN.	43
Figure 2.30 ORTEP drawing of [H-Me ₂ -Bz ₂ -CB-Cyclam][InBr ₄] (ellipsoids are at 50% probability).	44
Figure 2.31 ¹ H NMR spectrum of Hg-CB-DO2A in D ₂ O.	46
Figure 2.32 ¹³ C{ ¹ H} NMR spectrum of Hg-CB-DO2A in D ₂ O.	46
Figure 2.33 A dynamic C _{2v} -symmetric enantiomerization of Hg-CB-DO2A.	47
Figure 2.34 IR spectrum of Hg-CB-DO2A.	47
Figure 3.1 ¹ H NMR spectrum of (a) [InBr ₂ -CB-Cyclen]Br in D ₂ O (top); (b) [InBr ₂ -CB-Cyclen]Br in 0.97 N DCl/D ₂ O after 50 % Decomplexation (middle); (c) protonated CB-Cyclen in 0.97 N DCl/D ₂ O (bottom).	52
Figure 3.2 A kinetic plot of <i>ln</i> (N/N ₀) vs. time for [InBr ₂ -CB-Cyclen]Br in 0.97 N DCl/D ₂ O at room temperature.	52

Figure 3.3 A kinetic plot of $\ln(N/N_0)$ vs. time for $[\text{InBr}_2\text{-CB-Cyclen}]\text{Br}$ in 0.97 N $\text{DCI/D}_2\text{O}$ at 90 °C.	53
Figure 3.4 A kinetic plot of $\ln(N/N_0)$ vs. time for $[\text{InBr}_2\text{-CB-Cyclen}]\text{Br}$ in 5.05 N $\text{DCI/D}_2\text{O}$ at room temperature.	54
Figure 3.5 ^1H NMR spectrum in 0.97 N $\text{DCI/D}_2\text{O}$ of (a) $[\text{InBr}_2\text{-CB-Cyclam}]\text{Br}$ after 3 weeks at room temperature (top); (b) $[\text{InBr}_2\text{-CB-Cyclam}]\text{Br}$ at 90 °C (middle); (c) protonated CB-cyclam (bottom).	55
Figure 3.6 ^1H NMR spectrum in 5.05 N $\text{DCI/D}_2\text{O}$ of (a) $[\text{InBr}_2\text{-CB-Cyclam}]\text{Br}$ after 3 weeks at room temperature (top); (b) protonated CB-cyclam (bottom).	55
Figure 3.7 ^1H NMR spectrum in 5.05 N $\text{DCI/D}_2\text{O}$ of (a) $[\text{GaBr}_2\text{-CB-Cyclam}]\text{Br}$ after 1 month at 90 °C (top); (b) protonated CB-cyclam (bottom).	56
Figure 3.8 ^1H NMR spectra of (a) $[\text{Ga-CB-DO2A}]\text{NO}_3$ in D_2O (top); (b) $[\text{Ga-CB-DO2A}]\text{NO}_3$ in 0.97 N $\text{DCI/D}_2\text{O}$ at room temperature after 8 months (second from top); (c) $[\text{Ga-CB-DO2A}]\text{NO}_3$ in 0.97 N $\text{DCI/D}_2\text{O}$ at 90 °C after 2 months (third from top); (d) protonated CB-DO2A in 0.97 N $\text{DCI/D}_2\text{O}$ (bottom).	57
Figure 3.9 ^1H NMR spectrum of (a) $[\text{In-CB-DO2A}]\text{Cl}$ in D_2O (top); (b) $[\text{In-CB-DO2A}]\text{Cl}$ in 0.97 N $\text{DCI/D}_2\text{O}$ at 90 °C after 34 days (middle); (c) protonated CB-DO2A in 0.97 N $\text{DCI/D}_2\text{O}$ (bottom).	58
Figure 3.10 H/D exchange for two diastereotopic pendant-arm methylene protons.	59
Figure 3.11 H/D exchange of the methylene protons on the CH_2COO arms for $[\text{In-CB-DO2A}]\text{Cl}$ in D_2O over time.	60
Figure 3.12 ^1H NMR spectra of (a) $[\text{Zn-CB-DO2A}]$ in D_2O (top); (b) $[\text{Zn-CB-DO2A}]$ in 0.97 N $\text{DCI/D}_2\text{O}$ at room temperature after 4 minutes (middle); (c) protonated CB-DO2A in 0.97 N $\text{DCI/D}_2\text{O}$ (bottom).	61
Figure 3.13 A kinetic plot of $\ln(N/N_0)$ vs. time for $[\text{Zn-CB-DO2A}]$ in 0.97 N $\text{DCI/D}_2\text{O}$ at room temperature.	62
Figure 3.14 ^1H NMR spectra of (a) $[\text{Zn-CB-TE2A}]$ in D_2O (top); (b) $[\text{Zn-CB-TE2A}]$ in 0.97 N $\text{DCI/D}_2\text{O}$ at room temperature after 71 days (middle); (c) protonated CB-TE2A (bottom) in 0.97 N $\text{DCI/D}_2\text{O}$.	63

Figure 3.15 A kinetic plot of $\ln(N/N_0)$ vs. time for Zn-CB-TE2A in 0.97 N DCl/D ₂ O at 90 °C.	64
Figure 3.16 ¹ H NMR spectra in 5.05 N DCl/D ₂ O of (a) [Zn-CB-TE2A] (top); (b) protonated CB-TE2A (bottom).	64
Figure 3.17 A kinetic plot of $\ln(N/N_0)$ vs. time for Zn-CB-TE2A in 5.05 N DCl/D ₂ O at room temperature.	65
Figure 3.18 ¹ H NMR spectrum of (a) Cd-CB-DO2A in D ₂ O (top); (b) Cd-CB-DO2A in 0.97 N DCl/D ₂ O after 6 minutes at room temperature (middle); (c) protonated CB-DO2A in 0.97 N DCl/D ₂ O (bottom).	66
Figure 3.19 ¹ H NMR spectra of (a) [Cd-CB-TE2A] in D ₂ O (top); (b) [Cd-CB-TE2A] in 5.05 N DCl/D ₂ O after 5 minutes at room temperature (middle); (c) protonated CB-TE2A in 5.05 N DCl/D ₂ O (bottom).	67
Figure 3.20 NH/ND Exchange in D ₂ O or CD ₃ OD.	68
Figure 3.21 Possible mechanisms for NH/ND Exchange in D ₂ O and CD ₃ OD.	68
Figure 3.22 ¹ H NMR spectrum of In-CB-Cyclen at room temperature (a) in D ₂ O after 5 minutes (top); (b) in D ₂ O after 4 days (middle); (c) in 0.97 N DCl/D ₂ O after 43 days (bottom).	69
Figure 3.23 ¹ H NMR spectrum of Ga-CB-Cyclam at room temperature (a) in D ₂ O after 5 minutes (top); (b) in D ₂ O after 1 day (middle); (c) in 0.97 N DCl/D ₂ O after 16 days (bottom).	70
Figure 3.24 (a) Coordination geometry of a metal complex of the cross-bridged ligand. (left); (b) axial and equatorial ideal angles for a metal complex.	71
Figure 3.25 Proposed acid-promoted decomplexation mechanism for Cu-CB-Cyclam.	74

LIST OF TABLES

<u>Table</u>	<u>Page</u>
Table 1.1 Gallium and Indium Radionuclides.	3
Table 3.1 Metal cationic radii for 6-coordinate, octahedral coordination.	72
Table 3.2 X-ray structural data.	72
Table 3.3 Half-lives of selected metal complexes.	73

LIST OF SCHEMES

<u>Scheme</u>	<u>Page</u>
Scheme 1.1 Route to cross-bridged cyclam and H ₂ CB-TE2A.	12
Scheme 1.2 Route to dibenzo annelated cross-bridged cyclam.	12

ABSTRACT

**GROUP 12 AND GROUP 13 METAL COMPLEXES OF CROSS-BRIDGED
TETRAAMINE MACROCYCLES**

BY

Wei-Chih Lee

University of New Hampshire, September, 2006

The use of radiometal-based radiopharmaceuticals for the therapy and diagnostic imaging of various diseases is rapidly increasing. Metal complex stability *in vivo* is an important factor to keep the metal chelate intact under physiological conditions for the radiopharmaceutical application. A novel class of cross-bridged tetraazamacrocycles with nonadjacent nitrogens bridged by an ethylene unit was developed to make metal complexes with good thermodynamic stability and higher kinetic inertness towards dissociation. Complexes of Ga(III) and In(III) radionuclides are widely used in diagnostic imaging and their respective half-lives are convenient for specific diseases. The new complexes [In-CB-DO2A]⁺ and [In-CB-TE2A]⁺ have been prepared by direct and indirect routes respectively. In addition, to predict how these complexes will survive *in vivo*, their decomplexation half-lives under forcing conditions are used as first indicators. Related diamagnetic Ga³⁺, In³⁺, Zn²⁺, Cd²⁺, and Hg²⁺ complexes were also included for these acid decomplexation studies by NMR spectroscopy in DCl/D₂O solution. In general, relative inertness can be correlated to their solid-state structures.

CHAPTER I

INTRODUCTION

1.1 Background

The use of radiometal-based radiopharmaceuticals for the therapy and diagnostic imaging of various diseases is rapidly increasing and has been reviewed.¹⁻⁹ A targeting metallo-radiopharmaceutical is constituted from three major components: a radionuclide, a bifunctional chelator, and the targeting biomolecule (**Figure 1.1**). The targeting biomolecule, such as an antibody or peptide, is coupled through a bifunctional chelator which covalently links it while coordinated to the metallic radionuclide.

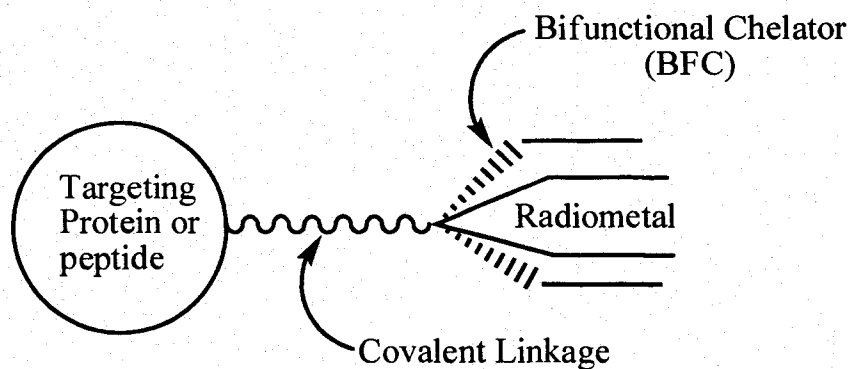


Figure 1.1⁵ A targeted metallo-radiopharmaceutical.

Somatostatin (**Figure 1.2**) is a 14-amino acid peptide involved in the regulation and release of a number of hormones.¹ Somatostatin receptors (SSRs), found on the cell surface, occur in a number of different normal organ systems, including the central nervous system, the gastrointestinal tract, and the exocrine and endocrine pancreas. In

addition, most human tumors originating from the somatostatin targeted tissue have conserved somatostatin receptors and are SSR-positive. While Somatostatin has a very short biological half-life, its analogs such as Octreotide have much longer residence times.⁴ For instance, Octreotide (**Figure 1.2**) is an 8-amino acid somatostatin analog which has a half-life of 117 minutes as compared to approximately one minute for Somatostatin itself, making it more suitable for therapeutic and imaging purposes. Octreotide has been labeled with ¹¹¹In using DTPA (¹¹¹In-DTPA-octreotide, **Figure 1.3**) and was approved in 1994 for human use in the U.S.A. and Europe as a diagnostic imaging agent for neuroendocrine tumors. The targeting of SSRs in tumors has been a goal in cancer diagnosis and treatment recently by using somatostatin analogs labeled with other radionuclides.^{2,3}

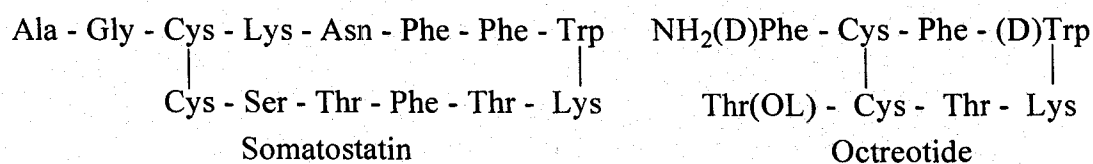


Figure 1.2³ Structures of Somatostatin and its analog, Octreotide.

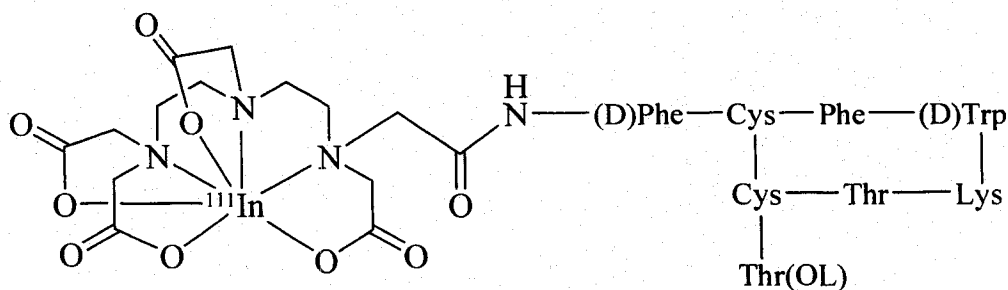


Figure 1.3¹⁰ Structure of ¹¹¹In-DTPA-Octreotide.

1.2 Gallium(III) and Indium(III) Chemistry

1.2.1 Gallium(III) and Indium(III) Radionuclides

One of the important factors for the selection of a radiopharmaceutical is its half-life. This must be long enough to carry out the desired chemistry to synthesize the radiopharmaceutical, but short enough to limit the dose to the patient.⁴ The *in vivo* half-life also depends on the time required for the pharmaceutical to localize in and clear the target tissue. Complexes of Ga(III) and In(III) radionuclides are widely used in diagnostic imaging and their coordination and radiopharmaceutical chemistry have been reviewed recently.^{1-5,11,12,13} The half-lives and decay modes of gallium and indium radionuclides are summarized in **Table 1.1**.⁴

Table 1.1⁴ Gallium and Indium Radionuclides.

Isotope	T _{1/2} (h)	Decay mode
⁶⁶ Ga	9.5	β ⁺ (56%) EC (44%)
⁶⁷ Ga	78.26	EC (100%)
⁶⁸ Ga	1.1	β ⁺ (90%) EC (10%)
¹¹¹ In	67.9	EC (100%)

1.2.2 Properties of Trivalent Gallium and Indium Cations in Aqueous Solution

Both gallium and indium are in Group 13 of the Periodic Table. Under physiological conditions, their most prevalent oxidation state in aqueous solution is +3, and this is thus most relevant for radiopharmaceutical chemistry.⁵ Due to their high charge density, Ga(III) and In(III) are both considered to be hard metal ions which prefer

chelators with hard donors, such as carboxylate-oxygen and phenolate-oxygen atoms with respect to the Hard/Soft Acid/Base theory. Since they are highly-charged cations, free hydrated Ga(III) is only present in acidic aqueous solutions ($pK_a = 2.6$),¹⁴ and hydrolyzes nearly completely over a wide pH range with a variety of hydroxide species forming as the pH is raised (**Figure 1.4, 1.5**). It was reported that insoluble Ga(OH)₃ is the primary species between pH 3 ~ 9.5, whereas above pH 9.6, the soluble gallate anion (Ga(OH)₄⁻) forms. Similarly, In(III) also hydrolyzes easily ($pK_a = 4$),¹⁴ forming insoluble hydroxides at pH > 3.4.⁵ This hydrolysis of Ga³⁺ and In³⁺, particularly at pH > 4, poses a significant challenge since the precipitation of Ga(OH)₃ and In(OH)₃ can occur before Ga(III) and In(III) complexations.²

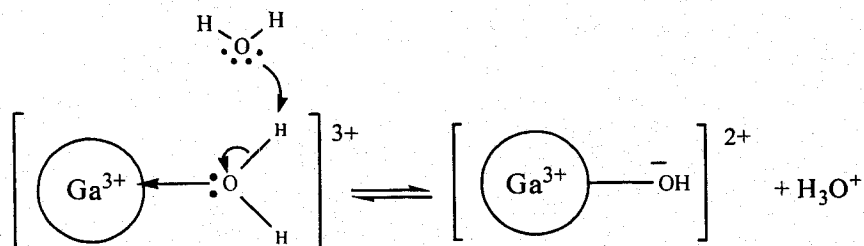


Figure 1.4 Hydrolysis of the hydrated Ga³⁺ cation.

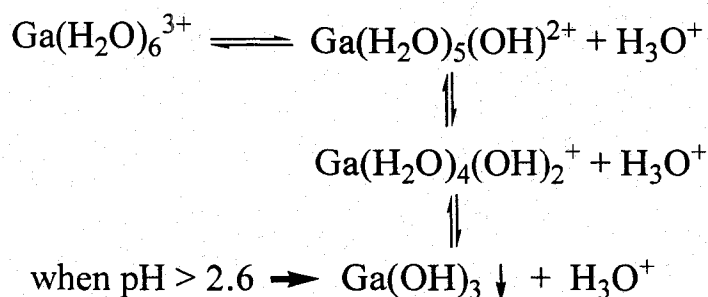


Figure 1.5 Hydrolysis of the hydrated Ga³⁺ cation.

In addition, trications are usually much more substitution-inert than dications.^{14,15} Some rate constants for water exchange of solvated cations are as follows:¹⁵ $\text{Cu}(\text{OH}_2)_6^{2+}$: $8 \times 10^9 \text{ s}^{-1}$; $\text{Zn}(\text{OH}_2)_6^{2+}$: $2 \times 10^7 \text{ s}^{-1}$; $\text{Ga}(\text{OH}_2)_6^{3+}$: $1 \times 10^3 \text{ s}^{-1}$; $\text{In}(\text{OH}_2)_6^{3+}$: $2 \times 10^5 \text{ s}^{-1}$. A relationship of these rate constants to the acidity of the metal cations exists: water molecules are much more strongly bound to more acidic metal cations resulting in a slower exchange and smaller rate constants during substitution reactions.

For their complexes, Ga(III) and In(III) have well-established coordination numbers of 3, 4, 5, and 6 depending on the ligand, while indium also forms seven- or eight-coordinate complexes due to its larger size (In^{3+} : 94 pm vs. Ga^{3+} : 76 pm for six-coordinate complexes).⁵

1.3 Bifunctional Chelators (BFCs)

One of important factors for the efficacy of a radiopharmaceutical is the metal complex stability *in vivo* in order to keep the metal chelate intact under physiological conditions.¹⁰ Macrocyclic chelators have been found to form metal complexes with more kinetic inertness towards dissociation and greater thermodynamic stability (macrocyclic effect) than their acyclic analogues.⁴ The reason for this drastic difference is due to the cyclic nature of the ligand, which hinders a stepwise dissociation from the metal ion and concomitant protonation of the amino groups.¹⁶

Bifunctional chelators are chelating agents that have a second functionality which can covalently attach it to a targeting moiety. There have been many bifunctional chelators developed for radiopharmaceutical applications, e.g. NOTA, DOTA, TRITA,

TETA (**Figure 1.6**) and their derivatives. Their related BFC coordination chemistry has been reviewed recently.^{4,17-22}

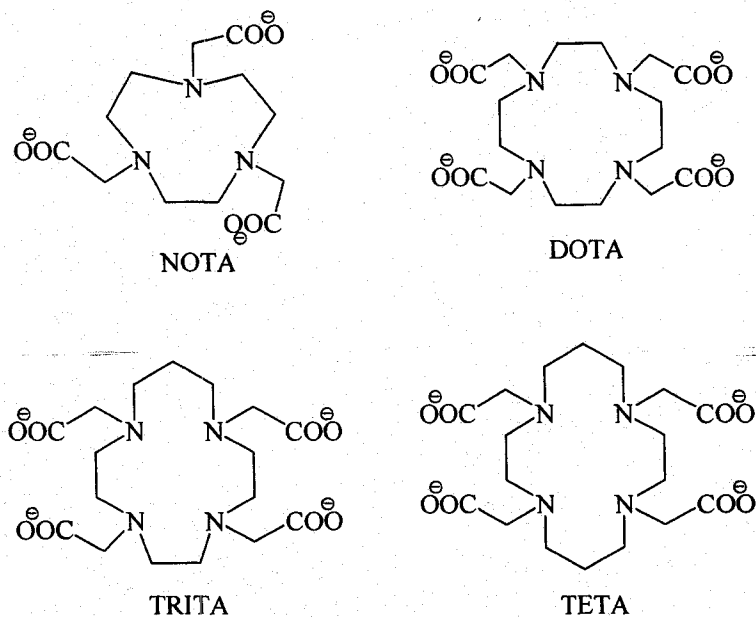


Figure 1.6 Some Common Bifunctional Chelators (BFCs).

1.4 Coordination Chemistry of Gallium and Indium Complexes of Cyclen, Cyclam and their derivatives

Bosnich reported in 1965 that cyclam has five possible coordination modes for the trans-isomers of their complexes and three for their cis-isomers (**Figure 1.7**). Cyclen has the same possible coordination modes except for the equivalence of trans-III and trans-IV.^{8,23} The complex of a specific metal cation, however, may favor one coordination configuration over the rest. This coordination chemistry of cyclam, cyclen, and their derivatives has been studied in detail.^{8, 23-28}

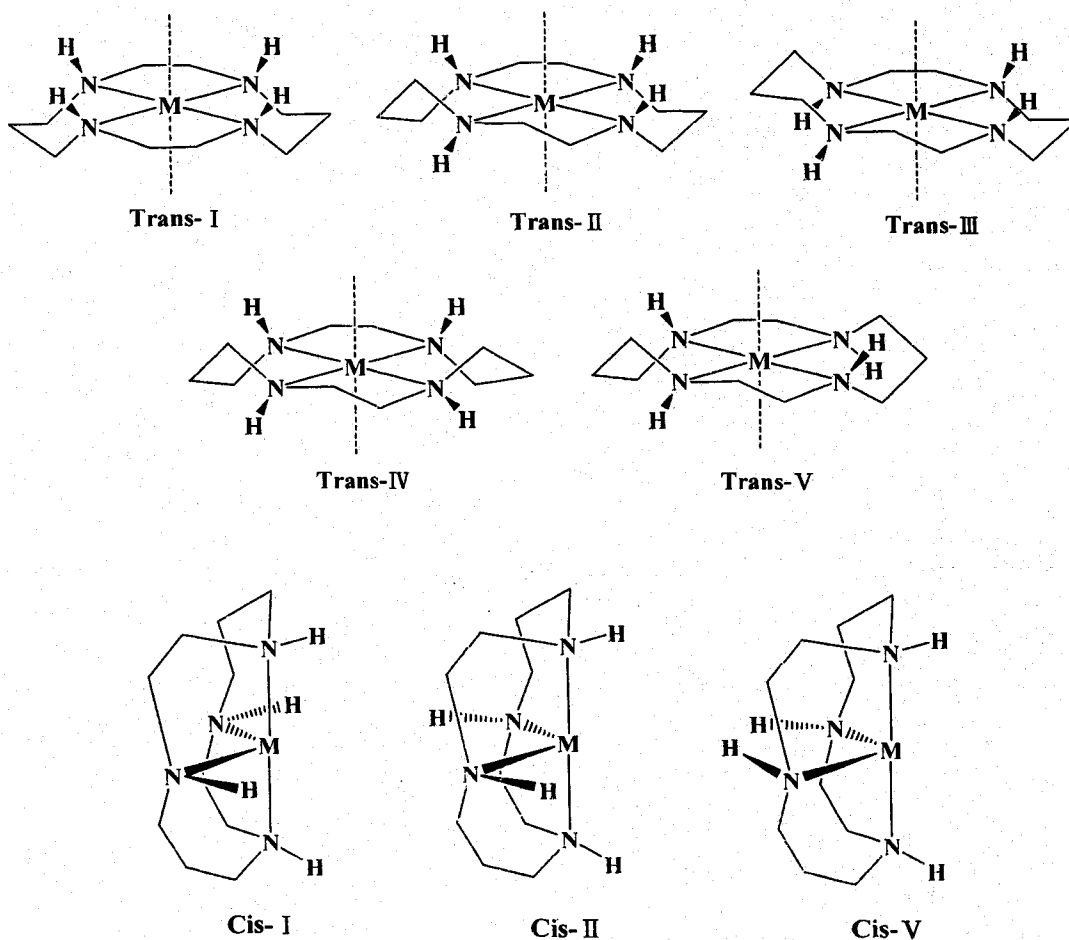


Figure 1.7^{8,23} Possible coordination modes of trans- (top) and cis- (bottom) isomers for cyclam.

DOTA and its derivatives are known to form thermodynamically and kinetically stable metal complexes with many di- and tri-valent metal ions.^{2,4,5,9,10,18,29} From the solid-state structure (**Figure 1.8**) of Ga-DOTA-d-PheNH₂,²⁹ the chelator adopts a cis- I pseudo-octahedral geometry with a folded macrocyclic unit. The hexadentate DOTA-d-PheNH₂ coordinates the Ga³⁺ ion with four nitrogen donors and two carboxylate groups. The axial angle 156.3(2)° of N3-Ga1-N5 reveals this distorted geometry. In addition, two transannular nitrogens (N2, N4) of the cyclen ring and two corresponding carboxylate-oxygen atoms form an almost perfect equatorial plane with a maximum deviation of

0.028 Å. Furthermore, the one uncoordinated carboxylate group is deprotonated at physiological pH; this structural feature is believed to contribute to a fast and efficient excretion of chemicals through the kidney.²⁹

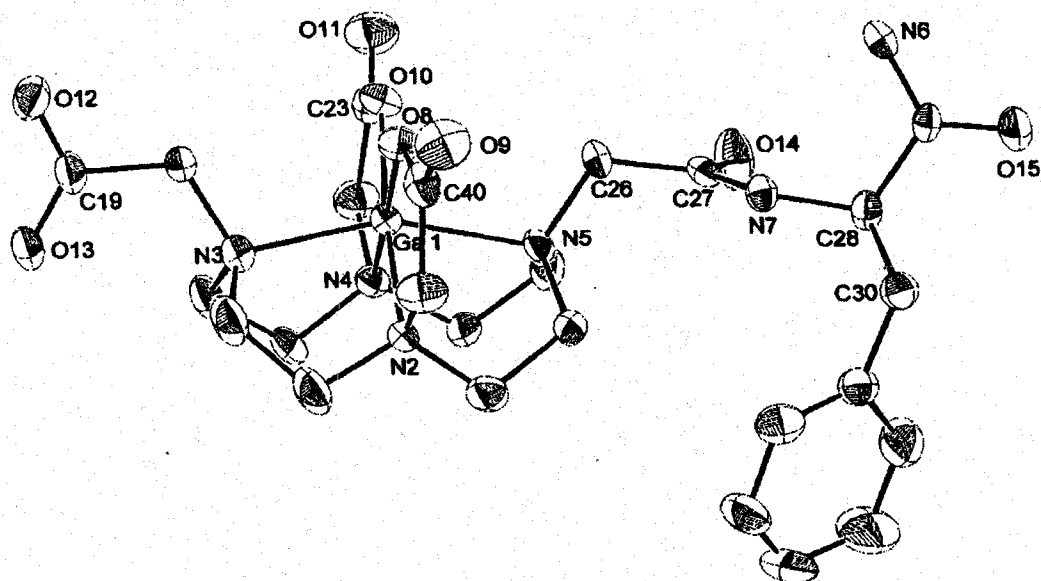


Figure 1.8²⁹ ORTEP plot of the crystal structure of [Ga-DOTA-d-PheNH₂].

Since the coordination number of In³⁺ is typically 6 or 7, only a few eight-coordinated In³⁺ complexes are known.³⁰ DOTA-AA (AA = *p*-Aminoanilide), as an octadentate ligand, coordinating In³⁺ with four amine-nitrogen, one amide carbonyl-oxygen, and three carboxylate-oxygen atoms to form a twisted square antiprismatic geometry in the solid state (**Figure 1.9**).³⁰ The carbonyl-oxygen, however, may become dissociated in solution to give a seven-coordinate solution complex as demonstrated by its ¹H NMR spectrum (**Figure 1.10**).

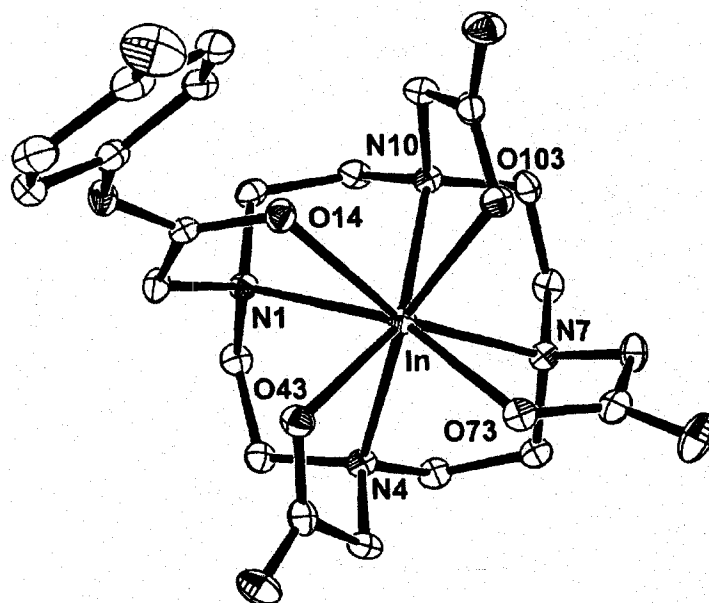


Figure 1.9 ORTEP drawing of In(DOTA-AA).

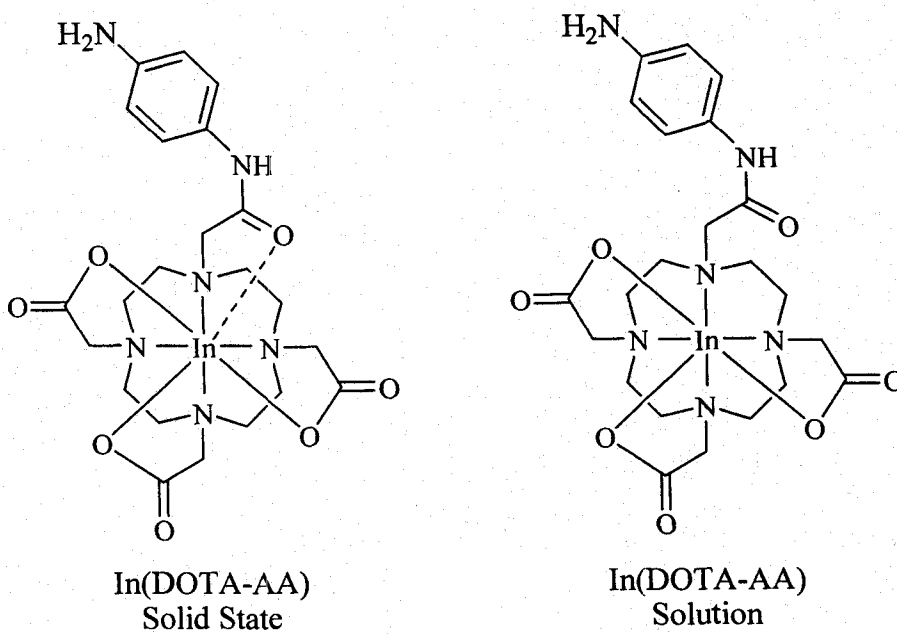
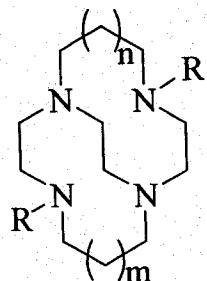


Figure 1.10³⁰ Comparison of the coordination geometry of In(DOTA-AA) in its solid state (left) and in solution (right).

1.5 Gallium and Indium Coordination Chemistry of Cross-bridged Tetraazamacrocyclic Ligands



$m=n=0$ and $R=H$, CB-Cyclen.
 $m=n=1$ and $R=H$, CB-Cyclam.
 $m=n=0$ and $R=CH_2COO^-$, CB-DO2A.
 $m=n=1$ and $R=CH_2COO^-$, CB-TE2A.

Figure 1.11 Generic structures of cross-bridged ligands.

A novel class of cross-bridged tetraazamacrocycles with nonadjacent nitrogens bridged by an ethylene unit was first reported in 1990 by Weisman at UNH.³¹ A series of refined synthetic methods to make the derivatives of the cross-bridged tetraazamacrocycles have also been developed (**Figure 1.11**).³²⁻³⁴ The cross-bridged ligands were designed to have all four nitrogen donor electron pairs convergent upon a molecular cleft (**Figure 1.12**) for optimal metal binding. These cross-bridged ligands improved the kinetic stability of metal complexes significantly compared to related cyclam and cyclen ligands or their derivatives. In addition, the cross-bridging ethylene allows only the *cis-V* coordinating ligand conformation (**Figure 1.13**). N-functionalization of these cross-bridged tetraazamacrocyclic ligands with one or two neutral or ionizable pendant arms can serve to more completely envelope a 6-coordinate guest cation and does impart significant kinetic inertness to their complexes (**Figure 1.13**). In addition, these cross-bridged ligands are proton sponges (for dimethyl CB-Cyclam, $pK_{a1} > 13.5$ (25 in MeCN) and $pK_{a2} = 10.8$).³¹ Therefore, in protic solvents only

most strongly-binding divalent transition metal ions like Cu^{2+} and Zn^{2+} readily form complexes with these ligands.^{31,32} This property makes metal complexation difficult under protic conditions because of the competition between protons and the metal cations for the nitrogen donors.

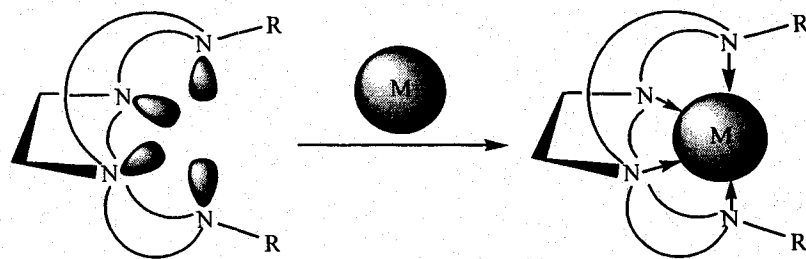


Figure 1.12 Metal complexation of cross-bridged ligands with all four nitrogen donor electron pairs convergent upon a molecular cleft

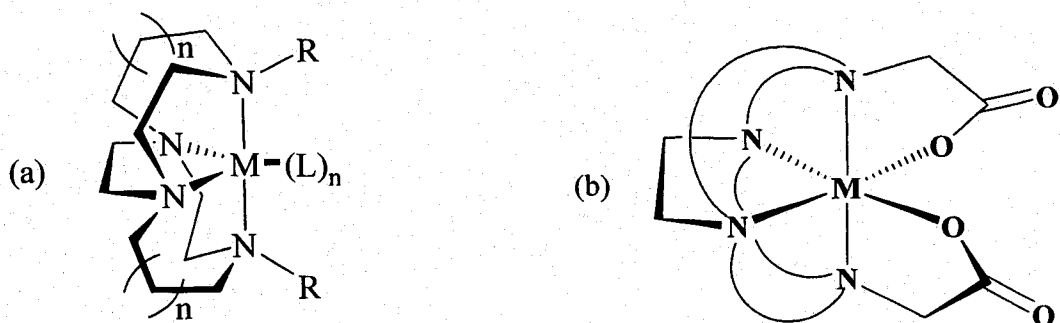
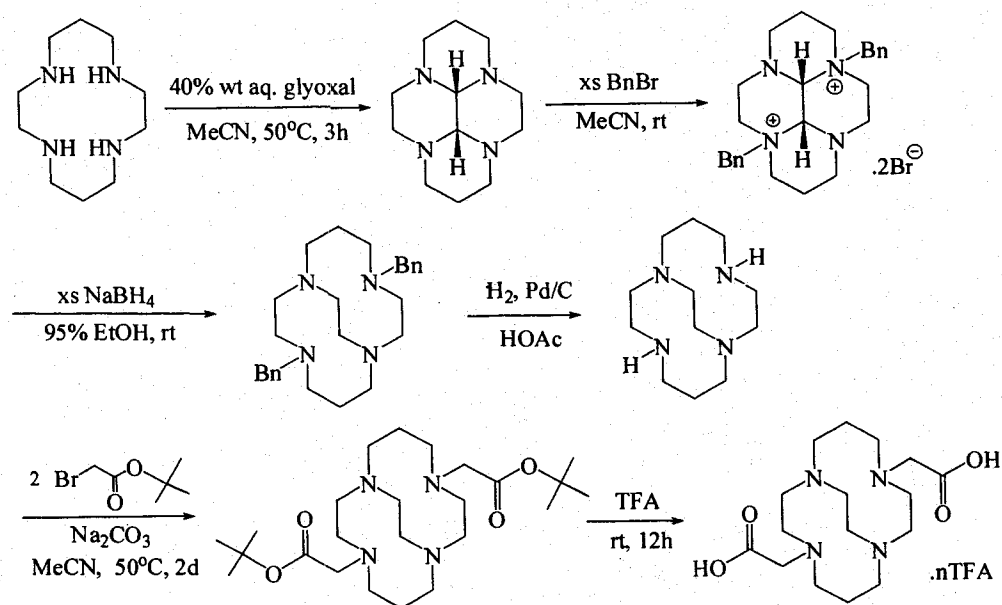


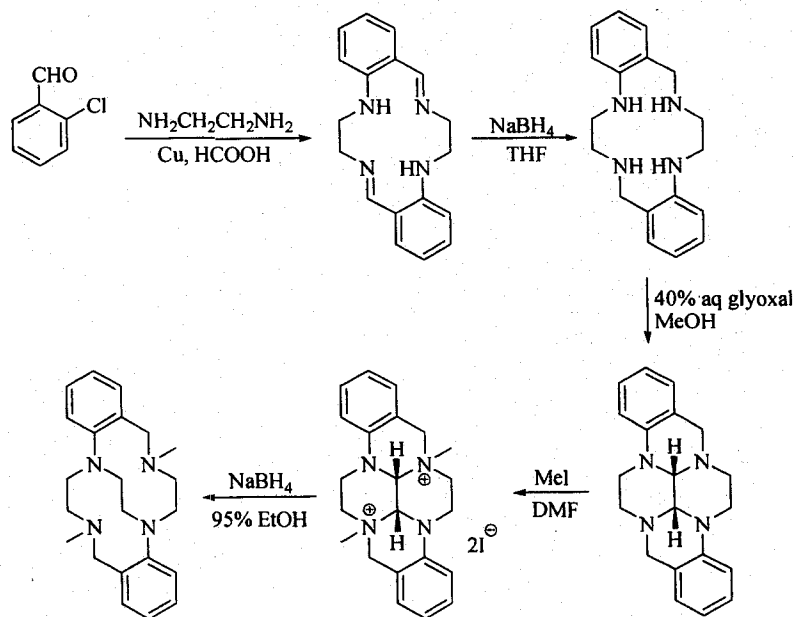
Figure 1.13 (a) Cis-V configuration for the metal complexes of cross-bridged ligands (left); (b) generic structure of a metal complex of a two carboxylate pendant-armed cross-bridged ligand (right).

The general synthetic route to make cross-bridged ligands is shown in **Scheme 1.1**. A broad series of metal complexes of the cross-bridged tetraazamacrocycles and their coordination chemistry has been reported, including: Li^+ , Cr^{2+} , Mn^{2+} , Mn^{3+} , Fe^{2+} , Fe^{3+} , Co^{2+} , Co^{3+} , Ni^{2+} , Cu^{1+} , Cu^{2+} , Ga^{3+} , In^{3+} , Pd^{2+} , Zn^{2+} , Cd^{2+} , Hg^{2+} , and Zr^{4+} .^{19,31-33,35-41} Various coordination geometries including octahedral, trigonal bipyramidal, square

pyramidal and tetrahedral have been observed. New dibenzo annelated cross-bridged cyclam was first synthesized by Jeffrey S. Condon (Scheme 1.2),⁴² and later modified by Dave Martin using MeOTs instead of MeI for alkylation to improve the yield. These



Scheme 1.1 Route to cross-bridged cyclam and H₂CB-TE2A.



Scheme 1.2 Route to dibenzo annelated cross-bridged cyclam.

ligands are designed to have decreased basicity relative to the corresponding derivatives of cross-bridged cyclams while still retaining the same superior coordination chemistry. The annelated aromatic rings also provide a framework for functionalization to attach a targeting biomolecule.

Gallium and indium complexes of cross-bridged ligands were first prepared and characterized by Niu. These include $[\text{GaCl}_2\text{-CB-Cyclen}]\text{Cl}$, $[\text{GaCl}_2\text{-CB-Cyclam}]\text{Cl}$, $[\text{InBr}_2\text{-CB-Cylen}]\text{Br}$, $[\text{InBr}_2\text{-CB-Cyclam}]\text{Br}$, and $[\text{Ga-CB-DO2A}]\text{NO}_3$.^{36,37} Their solid-state structures confirmed the cis-folded binding conformation of these cross-bridged ligands. These hexacoordinate metal centers all exhibit significant distortions from idealized octahedral geometry. The solid-state structure (**Figure 1.14**) of C_2 -symmetric $[\text{Ga-CB-DO2A}]\text{NO}_3$ revealed an enveloped Ga^{3+} cation within the ligand's cleft. The distortion from an idealized octahedral geometry is observed with an axial $\text{N}(2)\text{-Ga}(1)\text{-N}(2\text{A})$ angle of $164.56(9)^\circ$ and an equatorial $\text{N}(1)\text{-Ga}(1)\text{-N}(1\text{A})$ angle of $86.24(9)^\circ$. The pseudo-octahedral coordination geometry (**Figure 1.15**) of C_2 -symmetric $[\text{InBr}_2\text{-CB-}$

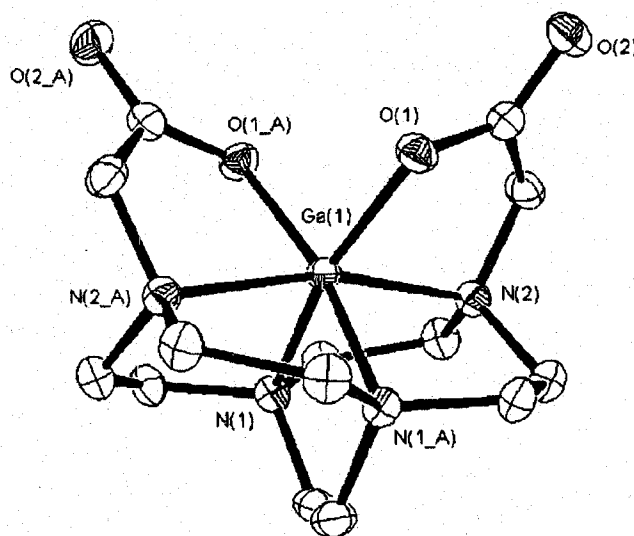


Figure 1.14 X-ray structure of $[\text{Ga-CB-DO2A}]\text{NO}_3$.

Cyclen]Br showed the most distorted geometry amongst the four gallium and indium complexes of CB-cyclam and CB-Cyclen with an axial N(2)-In(1)-N(4) angle of 143.95(12)° and equatorial N(1)-In(1)-N(3) angle of 76.78(12)°. This is the result of the misfit of the large In³⁺ in the small cyclen cavity.

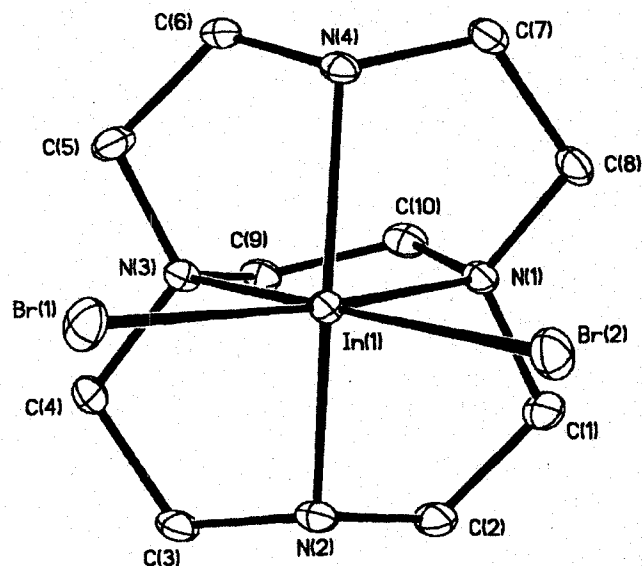


Figure 1.15 X-ray structure of [InBr₂-CB-Cylen]Br.

As was observed for Zn(II), Cd(II) and Hg(II) complexes of cross-bridged cyclam and cyclen,⁴⁰ N-H/N-D exchange at the secondary ligand nitrogens (**Figure 1.16**) was observed for all gallium and indium complexes of cross-bridged cyclam and cyclen in D₂O or CD₃OD (see Chapter 3), suggesting that these N-H protons may be acidic.³⁶ In addition, the half-lives of these N-H/N-D exchange for Zn(II), Cd(II) and Hg(II) complexes were also determined by Niu.⁴³

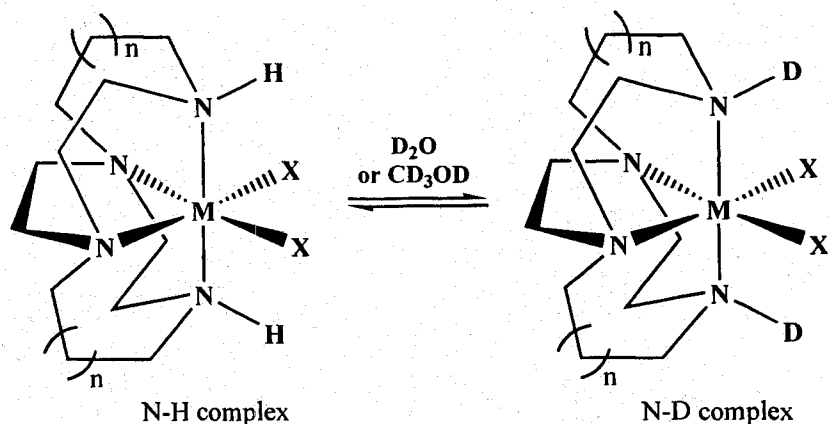


Figure 1.16 NH/ND exchange process in D_2O or CD_3OD .

1.6 Research Goals

This thesis will focus on the gallium(III) and indium(III) complexation with a family of ethylene cross-bridged tetraazamacrocycles with two carboxylate pendant arms. These are of interest because of their potential radiopharmaceutical applications. Besides $[\text{Ga-CB-DO2A}]\text{NO}_3$ made by Niu, Ga(III) and In(III) complexes of cross-bridged tetraazamacrocycles with two carboxylate arms and dibenzo derivatives are still unknown. In order to synthesize these complexes, ligands used were prepared according to previous work. The diamagnetic nature of the gallium and indium complexes allowed for routine NMR spectral assays of reaction progress. Metal complexes thus synthesized were characterized by IR, ^1H and $^{13}\text{C}\{^1\text{H}\}$ NMR spectrometry, and ESI-MS methods. Acid-promoted dissociation studies were then used to compare the relative kinetic inertness of selected complexes.

CHAPTER II

Ga(III) AND In(III) COMPLEXES OF CROSS-BRIDGED TETRAAZAMACROCYCLIC LIGANDS

2.1 Introduction

Ga(III) and In(III) complexes of pendant-armed cyclam and cyclen derivatives are of interest because of their potential radiopharmaceutical application.^{1-5,11-13} Besides [Ga-CB-DO2A]NO₃ made by Niu,³⁷ Ga(III) and In(III) complexes of the ethylene cross-bridged tetraazamacrocycles with two carboxylate arms and a dibenzo annelated derivative (Figure 2.1) are still unknown.

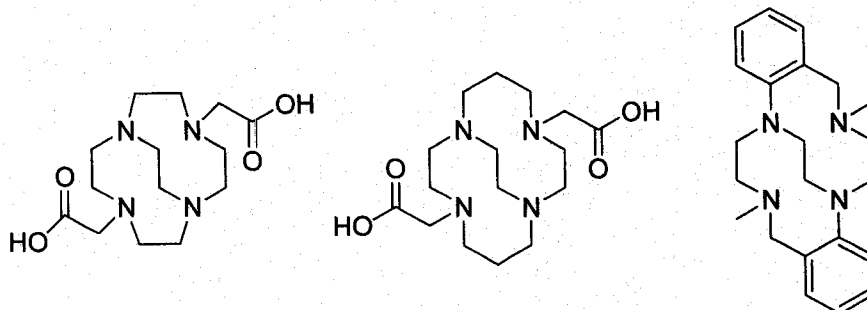


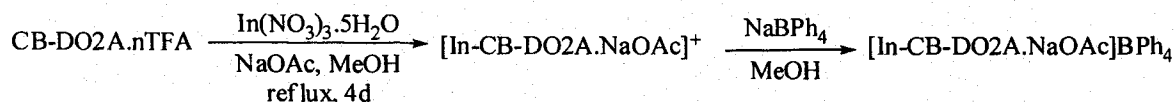
Figure 2.1 Cross-bridged ligands studied in Ga(III) and In(III) complexations.

The significant challenge in trivalent metal (Ga^{3+} and In^{3+}) complexation in aqueous solution is that the precipitation of $\text{Ga}(\text{OH})_3$ and $\text{In}(\text{OH})_3$ may occur before the pH is high enough for Ga(III) and In(III) complexes to form.^{2,5} Furthermore, the proton-sponge nature^{31,32} of cross-bridged tetraazamacrocyclic ligands makes the metal ion

binding even more challenging because these ligands bind at least one proton very tightly and higher pH is needed to remove the last one or two protons on the protonated cross-bridged ligand. Only strongly binding metal ions can compete with that proton for the cavity. In addition, trivalent metal (Ga^{3+} and In^{3+}) ions are much more kinetically inert than divalent Zn^{2+} , Cd^{2+} , Hg^{2+} , and Cu^{2+} as seen from the reaction rates of their octahedral complexes in exchange of solvent water. This can be attributed to a higher electrostatic attraction between the central atom and the attached ligands, which will slow down any dissociative exchange.^{14,15} The combination of these properties, therefore, ensures that the binding rate of Ga^{3+} and In^{3+} in competition with protons for the ligand cavity in protic solvents would be much slower than those of most other divalent metal ions and makes successful complexation challenging.

2.2 Synthesis and Characterization

2.2.1 Synthesis of the In(III) Complex of $\text{H}_2\text{-CB-DO2A} \cdot n\text{TFA}$



The same published literature procedures used to prepare $[\text{Ga-CB-DO2A}]\text{NO}_3$ developed by Niu were used.³⁷ One equivalent of $\text{H}_2\text{-CB-DO2A} \cdot n\text{TFA}$ ($n=4$ from its proton NMR spectrum) in MeOH was added into a solution of $\text{In(NO}_3)_3$ pentahydrate in MeOH and stirred for 10 minutes. Excess sodium acetate (10 equivalents) was then added in one portion to this stirred solution. After 4 days of refluxing, an insoluble solid was centrifuged off from the cloudy solution and the supernatant was separated and evaporated to dryness to give the crude product. From its IR spectrum, the methanol-

insoluble solid contained only sodium acetate and indium hydroxide. Instead of the downfield singlet proton NMR resonance (δ 3.74) of the methylene protons of the free ligand CH_2COO arms, a downfield AB pattern was found for the crude product in CD_3OD (**Figure 2.2(a)**). The other proton resonances cannot be readily assigned. The $^{13}\text{C}\{^1\text{H}\}$ NMR spectrum of the crude product showed at least five signals between 52 and 66 ppm compared to only four signals in the aliphatic region of the free ligand $\text{H}_2\text{-CB-DO2A}$.

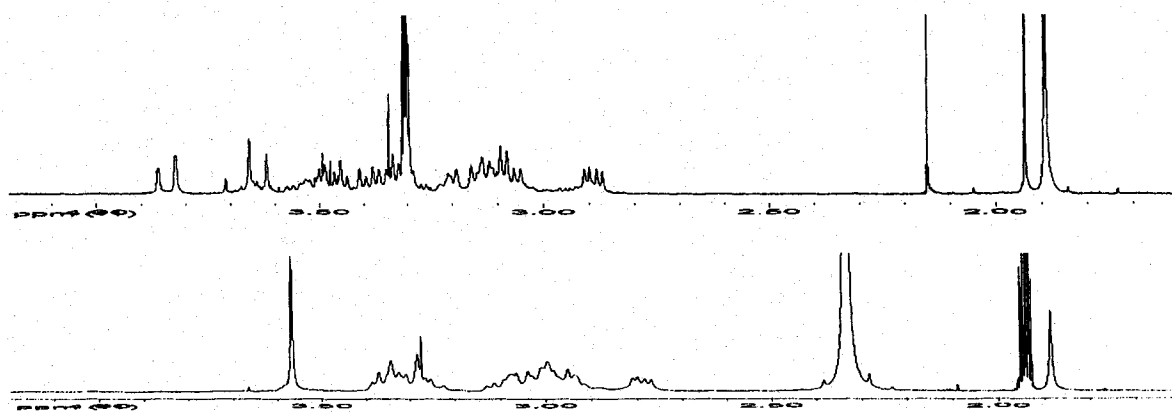


Figure 2.2 ^1H NMR spectra comparison (a) crude product in CD_3OD (top); (b) $[\text{In-CB-DO2A} \cdot \text{NaOAc}]\text{BPh}_4$ in CD_3CN (bottom).

Addition of one equivalent of sodium tetraphenylborate to a MeOH solution of the crude product precipitated a white solid (67% yield) which showed eight signals (δ 177.71, 65.23, 61.18, 58.54, 57.11, 54.82, 49.43, 47.98) in the $^{13}\text{C}\{^1\text{H}\}$ NMR spectrum and two extra signals at δ 23.46, 174.93 from sodium acetate. These data are very different from Niu's $[\text{Ga-CB-DO2A}]\text{NO}_3$ which precipitated from the MeOH and whose $^{13}\text{C}\{^1\text{H}\}$ NMR spectrum showed only seven peaks. It is also interesting that the AB pattern of the methylene protons on the complex arms in the proton NMR spectrum of $[\text{In-CB-DO2A}]^+$ in CD_3OD became a singlet (δ 3.57) in CD_3CN (**Figure 2.2(b)**).

From the major peak ($m/z = 509$) of the compound's FAB Mass spectrum (**Figure 2.3**), $[\text{In-CB-DO2A} \cdot \text{NaOAc}]^+$ exists as an entity. There is thus an additional sodium acetate attached to the In(III) complex core. This is confirmed by its IR spectrum (**Figure 2.4**) which showed two carbonyl stretching bands ($1659.2, 1620.9 \text{ cm}^{-1}$): one is from the pendant arm carboxylate and the other is from acetate. Further, the integration of the singlet proton NMR resonance at $\delta 3.60$ versus that of the phenyl resonance at $\delta 6.85$ reveals one tetraphenylborate anion for each $[\text{In-CB-DO2A} \cdot \text{NaOAc}]^+$ complex cation, suggesting the empirical formula to be $[\text{In-CB-DO2A} \cdot \text{NaOAc}]\text{BPh}_4$. This has been confirmed by CHN analyses. However, none of the proposed structures (**Figure 2.5**), while consistent with the ^{13}C data, can explain the downfield methylene singlet at $\delta 3.57$ in the proton NMR spectrum unless they are accidentally overlapping (isochronous) and chemical shifts may thus make the diastereotopic H_a and H_b equivalent (a singlet). Despite numerous attempts to obtain X-ray quality crystals only laminated plates formed.

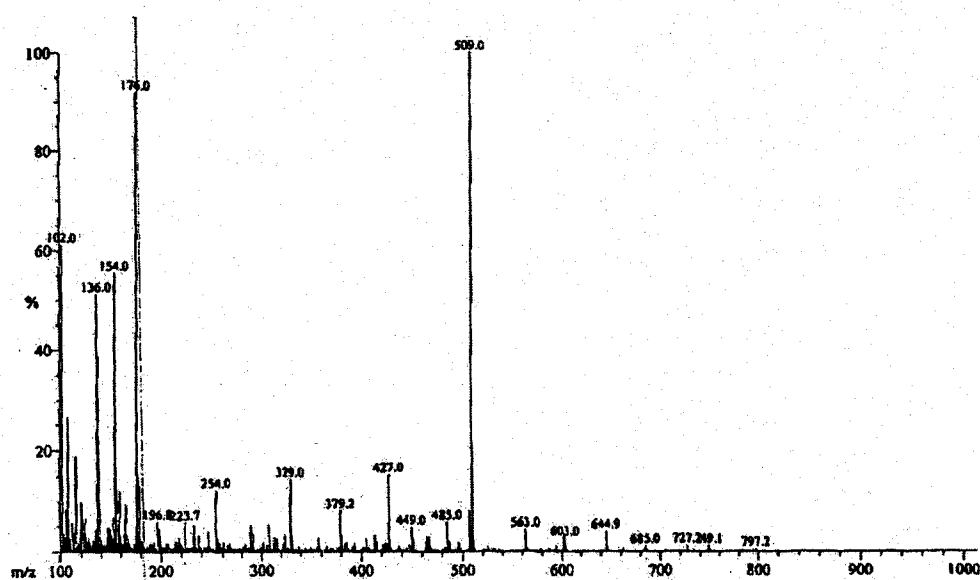


Figure 2.3 FAB (positive mode) mass spectrum of $[\text{In-CB-DO2A} \cdot \text{NaOAc}]\text{BPh}_4$.

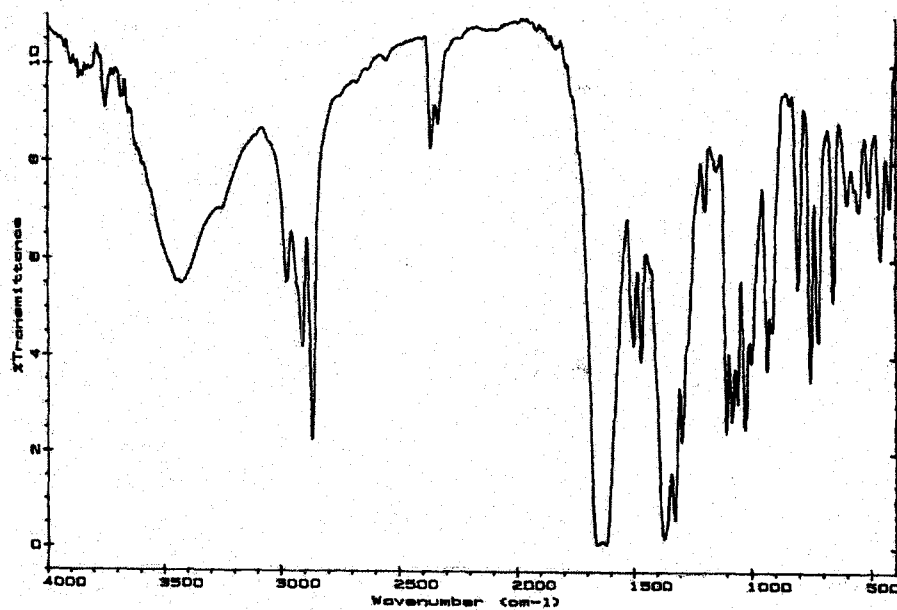


Figure 2.4 IR spectrum of $[\text{In-CB-DO2A} \cdot \text{NaOAc}]\text{BPh}_4$.

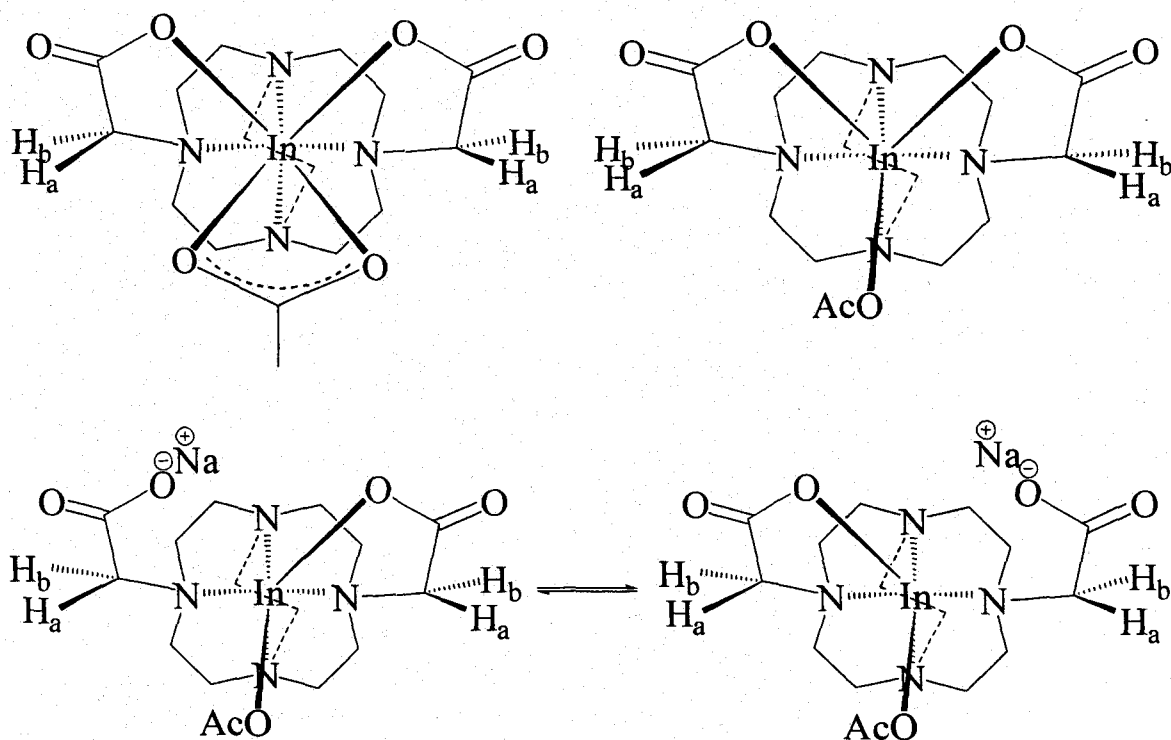


Figure 2.5 Possible structures of $[\text{In-CB-DO2A} \cdot \text{NaOAc}]\text{BPh}_4$.

A second method to isolate the $[\text{In-CB-DO2A}]^+$ cation was tried. Addition of concentrated aqueous HCl to a CH_3CN solution of $[\text{In-CB-DO2A} \cdot \text{NaOAc}]\text{BPh}_4$ precipitated a white solid. Interestingly, the AB pattern of the CH_2COO arms in the proton NMR spectrum in D_2O appeared and the relative integrations are: δ 3.74 (AB pattern of CH_2COO , 4H), 3.62-3.44 (m, 6H), 3.36-3.12 (m, 12H), 2.98-2.90 (dd, 2H) (Figure 2.6). The $^{13}\text{C}\{^1\text{H}\}$ NMR spectrum showed eight resonances as before (Figure

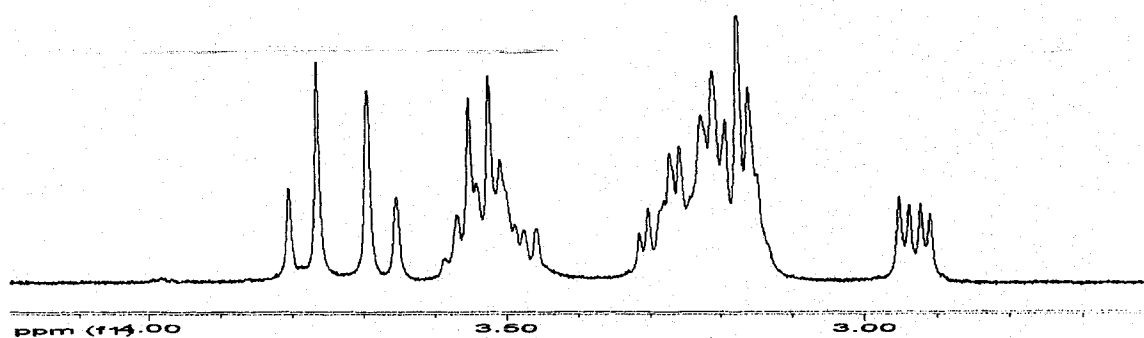


Figure 2.6 ^1H NMR spectrum of $[\text{In-CB-DO2A}]^+$.

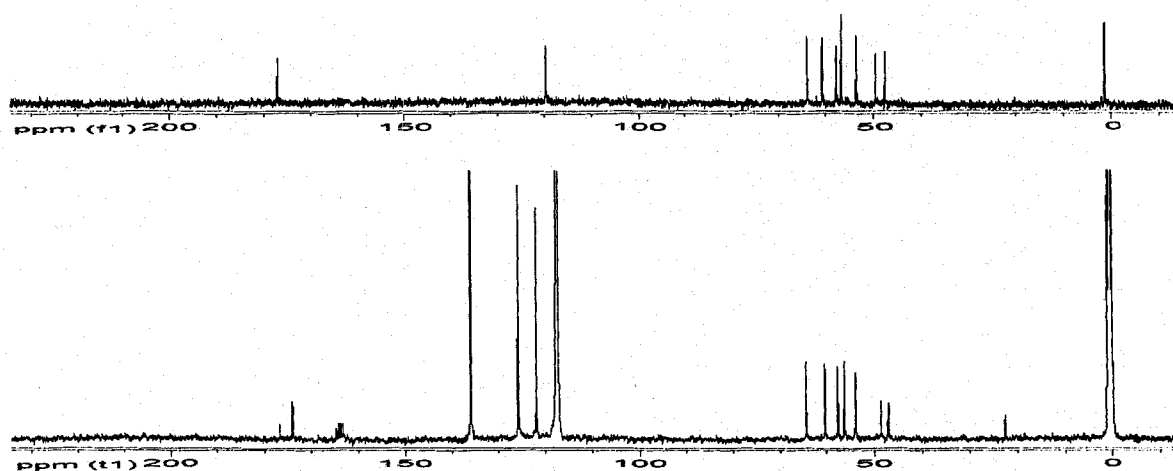


Figure 2.7 $^{13}\text{C}\{^1\text{H}\}$ NMR spectra comparison (a) $[\text{In-CB-DO2A}]\text{Cl}$ in D_2O (top); (b) $[\text{In-CB-DO2A} \cdot \text{NaOAc}]\text{BPh}_4$ in CD_3CN (bottom).

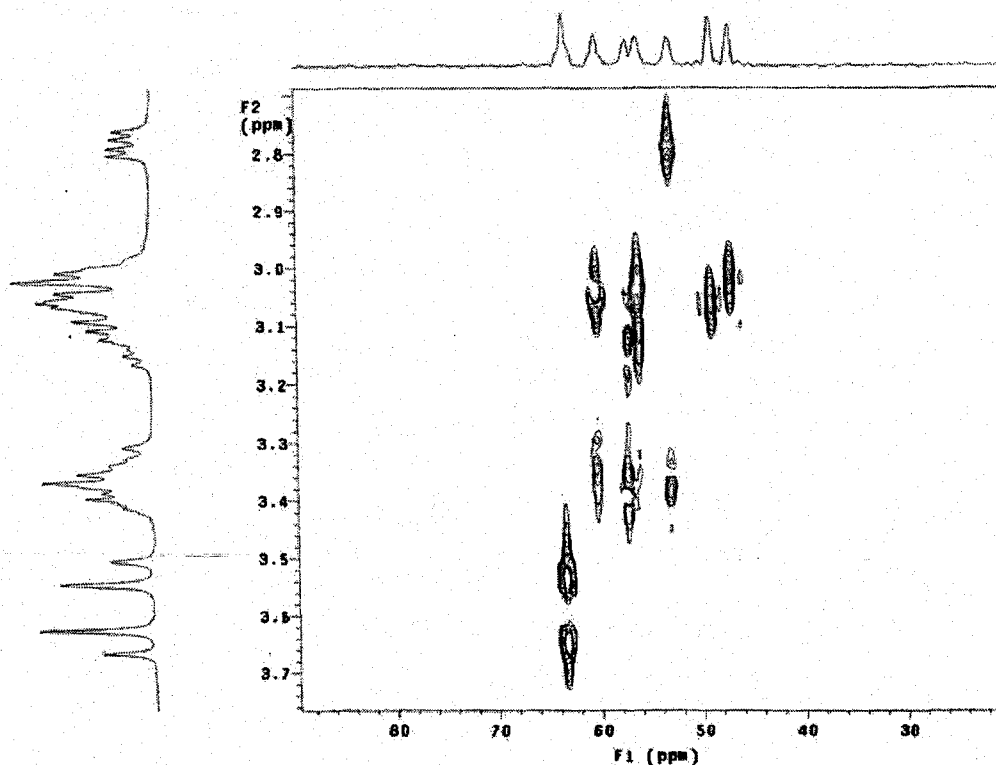


Figure 2.8 2D [^1H , ^{13}C] HMQC spectrum of “[In-CB-DO2A]Cl”.

2.7). In addition, the most downfield methylene resonance (δ 64.20) in its $^{13}\text{C}\{^1\text{H}\}$ NMR spectrum can be assigned to the methylene carbon of the acetate arm by a 2D [^1H , ^{13}C] HMQC spectrum (**Figure 2.8**). The acetate anion coordinated to the indium(III) ion center in the [In-CB-DO2A·NaOAc]BPh₄ is now absent, as confirmed by its ^1H and $^{13}\text{C}\{^1\text{H}\}$ NMR spectra in D₂O. Although its IR spectrum (**Figure 2.9**) showed that the two carboxylate pendant arms are fully protonated (ν_{COOH} :1726.8 (s) cm^{-1}), the AB pattern of the CH₂COO arms in the ^1H NMR is evidence that the arms remain coordinated to the indium(III) ion center, most likely through the carbonyl oxygens. Furthermore, the ESI-MS (positive mode) spectrum (**Figure 2.10**) of [In-CB-DO2A]Cl showed $m/z = 482.2$ for $\{[\text{In-CB-DO2A}]\text{Cl} + \text{Na}\}^+$ and $m/z = 427.2$ for $[\text{In-CB-DO2A}]^+$.

However, the yield is low (30-40%) and the CHN analyses showed the product to contain extra HCl as well as NaCl: $[\text{In-CB-DO2A}]\text{Cl}(\text{NaCl})_2(\text{HCl})_3$. Efforts to grow X-ray quality crystals were unsuccessful.

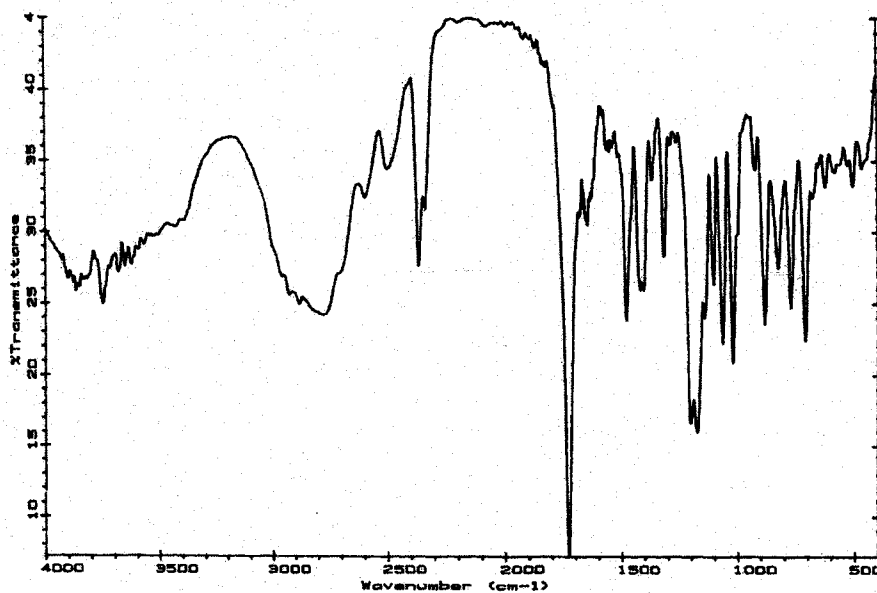


Figure 2.9 IR spectrum of “[In-CB-DO2A]Cl”.

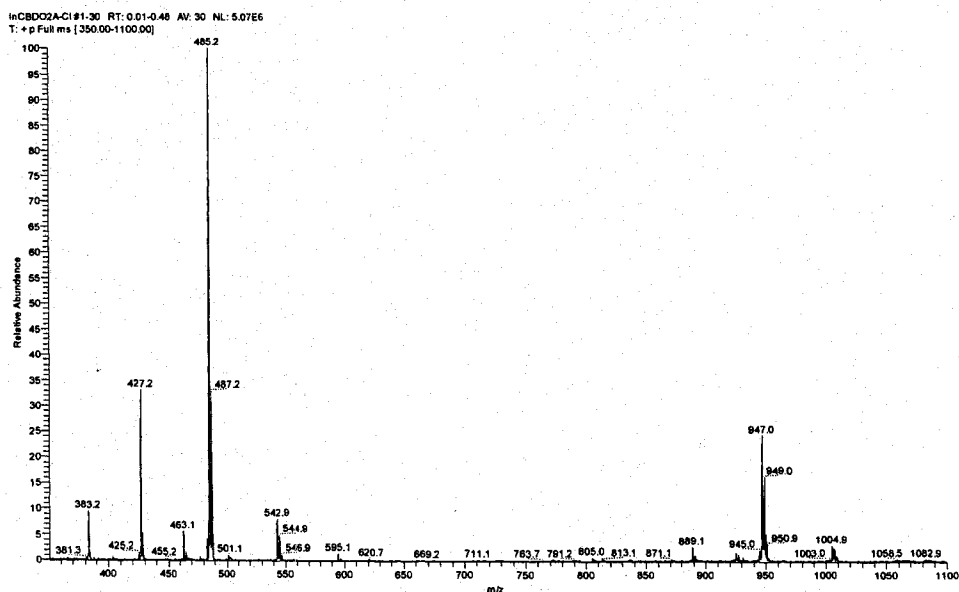
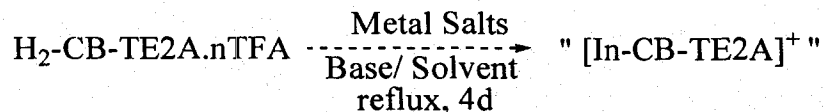


Figure 2.10 ESI-MS (positive mode) spectrum of “[In-CB-DO2A]Cl”.

In a third variation, several other counterions were tried to precipitate the [In-CB-DO2A · NaOAc]⁺ cation from methanol solution. These included NaClO₄, NaSCN, NH₄PF₆, KOC₆H₂(NO₂)₃ (potassium picrate), NaBF₄, and KI. Since none of these precipitated the cation [In-CB-DO2A · NaOAc]⁺, the solutions were left in the hood to evaporate slowly. However, no X-ray quality crystal ever formed.

Finally, since excess nitrate and acetate anions are present in the crude reaction mixture, the crude reaction solution was dissolved in water and passed through an anion exchange resin saturated with Cl⁻. The eluant was collected and evaporated to dryness. From its ¹H and ¹³C{¹H} NMR spectra in D₂O, no sodium acetate remained. Crystal growing was tried but again no X-ray quality crystals formed.

2.2.2 Attempted H₂-CB-TE2A.nTFA complexation of Ga(III) and In(III)



Base/Solvent: ① NaOH/H₂O
 ② NaOAc/MeOH, Na₂CO₃/MeOH, or Cs₂CO₃/EtOH
 ③ Cs₂CO₃/CH₃CN, NaH/THF, K₃PO₄/DMF, or
 Phosphazene Base P₂-t-Bu (pK_a = 30.25 in DMSO)^{44(a)}
 /THF

Several different reaction environments were tried including aqueous solution, protic and aprotic solvents with various bases. General procedures for these conditions were as follows.

① In order to reduce the number of protons on the protonated ligand in aqueous solution, enough aqueous sodium hydroxide was added to adjust the pH to 9 or even 12,

followed by addition of indium or gallium nitrate hydrate. After refluxing for 4 days, only protonated ligand was obtained, as shown by its ^1H and $^{13}\text{C}\{^1\text{H}\}$ NMR spectra.

② To a stirred solution of indium or gallium nitrate hydrate, or anhydrous indium bromide or gallium chloride in anhydrous alcoholic solvent (methanol or ethanol), an equivalent of $\text{H}_2\text{-CB-TE2A}\cdot n\text{TFA}$ in the same anhydrous alcoholic solvent was added in one portion. Excess sodium acetate, sodium carbonate, or cesium carbonate in anhydrous alcoholic solvent was then added into this solution. The reaction was refluxed 4 days and then centrifuged to remove the insolubles. The supernatant was evaporated to dryness. To compare the $^{13}\text{C}\{^1\text{H}\}$ NMR spectra, $\text{H}_2\text{-CB-TE2A}\cdot n\text{TFA}$ was dissolved in CD_3OD and then excess sodium acetate was added. Its $^{13}\text{C}\{^1\text{H}\}$ NMR spectrum showed almost the same signals as for the reaction mixture, indicating presence of protonated uncomplexed ligand only.

③ To the aprotic solvent suspension of the $\text{H}_2\text{-CB-TE2A}\cdot n\text{TFA}$ was added cesium carbonate, sodium hydride, potassium phosphate, or phosphazene base $\text{P}_2\text{-t-Bu}$ ($\text{pK}_a = 30.25$ in DMSO)^{44(a)} for deprotonation. A slight excess of anhydrous metal salt (GaCl_3 or InBr_3) in the aprotic solvent was then added to this mixture. After 4 days of refluxing and normal workup, there is only protonated ligand produced as confirmed by its ^1H and $^{13}\text{C}\{^1\text{H}\}$ NMR spectra.

All attempts at making Ga(III) and In(III) complexes of CB-TE2A have failed so far. There are some conclusions to be made from the above attempts. When higher pH was used to help deprotonate the ligand in aqueous solution in ①, since free hydrated Ga(III) is only stable under acidic conditions, it hydrolyzes nearly completely over a wide pH range forming with various hydroxide species as the pH is raised. It was previously

reported that insoluble $\text{Ga}(\text{OH})_3$ is the primary species between pH 3 ~ 9.5, whereas above pH 9.6, the soluble gallate ion ($\text{Ga}(\text{OH})_4^-$) forms.^{2,5} Most gallium complexes actually decompose to $\text{Ga}(\text{OH})_4^-$ at high pH. In(III) also hydrolyzes easily, forming insoluble hydroxides at pH > 3.4.

Carbonate is a not strong enough base to completely deprotonate $\text{H}_2\text{-CB-TE2A}$. The attempted complexation of anhydrous indium bromide with $\text{H}_2\text{-CB-TE2A.nTFA}$ by using cesium carbonate in absolute ethanol for several days yielded only oligomeric products from its ESI-MS spectrum (**Figure 2.11**) although its $^{13}\text{C}\{^1\text{H}\}$ NMR spectrum (**Figure 2.12**) looked promisingly simple.

When a stronger base than OH^- was used for deprotonation in ③, any moisture should be avoided due to the immediate precipitation of $\text{Ga}(\text{OH})_3$ and $\text{In}(\text{OH})_3$. Such moisture may be from the nitrogen atmosphere, glassware, sample preparation in the air, or cross-bridged ligands. Absolutely anhydrous conditions may be required to make this complex successfully.

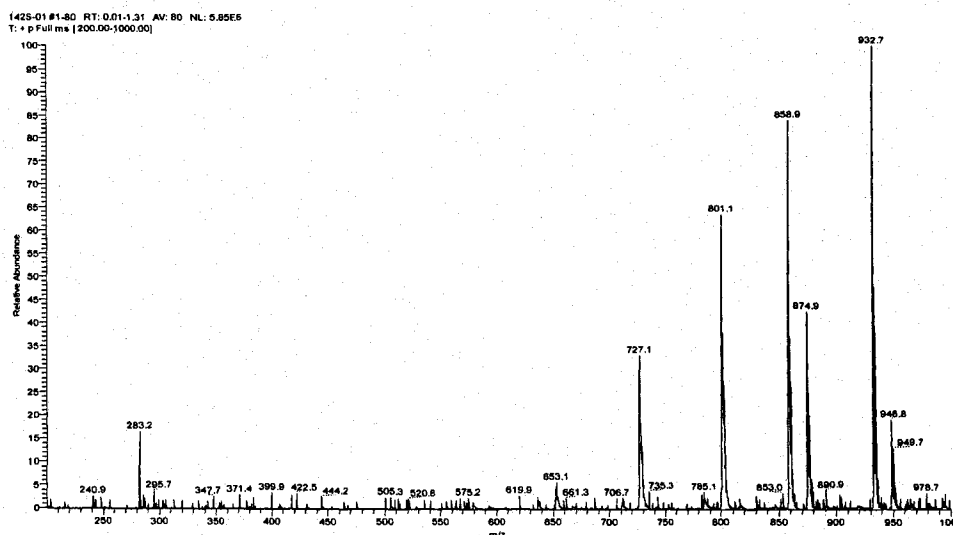


Figure 2.11 ESI-MS spectrum of crude product of attempted complexation in EtOH.

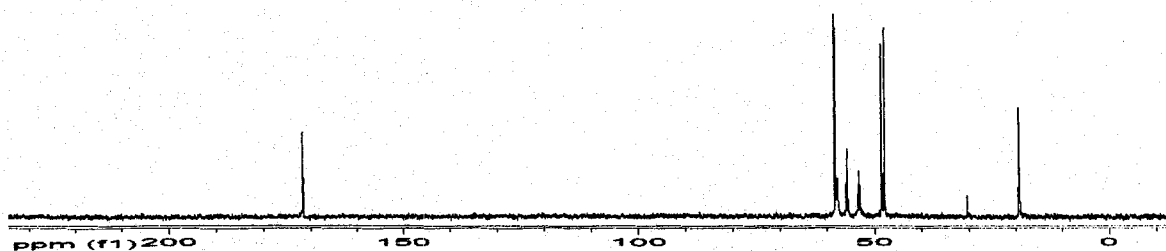


Figure 2.12 $^{13}\text{C}\{^1\text{H}\}$ NMR spectrum of crude product of attempted complexation in EtOH.

Indirect Routes

2.2.3 Attempted In(III) Complexation with $^t\text{Bu}_2\text{-CB-TE2A}$

To avoid protonated ligand formation from residual TFA used in deprotection, the diester tert-Bu₂-CB-TE2A was used to complex the indium cation first. Afterwards, the tert-butyl groups may be deprotected by excess TFA. $^t\text{Bu}_2\text{-CB-TE2A}$ was therefore reacted with 1 equiv of indium bromide in the anhydrous aprotic solvent acetonitrile or toluene by 4 days of refluxing. From the IR spectrum (**Figure 2.13**) of the precipitated product, the carbonyl stretching region showed two bands: 1625 cm⁻¹ (major band), and 1736.7 cm⁻¹, suggesting that some of the ^tBu -ester had been deprotected, most likely by the strongly Lewis acid In³⁺. There are some examples in the literature for ester deprotection using TiCl₄, AlBr₃, BCl₃, and SnCl₄ Lewis acids.^{44(b,c)} Furthermore, the $^{13}\text{C}\{^1\text{H}\}$ NMR spectrum of the precipitate in D₂O showed almost the same resonance with that of the protonated H₂-CB-TE2A · nTFA (**Figure 2.14**). Silver nitrate in H₂O was used to precipitate silver bromide from the precipitate product in H₂O, suggesting the presence of bromide anions contained in this precipitate mixture.

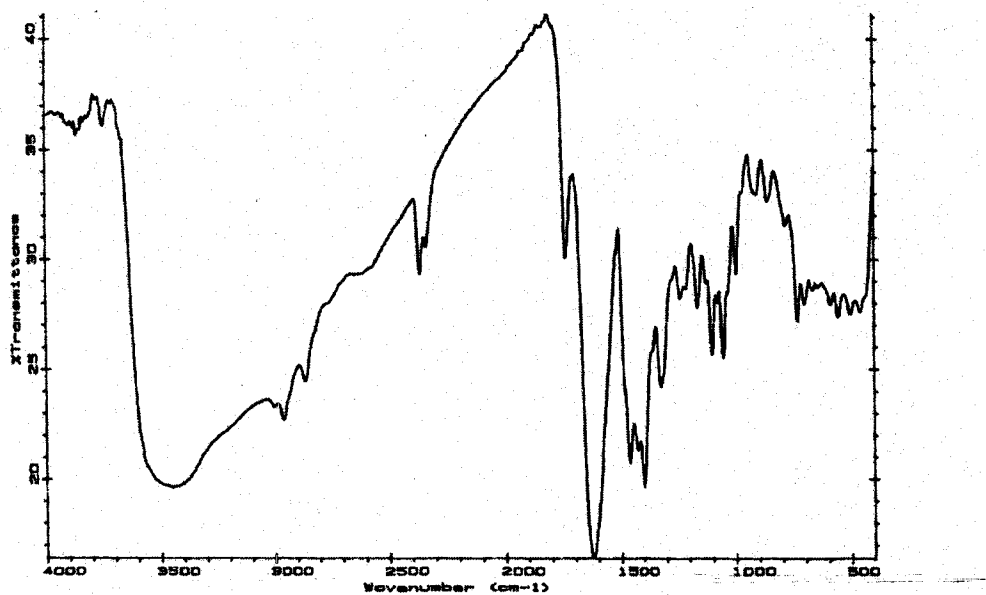


Figure 2.13 IR spectrum of precipitated product of attempted In(III) complexation of $t\text{Bu}_2\text{-CB-TE2A}$.

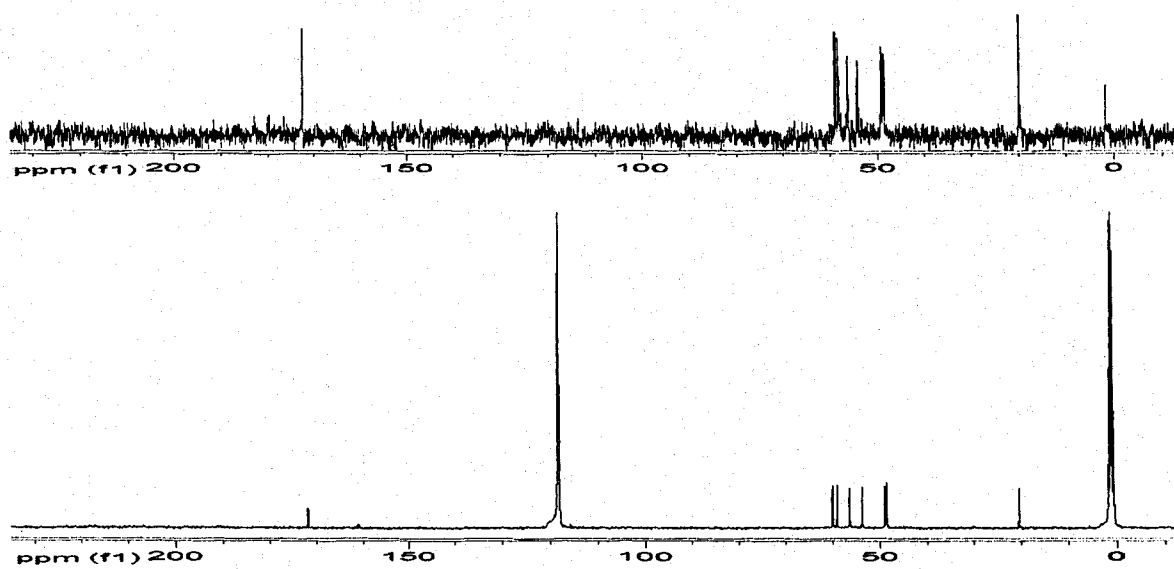
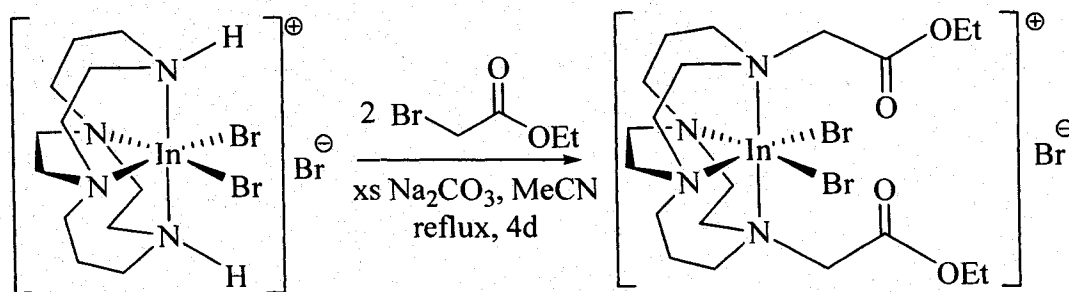


Figure 2.14 $^{13}\text{C}\{^1\text{H}\}$ NMR spectra comparison (a) precipitated product in D_2O (top); (b) protonated $\text{H}_2\text{-CB-TE2A.nTFA}$ in CD_3CN (bottom).

2.2.4 Arming (alkylation) of [InBr₂-CB-Cyclam]Br



[InBr₂-CB-Cyclam]Br and [GaBr₂-CB-Cyclam]Br were first synthesized by Niu and their NH/ND exchanges were observed in D₂O or CD₃OD,³⁶ suggesting these protons are acidic enough to exchange with deuteriums in solution. In addition, because free trivalent indium or gallium ion is more likely to precipitate out of solution than their complexes, the idea here is to use [InBr₂-CB-Cyclam]Br or [GaBr₂-CB-Cyclam]Br as the precursor for arming by alkylation.

Early attempts were performed in basic aqueous solution (2 equiv. NaOH) by using sodium bromoacetate (2 equiv.) as the alkylating agent, (sodium bromoacetate was prepared as described previously),⁴⁵ with [InBr₂-CB-Cyclam]Br. After 4 days of refluxing, the evidence from the crude product ¹H NMR (a singlet for the CH₂COO) in D₂O and ESI-MS spectrum showed no armed product. Instead, HOCH₂COOH (glycolic acid) was produced during this reaction as confirmed by its ¹H and ¹³C{¹H} NMR data.⁴⁶ Clearly, sodium bromoacetate is not very stable to hydrolysis and it may even oligomerize in aqueous solution under reflux.⁴⁷

An alternative way was tried using excess ethyl bromoacetate as the alkylating agent (excess alkylating agent was used to improve the yield) and excess sodium

carbonate as the base were added into an anhydrous MeCN solution of [InBr₂-CB-Cyclam]Br. This cloudy mixture was stirred at reflux under nitrogen. After 4 days, the insoluble sodium carbonate was centrifuged and the supernatant was decanted off and evaporated to dryness to give the crude product after washing out excess alkylating agent (ethyl bromoacetate) with diethyl ether to give an off-white solid (77 % yield).

This complex has been characterized by elemental analysis, IR, ESI-MS, ¹H and ¹³C{¹H} NMR methods. Instead of the singlet proton NMR resonance of the methylene protons of the alkylating agent ethyl bromoacetate, an AX pattern for the CH₂COOEt arms was found in CD₃CN (**Figure 2.15**). This confirmed that the CH₂COOEt arms have been successfully attached to the [InBr₂-CB-Cyclam]Br complex. From its ¹H NMR spectrum, a doublet of multiplets of the most upfield resonance (δ 1.76-1.84) can be assigned to the equatorial protons of the β-methylene in the six-membered chelate ring (β-CHH_{eq}), whereas the second-most upfield resonance (δ 2.28-2.42) belongs to the axial protons (β-CHH_{ax}). The resonances of the AX pattern (δ 4.32 and 3.81, J = 17.44 Hz) of the CH₂COOEt arms for [InBr₂-Et₂-CB-TE2A]Br are farther apart compared to those (AB, δ 3.08 and 3.20, J = 16.7 Hz) for the ligand Et₂-CB-TE2A.³³ As expected for C₂ symmetry, there are ten resonances in its ¹³C{¹H} NMR spectrum (**Figure 2.16**): δ 168.46, 62.24 (OCH₂CH₃), 60.04, 57.74 (CH₂COO), 56.22, 54.91, 49.50, 46.70, 23.79 (CH₂CH₂CH₂), 14.41 (OCH₂CH₃). The assignments for δ 62.24, 57.74, 23.79 and 14.41 signals were deduced from its 2D [¹H, ¹³C] HMQC spectrum (**Figure 2.17**)

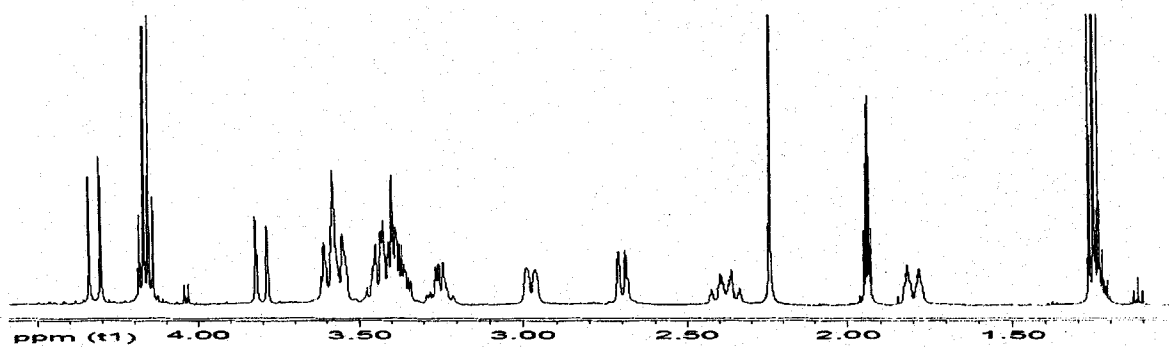


Figure 2.15 ^1H NMR spectrum of $[\text{InBr}_2\text{-Et}_2\text{-CB-TE2A}]\text{Br}$ in CD_3CN .

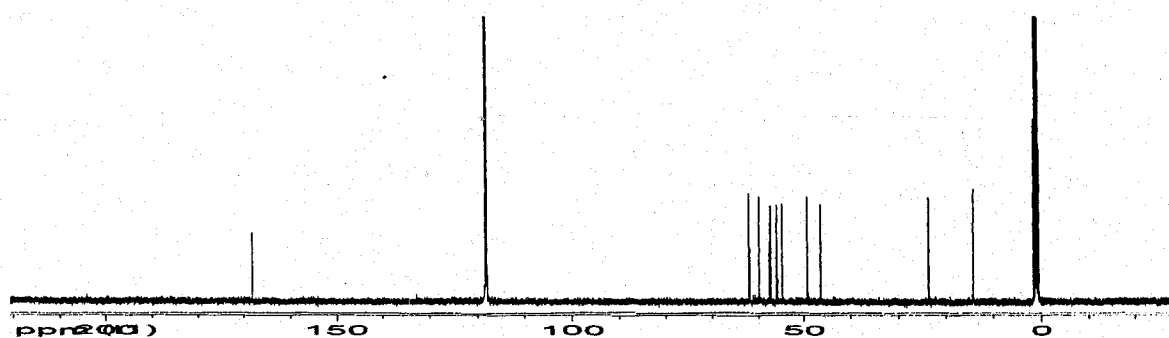


Figure 2.16 $^{13}\text{C}\{^1\text{H}\}$ NMR spectrum of $[\text{InBr}_2\text{-Et}_2\text{-CB-TE2A}]\text{Br}$ in CD_3CN .

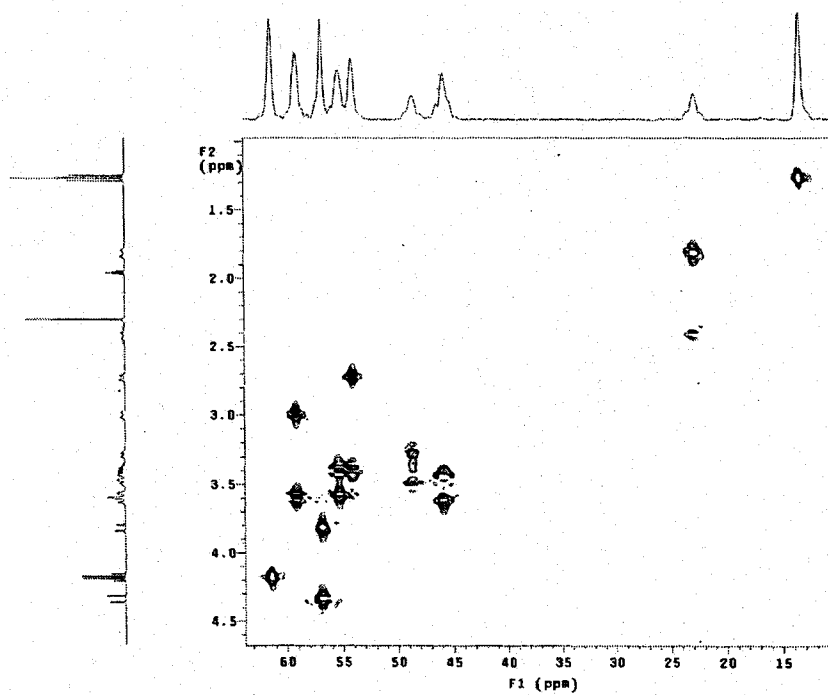


Figure 2.17 2D $[^1\text{H}, ^{13}\text{C}]$ HMQC spectrum of $[\text{InBr}_2\text{-Et}_2\text{-CB-TE2A}]\text{Br}$

The ESI-MS (positive mode) spectrum (**Figure 2.18**) of $[\text{InBr}_2\text{-Et}_2\text{-CB-TE2A}]\text{Br}$ showed a molecular ion at $m/z = 673.2$ for $[\text{InBr}_2\text{-Et}_2\text{-CB-TE2A}]^+$. The IR spectrum (**Figure 2.19**) of $[\text{InBr}_2\text{-Et}_2\text{-CB-TE2A}]\text{Br}$ showed a strong band at 1740 cm^{-1} due to the uncoordinated ethyl ester carbonyl groups, and a strong and broad band at 3450 cm^{-1} due to waters of crystallization. The elemental analysis data are completely consistent with the proposed formula $[\text{InBr}_2\text{-Et}_2\text{-CB-TE2A}]\text{Br}\cdot\text{H}_2\text{O}$ whose structure has been confirmed by a low-quality X-ray structure (**Figure 2.20**).

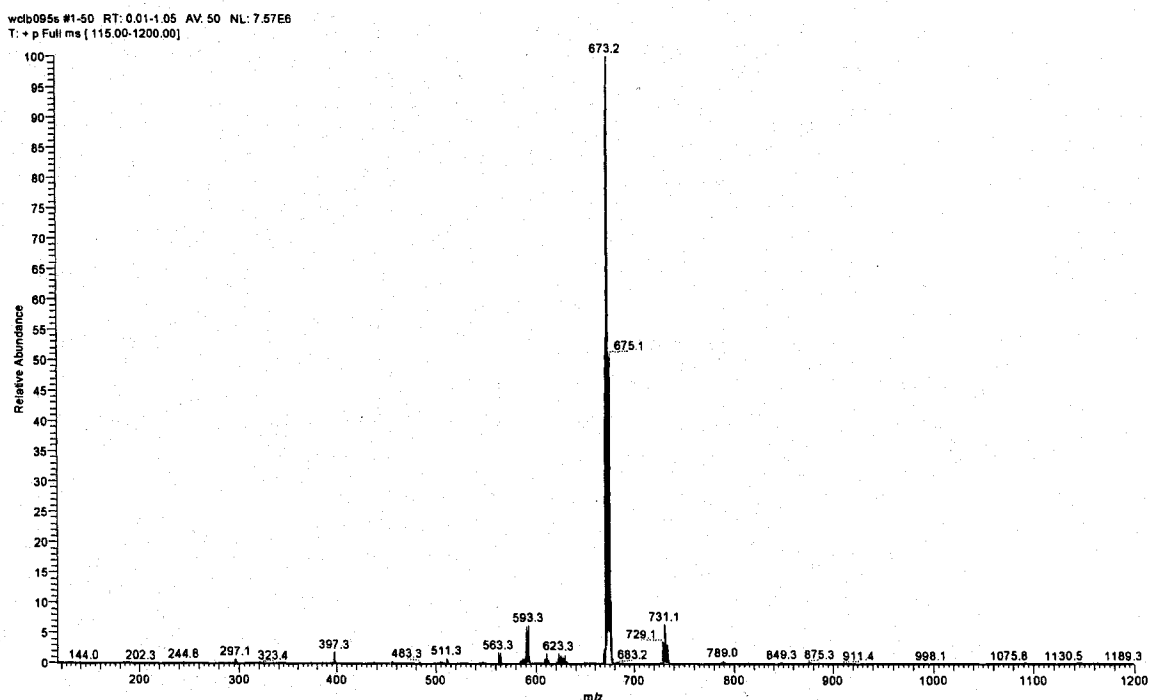


Figure 2.18 ESI-MS (positive mode) spectrum of $[\text{InBr}_2\text{-Et}_2\text{-CB-TE2A}]\text{Br}$.

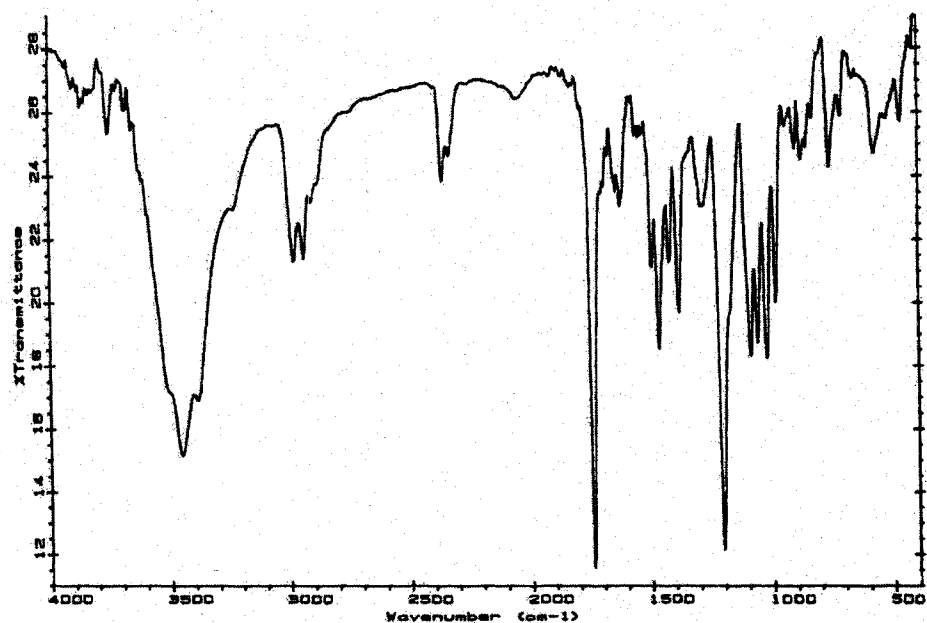


Figure 2.19 IR spectrum of $[\text{InBr}_2\text{-Et}_2\text{-CB-TE2A}]\text{Br}\cdot\text{H}_2\text{O}$.

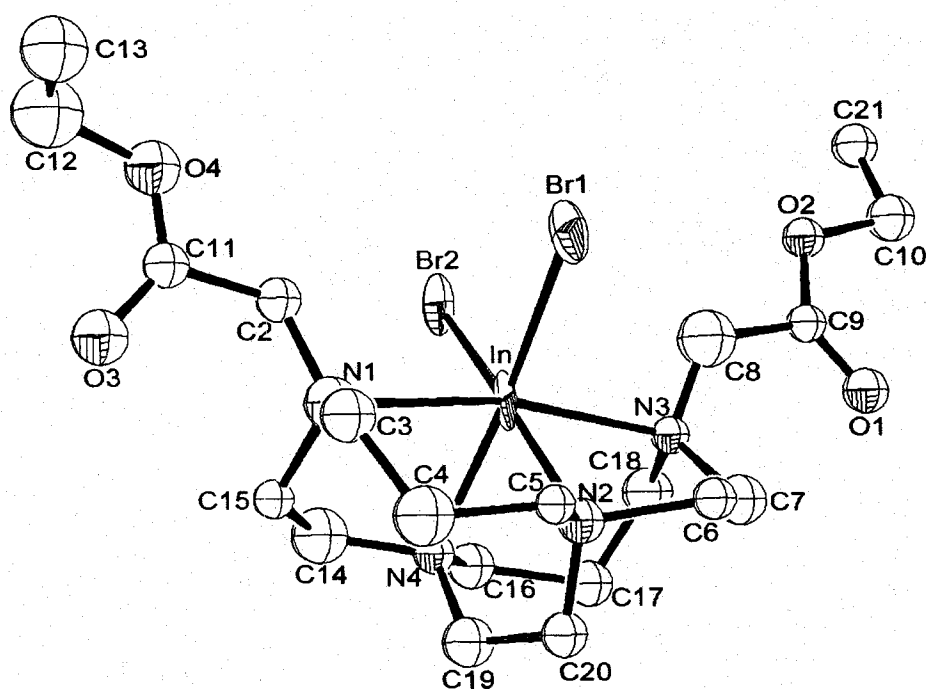


Figure 2.20 ORTEP drawing of $[\text{InBr}_2\text{-Et}_2\text{-CB-TE2A}]\text{Br}\cdot\text{H}_2\text{O}$ (ellipsoids are at 50% probability). Water molecules, uncoordinated bromide and hydrogen atoms are omitted for clarity. Selected bond distances (Å) and bond angles (deg): In-N2 2.22(3), In-N4 2.31(3), In-N3 2.39(2), In-N1 2.41(3), In-Br1 2.565(5), In-Br2 2.598(5), N1-In-N3 167.5(9), N2-In-N4 77.8(10).

The X-ray structure (**Figure 2.20**) of the $[\text{InBr}_2\text{-Et}_2\text{-CB-TE2A}]\text{Br}$ complex confirmed that two CH_2COOEt arms are indeed attached to the precursor $[\text{InBr}_2\text{-CB-Cyclam}]\text{Br}$ complex. It has a distorted octahedral coordination geometry with an axial N1-In-N3 bond angle of $167.5(9)^\circ$ and equatorial N2-In-N4 angle of $77.8(10)^\circ$, which are similar to its precursor $[\text{InBr}_2\text{-CB-Cyclam}]\text{Br}$ data ($164.29(12)^\circ$ and $78.89(9)^\circ$ respectively).³⁶ The equatorial In-N bonds are slightly shorter ($2.22(3)$ and $2.31(3)$ Å) than the axial ones ($2.39(2)$ and $2.41(3)$ Å). In addition, the two In-Br bond lengths are $2.565(5)$ and $2.598(5)$ Å, which are similar to those for $[\text{InBr}_2\text{-CB-Cyclam}]\text{Br}$ ($2.5806(4)$ and $2.6079(4)$ Å).

2.2.5 Synthesis of “[In-CB-TE2A]Br”

Synthesis of $[\text{In-CB-TE2A}]\text{Br}$ from $[\text{InBr}_2\text{-Et}_2\text{-CB-TE2A}]\text{Br}$ was straightforward. Two equivalents of aqueous sodium hydroxide solution (1.0441 N) was added to hydrolyze the two ethyl acetate arms (CH_2COOEt) of the complex $[\text{InBr}_2\text{-Et}_2\text{-CB-TE2A}]\text{Br}$. After 24 hours of refluxing, this clear aqueous solution was evaporated to dryness to give an off-white crude product. This has been characterized by IR, ESI-MS, and ^1H and $^{13}\text{C}\{^1\text{H}\}$ NMR methods. From the major peak ($m/z = 455.3$) of the compound's ESI-MS (positive mode) mass spectrum (**Figure 2.21**), $[\text{In-CB-TE2A}]^+$ exists as an entity consistent with no bromide attached to the indium (III) ion center, and the two ethyl acetate arms had indeed hydrolyzed to give coordinated carboxylates. The IR spectrum (**Figure 2.22**) of $[\text{In-CB-TE2A}]\text{Br}$ shows strong asymmetric carboxylate bands at 1643.9 and 1627.0 cm^{-1} .

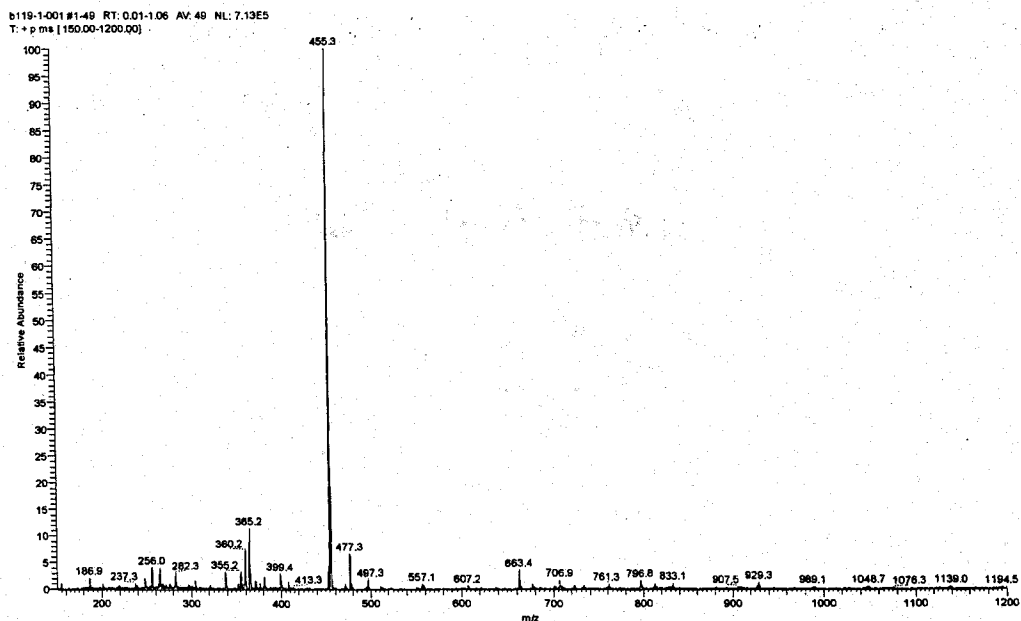


Figure 2.21 ESI-MS (positive mode) spectrum of $[\text{InBr}_2\text{-CB-TE2A}]\text{Br}$.

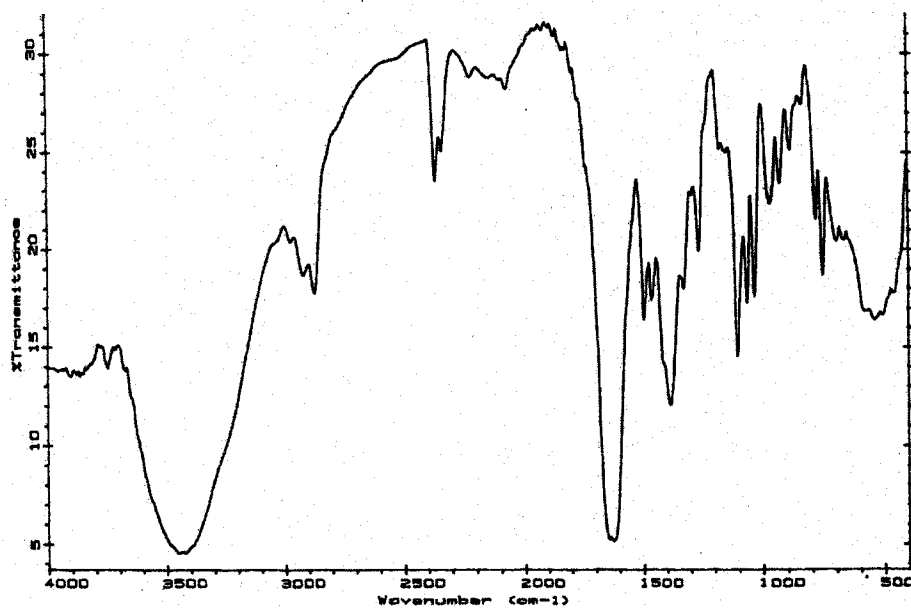


Figure 2.22 IR spectrum of $[\text{In-CB-TE2A}]\text{Br}$.

The ^1H (Figure 2.23) and $^{13}\text{C}\{^1\text{H}\}$ (Figure 2.24(a)) NMR spectra in D_2O are dynamically broadened, suggesting that $[\text{In-CB-TE2A}]^+$ is fluxional in solution at room

temperature most likely due to a dynamic equilibrium involving carboxylate arms/solvent exchange in D₂O (Figure 2.25). This dynamic process is relatively slow on the NMR time scale leading to broadened signals. To further investigate this, variable temperature ¹H and ¹³C{¹H} NMR spectral studies were carried out. Three deuterated NMR solvents (D₂O, CD₃CN, CD₃OD) were used to perform variable-temperature studies.

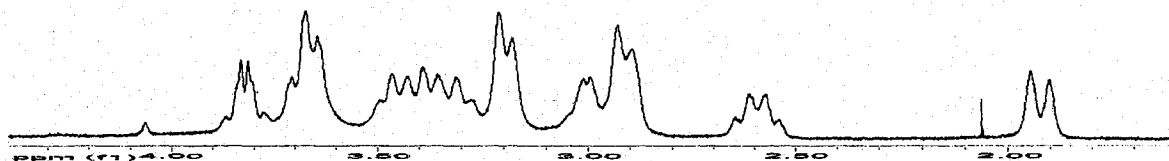


Figure 2.23 ¹H NMR spectrum of [In-CB-TE2A]Br in D₂O.

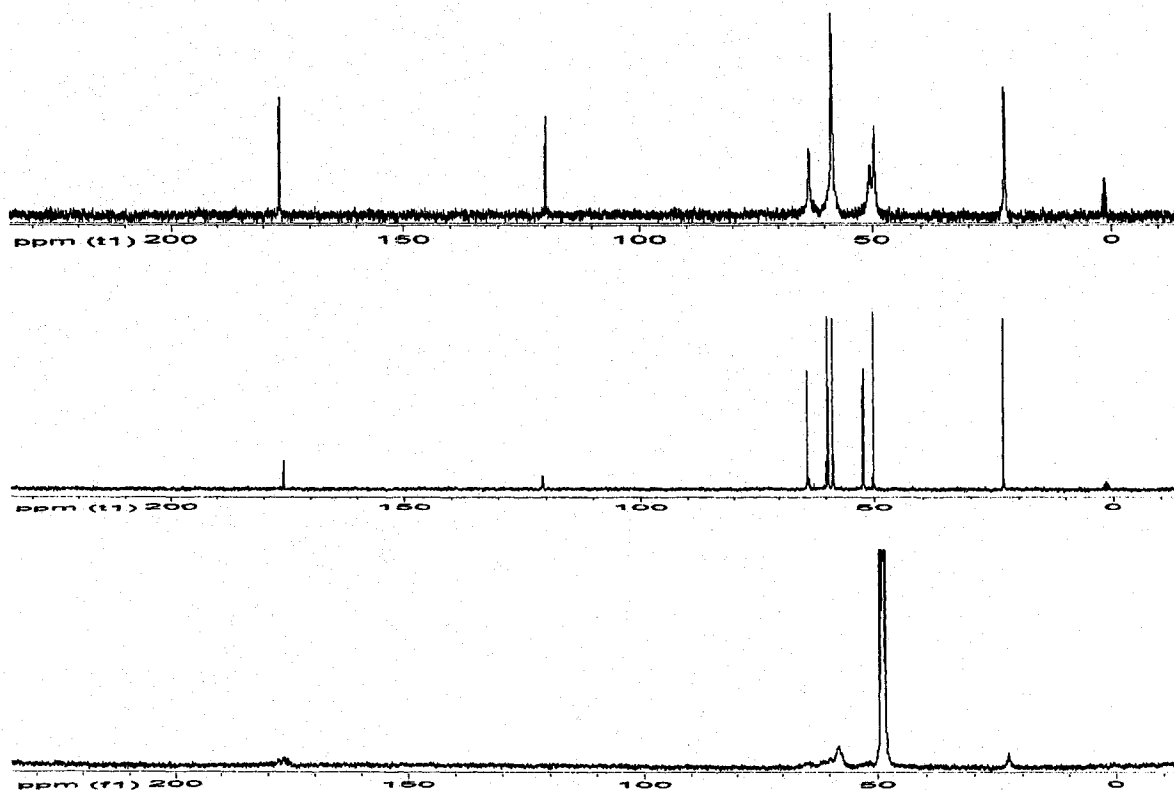


Figure 2.24 Variable temperature ¹³C{¹H} NMR spectra of [In-CB-TE2A]Br at (a) 25 °C in D₂O (top); (b) 85 °C in D₂O (middle); (c) -80 °C in CD₃OD (bottom).

As the temperature was increased to 85 °C in D₂O from room temperature all resonances in the aliphatic region sharpened (**Figure 2.24(b)**), suggesting a faster dynamic exchange process on the NMR timescale consistent with time-averaged C₂ symmetry showing 8 resonances.

Low-temperature NMR experiments can be used to slow down this process. Two low-temperature NMR experiments were performed. Addition of a saturated methanol solution of sodium tetraphenylborate to the crude product in methanol precipitated a white solid, assumed to be “[In-CB-TE2A]BPh₄”. This was dissolved in CD₃CN. The other experiment used the crude [In-CB-TE2A]⁺ in CD₃OD. Low temperatures of -49°C in CD₃CN and -80°C for CD₃OD (**Figure 2.24(c)**) were reached. However, we were not able to reach the slow-exchange limit as only broadened ¹H and ¹³C{¹H} NMR spectra were observed. This suggested that the slow exchange limit was not reached even at -80°C in CD₃OD. Further investigation was curtailed because of the low-temperature limitation (-80°C) of the Varian NMR instrument.

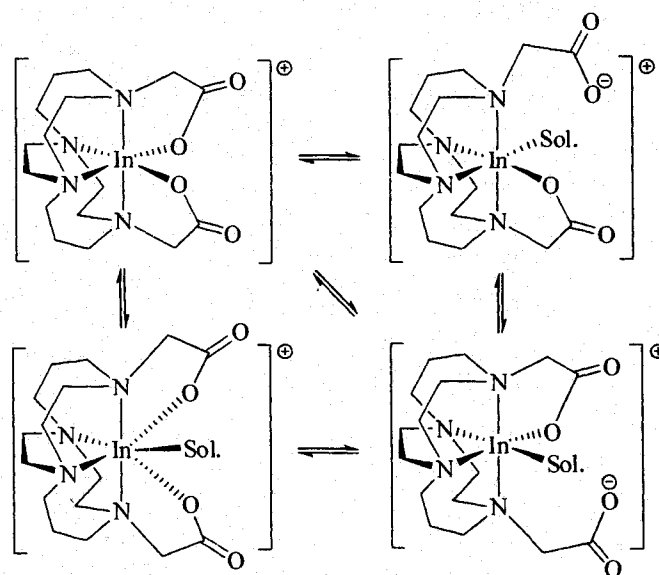


Figure 2.25 A possible dynamic process of [In-CB-TE2A]⁺. (Sol. = solvent)

Attempts to grow X-ray quality crystals were made by exchanging the counterion of the crude product $[\text{In-CB-TE2A}]\text{Br}$. A saturated methanol solution of sodium tetraphenylborate was used to precipitate $[\text{In-CB-TE2A}]^+$ from methanol. The CHN analyses, however, did not confirm the expected formula of $[\text{In-CB-TE2A}]\text{BPh}_4$, showing a mixture containing excess tetraphenylborate anions for each cation part instead. $[\text{In-CB-TE2A}]\text{ClO}_4$ was precipitated from ethanol solution of the crude product with sodium perchlorate. Diethyl ether diffusion was used to grow crystals in CH_3CN . No precipitate was formed from methanol solutions of the crude product with either NH_4PF_6 or potassium picrate, so these solutions were left for slow evaporation. In addition, 0.1 M and 1 M perchloric acid solutions of the product were similarly used for crystal growing. Unfortunately, none of these methods gave X-ray quality crystals.

2.2.6 Attempted Synthesis of the Gallium (III) Complex of CB-TE2A (Attempted alkylation of $[\text{GaBr}_2\text{-CB-Cyclam}]\text{Br}$)

Since $[\text{InBr}_2\text{-Et}_2\text{-CB-TE2A}]\text{Br}$ was successfully made by using $[\text{InBr}_2\text{-CB-Cyclam}]\text{Br}$ as the precursor, the same synthetic method was carried out for the Ga analogue. Excess ethyl bromoacetate as the alkylating agent and excess sodium carbonate as the base were added to an anhydrous MeCN solution of $[\text{GaBr}_2\text{-CB-Cyclam}]\text{Br}$, which showed poor solubility in CH_3CN . This cloudy mixture was stirred with reflux under nitrogen. After 4 days, the insoluble solid was centrifuged off and the clear supernatant was separated and evaporated to dryness to give the crude product. Washing out the excess ethyl bromoacetate in the crude product with diethyl ether gave an off-white solid residue. Unlike the well-resolved ^1H and $^{13}\text{C}\{^1\text{H}\}$ NMR spectra for the $[\text{InBr}_2\text{-CB-}$

Cyclam]Br alkylation reaction described above, these ^1H , $^{13}\text{C}\{^1\text{H}\}$ NMR, and ESI-MS spectra, however, showed mixtures including the starting material $[\text{GaBr}_2\text{-CB-Cyclam}]\text{Br}$. In order to improve the precursor Ga complex's solubility problem, more solvent, ethyl bromoacetate, and sodium carbonate were used. Reaction time was extended to 14 days of refluxing. After the same workup procedure as before, ^1H , $^{13}\text{C}\{^1\text{H}\}$ NMR, and ESI-MS spectra still showed a complicated mixture. The ESI-MS (positive mode) spectrum (Figure 2.26) of this solid product showed several species but not the target product $[\text{GaBr}_2\text{-Et}_2\text{-CB-TE2A}]^+$. Some proposed species were suggested and the isotope patterns simulated for these peaks (Figure 2.27).⁴⁸

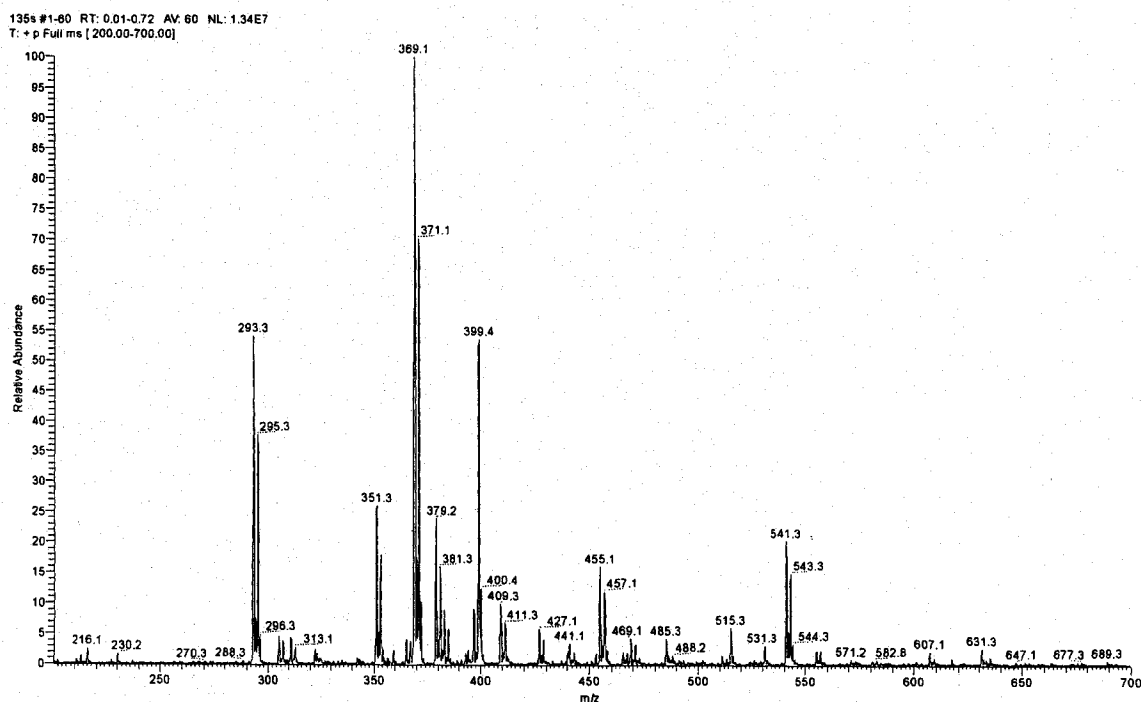


Figure 2.26 ESI-MS (positive mode) spectrum of the supernatant for the preparation of $[\text{GaBr}_2\text{-Et}_2\text{-CB-TE2A}]^+$.

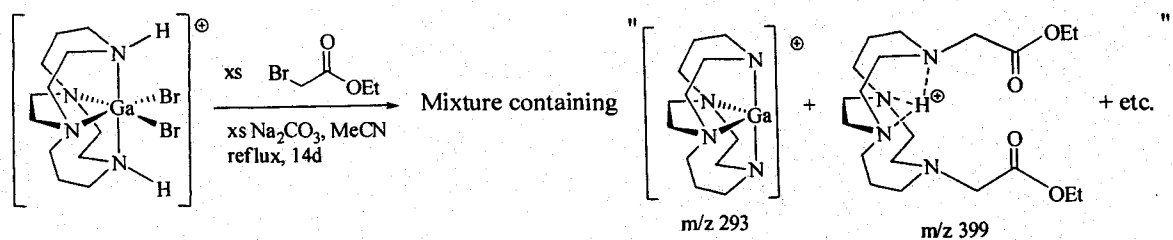


Figure 2.27 Proposed products based on the ESI-MS spectrum.

There are several possible explanations for this failure to alkylate. While the high positive charge and small size for gallium (III) should render the N-H protons on the $[\text{GaBr}_2\text{-CB-Cyclam}]\text{Br}$ more acidic than those on the corresponding indium (III) complex, the resulting nitrogen lone pairs of the deprotonated gallium complex should be less nucleophilic. In addition, there are two large bromide anions attached to the small gallium and their steric hindrance may also prevent a facile alkylation process. Furthermore, poor solubility of the $[\text{GaBr}_2\text{-CB-Cyclam}]\text{Br}$ complex and heterogeneous nature of sodium carbonate in CH_3CN probably made the alkylation even slower.

In order to test how acidic the N-H protons in $[\text{GaBr}_2\text{-CB-Cyclam}]\text{Br}$ are, sodium carbonate (6 equiv.) and sodium acetate (20 equiv.) were used as base respectively. From the extent of NH/ND exchange in the ^1H NMR spectra (**Figure 2.28**) in D_2O , 6 equivalents of sodium carbonate were sufficient to exchange $[\text{GaBr}_2\text{-CB-Cyclam}]\text{Br}$ in 5 minutes while even 20 equivalents of sodium acetate were not. Therefore, the 10 equiv. sodium carbonate actually used for the alkylation reaction should be enough to exchange it. From the $m/z = 293.3$ peak of the ESI-MS spectrum (**Figure 2.26**), $[(\text{Ga-CB-Cyclam})\text{-}2\text{H}]^+$ did appear to be present in the reaction mixture.

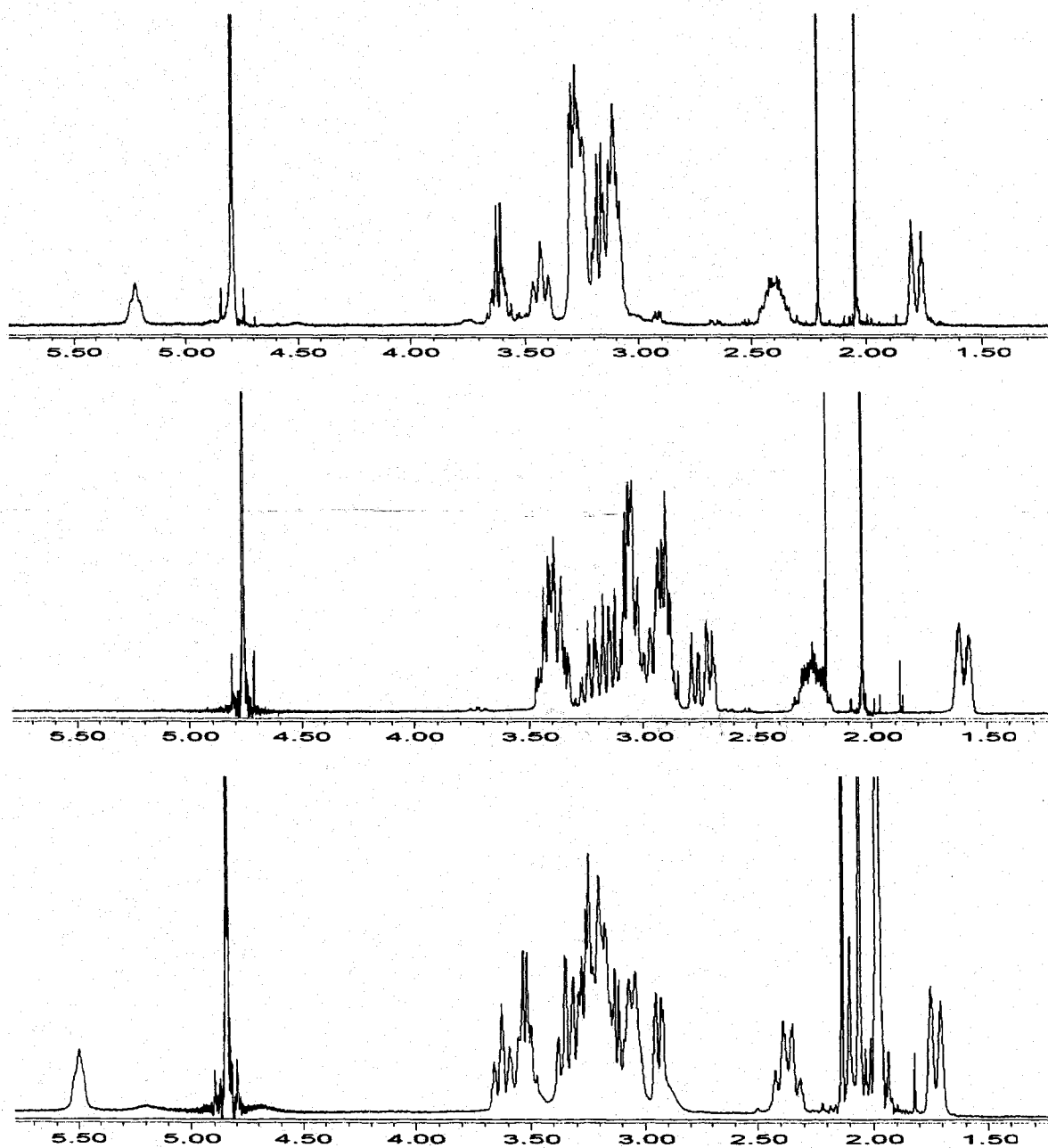


Figure 2.28 ^1H NMR spectra of NH/ND exchange of $[\text{GaBr}_2\text{-CB-Cyclam}]\text{Br}$ in D_2O : (a) complex only (top); (b) complex + 6 eqv. sodium carbonate (middle); (c) complex + 20 eqv. sodium acetate (bottom).

Although several attempts to make $[\text{GaBr}_2\text{-Et}_2\text{-CB-TE2A}]\text{Br}$ were failed, the successful preparation of $[\text{InBr}_2\text{-Et}_2\text{-CB-TE2A}]\text{Br}$ suggests that if the right aprotic

solvent or solvent mixture can be found to improve the solubility of [GaBr₂-CB-Cyclam]Br, it may eventually be possible to synthesize [GaBr₂-Et₂-CB-TE2A]Br. In addition, microwave irradiation is a promising future procedure to use to overcome this solubility problem and the heterogeneous nature of this synthesis.

2.2.7 Attempted In(III) Complexation of Dibenzo Annelated Cross-Bridged Cyclam

New C₂-symmetric dibenzo annelated cross-bridged cyclams have been synthesized first by Jeffery Condon.⁴² An improved synthetic procedure was attained by David Martin. It is believed that these compounds will have decreased basicity compared to corresponding cross-bridged cyclams. Because copper(II) complexes of dibenzo annelated cross-bridged cyclams were successfully prepared from refluxing methanol solution, similar conditions were used here. To a suspension of N,N'-dimethyl dibenzo cross-bridged cyclam (supplied by David Martin) in anhydrous methanol, one equivalent of indium bromide in anhydrous methanol was added. After 4 days of refluxing, a small amount of insoluble solid was centrifuged off, and the supernatant was separated and evaporated to dryness. The ¹H NMR spectrum (**Figure 2.29(a)**) of the crude product in D₂O showed only broadened peaks, suggesting a dynamic process for the product. However, there are several small broad signals around δ 10-13 (**Figure 2.29(b)**) in CD₃CN likely due to N-H protons of a protonated ligand. This was confirmed by its ESI-MS spectrum. X-ray quality crystals of this protonated ligand were obtained by diffusion of diethyl ether into the crude product in methanol.

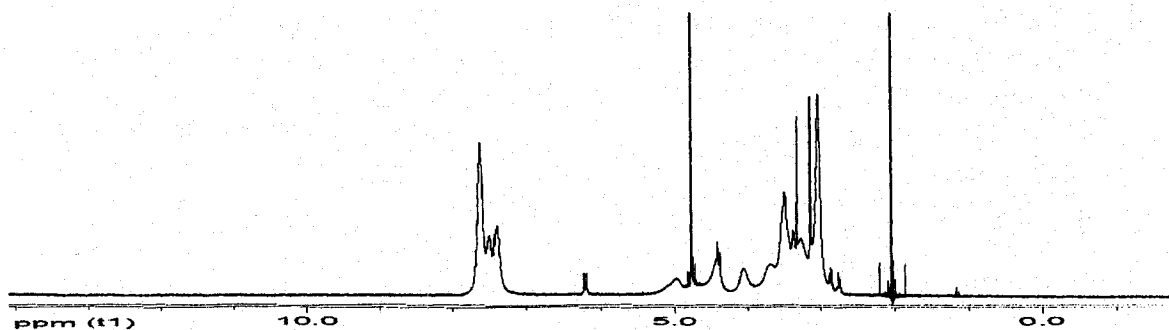


Figure 2.29 (a) ^1H NMR spectrum of protonated dibenzo annelated dimethyl CB-Cyclam in D_2O .

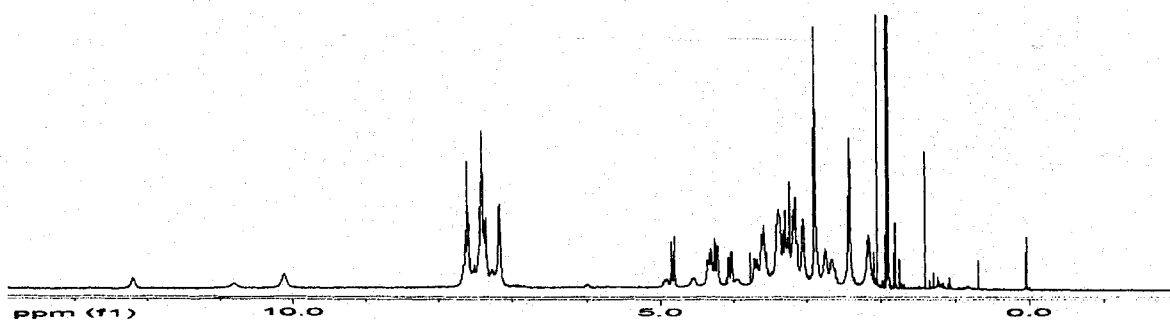


Figure 2.29 (b) ^1H NMR spectrum of protonated dibenzo annelated dimethyl CB-Cyclam in CD_3CN .

The crystal structure (**Figure 2.30**) obtained shows a mono-protonated ligand with an indium tetrabromide anion: $[\text{H-Me}_2\text{-Bz}_2\text{-CB-Cyclam}]^+[\text{InBr}_4]^-$. All four nitrogen lone pairs are convergent upon the ligand cleft and the two amino pairs are pointed directly at one another. The protonation hydrogen was not located in the crystal structure; however, according to the bond angle data, the proton is most likely located between N2 and N4 due to their nearly tetrahedral angles.

Because of the proton-sponge character of the cross-bridged ligands, the presence of any moisture or acidic proton sources easily results in the formation of undesired protonated ligands. Early attempts at Ga(III) or In(III) complexations of cross-bridged

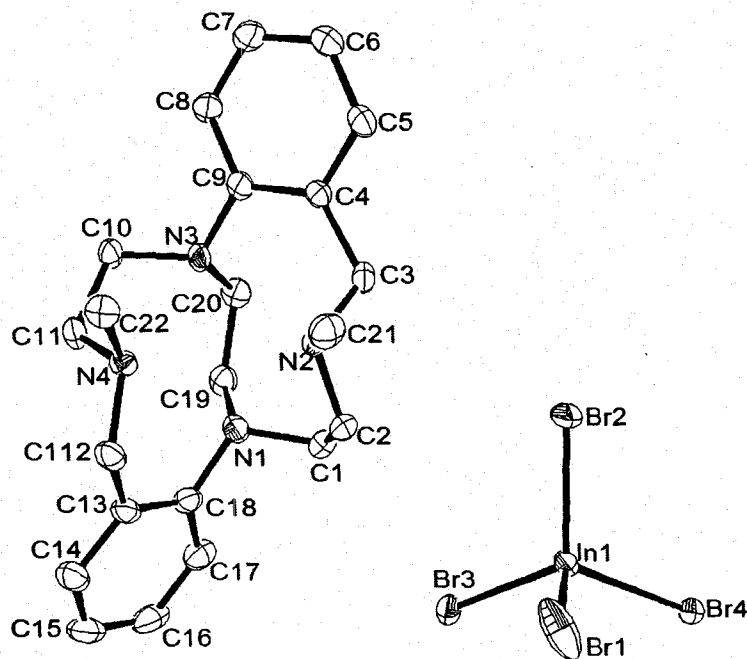


Figure 2.30 ORTEP drawing of $[\text{H-Me}_2\text{-Bz}_2\text{-CB-Cyclam}][\text{InBr}_4]$ (ellipsoids are at 50% probability). Hydrogen atoms are omitted for clarity. Selected bond angles (deg): C18–N1–C1 113.5(5), C18–N1–C19 112.3(4), C1–N1–C19 114.4(5), C21–N2–C2 109.9(4), C21–N2–C3 108.4(4), C2–N2–C3 110.7(4), C9–N3–C10 115.4(5), C9–N3–C20 114.7(5), C10–N3–C20 114.8(5), C22–N4–C11 113.0(5), C22–N4–C112 107.2(5), C11–N4–C112 108.5(5).

ligands indeed yielded a mixture of complex and protonated ligand when using metal hydrate salts or reactions in protic solvent.⁴³ This was overcome by using anhydrous metal salts in anhydrous aprotic solvent to successfully make $[\text{GaCl}_2\text{-CB-Cyclam}]\text{Cl}$, $[\text{GaCl}_2\text{-CB-Cyclen}]\text{Cl}$, $[\text{InBr}_2\text{-CB-Cyclam}]\text{Br}$, and $[\text{InBr}_2\text{-CB-Cyclen}]\text{Br}$.³⁶ However, several trials here using anhydrous metal salts and aprotic solvents still failed to yield Ga(III) or In(III) complexes of N,N'-dimethyl pendant-armed dibenzo annelated cross-bridged cyclam, suggesting that strictly anhydrous condition may be critical for successful metal complexation.

Hubin et al. reported a series of transition metal complexes of N,N'-dimethyl cross-bridged cyclams by reacting anhydrous metal salts and completely deprotonated ligands (vacuum distillation from KOH after benzene extraction from pH ≥ 14 water) in rigorously dry aprotic solvents in an inert atmosphere glovebox.³⁵ Because N,N'-dimethyl dibenzo annelated cross-bridged cyclams should be less basic than N,N'-dimethyl cross-bridged cyclam, their Ga(III) or In(III) complexes should be possible to prepare using similar methods.

2.3 Synthesis of Hg-CB-DO2A

In order to investigate the kinetic inertness of the Hg²⁺ complex of CB-DO2A in Chapter 3 and since there was no preparative procedure for it previously, a similar synthetic preparation for Niu's Zn(II) and Cd(II) complexes of CB-DO2A was used.³⁷ In the presence of a stoichiometric amount of aqueous sodium hydroxide, a methanol solution of HgCl₂ and CB-DO2A.2TFA was refluxed for 48 hours. Some white insoluble precipitate was centrifuged off. Diethyl ether vapor diffusion into this supernatant yielded a white crystalline solid.

This complex has been characterized by IR, and ¹H and ¹³C{¹H} NMR spectroscopic methods. ¹⁹⁹Hg has a nuclear spin $I = 1/2$, a natural abundance of 16.84% and reasonable receptivity (5.42 with respect to ¹³C).⁴⁹ This provides a useful tool for investigation and characterization of mercury (II) complexes. This mercury (II) complex indeed exhibited ¹H-¹⁹⁹Hg and ¹³C-¹⁹⁹Hg coupling satellites in its respective ¹H and ¹³C{¹H} NMR spectra in D₂O. The ¹H NMR spectrum (Figure 2.31) clearly showed ¹⁹⁹Hg satellites around both the methylene of the pendant arm (singlet at δ 3.48, CH₂COO,

$J = 30.2$ Hz) and the cross-bridged ethylene (singlet at $\delta 2.92$, cross-bridging CH_2CH_2 , $J = 26.0$ Hz). The ^{13}C - ^{199}Hg coupling satellites in its $^{13}\text{C}\{^1\text{H}\}$ NMR spectrum (Figure 2.32) in D_2O appeared around all five signals including the carboxylate carbon resonance. Their coupling constants are as follows: $\delta 178.40$ ($J = 11.7$ Hz), 64.77 ($J = 5.4$ Hz), 60.15 ($J = 8.9$ Hz), 57.01 ($J = 20.7$ Hz), 46.27 ($J = 22.9$ Hz). These confirmed that the Hg^{2+} cation in this complex is coordinated by all four amine nitrogen donors from the hexadentate CB-DO2A in D_2O and that the CB-ligand remains fully coordinated in solution. Further, the implied C_{2v} structural symmetry suggests that the pendant arms are

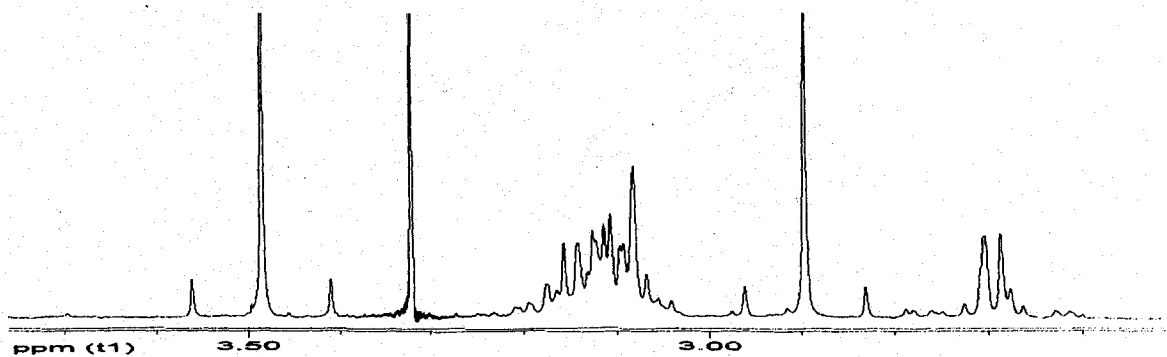


Figure 2.31 ^1H NMR spectrum of Hg-CB-DO2A in D_2O .

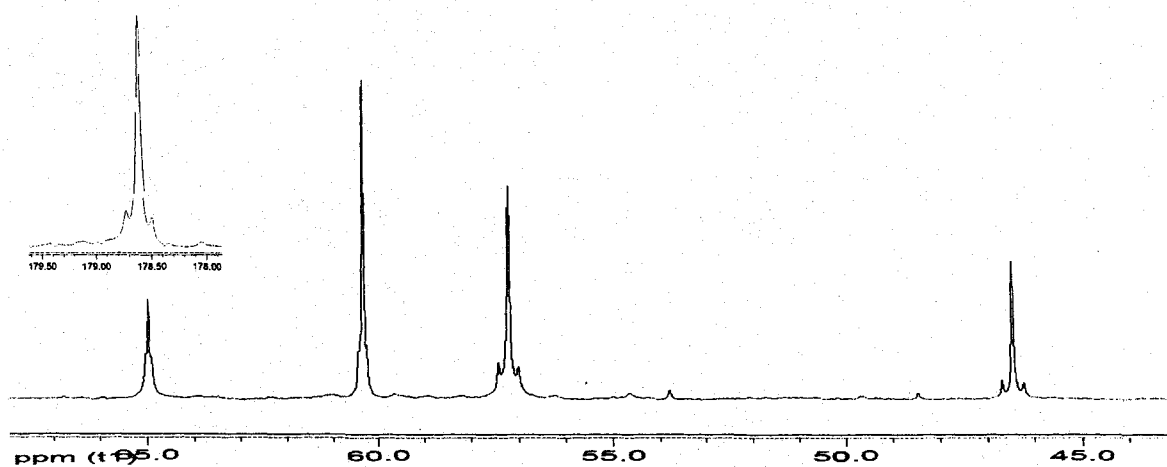


Figure 2.32 $^{13}\text{C}\{^1\text{H}\}$ NMR spectrum of Hg-CB-DO2A in D_2O .

rapidly exchanging (**Figure 2.33**) as previously observed for the zinc analog.^{37(a)} Its IR spectrum (**Figure 2.34**) showed strong carboxylate asymmetric stretching bands at 1578 and 1570 cm^{-1} .

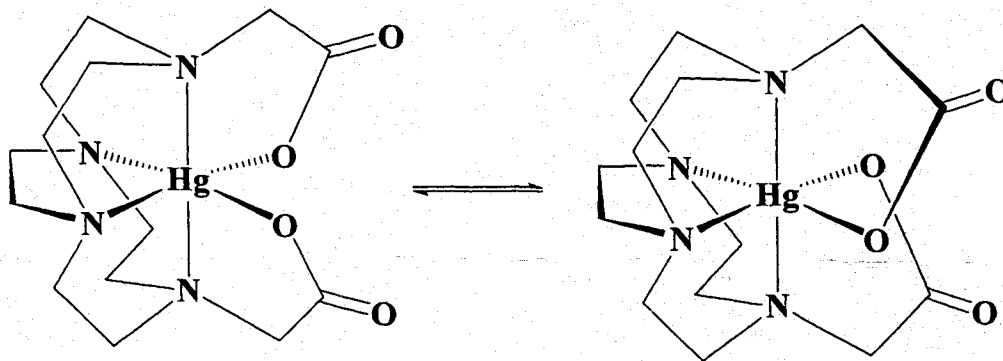


Figure 2.33 A dynamic C_{2v} -symmetric enantiomerization of Hg-CB-DO2A.

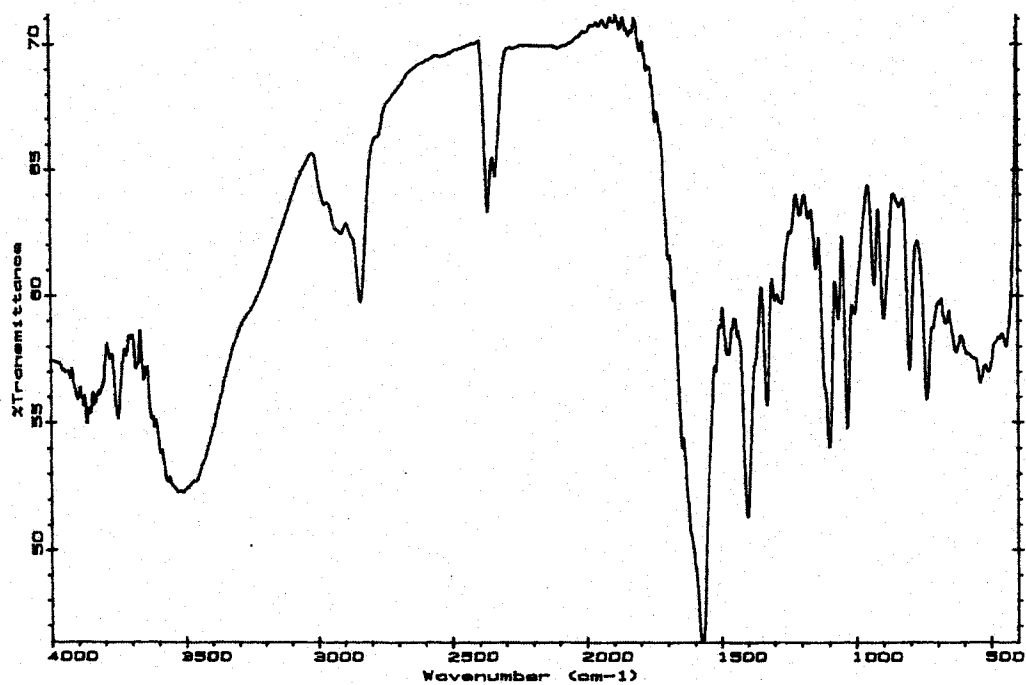


Figure 2.34 IR spectrum of Hg-CB-DO2A.

2.4 Summary and Conclusions

The [In-CB-DO2A · NaOAc]BPh₄ and [In-CB-DO2A]Cl complexes were successfully made and characterized by elemental analysis, IR, MS, ¹H and ¹³C{¹H} NMR methods. However, there is no proposed structure consistent with both its ¹H and ¹³C{¹H} NMR spectra unless there are accidentally overlapping (isochronous) and chemical shifts may thus make the diastereotopic H_a and H_b equivalent (a singlet).

Successful alkylation (arming) of [InBr₂-CB-Cyclam]Br yielded [InBr₂-Et₂-CB-TE2A]Br · H₂O which has been characterized by elemental analysis, IR, ESI-MS, ¹H and ¹³C{¹H} NMR methods, as well as a low quality X-ray structure. [In-CB-TE2A]Br was successfully made through hydrolysis of [InBr₂-Et₂-CB-TE2A]Br and showed a dynamic equilibrium in methanol even down to -80 °C.

Several attempts at alkylation of [GaBr₂-CB-Cyclam]Br to make [GaBr₂-Et₂-CB-TE2A]Br have failed due to poor solubility of [GaBr₂-CB-Cyclam]Br, and perhaps lowered nucleophilicity as well as more hindered nitrogen lone pairs relative to those of the corresponding indium complex. Interestingly, the ESI-MS spectrum showed that the product mixture may contain [(Ga-CB-Cyclam)-2H]⁺. In the future, microwave irradiation will be a good choice to overcome these slow alkylation problems.

CB-TE2A complexation with trivalent metals remains challenging due to its proton sponge nature. As mentioned before, the binding rate of Ga³⁺ and In³⁺ when competing with protons for the binding cavity in protic solvents should be much slower than those of most divalent metal ions to make complexation challenging. Microwave irradiation should also speed up this slow complexation to drive the reactions to completion.

Because N,N'-dimethyl dibenzo annelated cross-bridged cyclams should be less basic than N,N'-dimethyl cross-bridged cyclams, Ga(III) or In(III) complexes of N,N'-dimethyl pendant-armed dibenzo annelated cross-bridged cyclams should be accessible using strictly anhydrous reaction conditions.

To prepare Ga(III) and In(III) complexes, a transfer ligand exchange is often used since the precipitation of Ga(OH)₃ and In(OH)₃ occurs more rapidly than slow complexation with some ligands.⁵ This was actually attempted by making a Ga-citrate complex first in situ,⁵⁰ then adding sufficient base with protonated H₂-CB-TE2A in aqueous solution. However, no reaction was detected by NMR after two weeks of refluxing. Finally, metal exchange or transmetallation is also an alternate approach to make these complexes. For example, the known Hg or Cd complex of CB-TE2A may be used to transmetallate Ga³⁺ or In³⁺ in an appropriate solvent.

CHAPTER III

KINETIC INERTNESS STUDIES OF DIAMAGNETIC METAL COMPLEXES OF CROSS-BRIDGED LIGANDS

3.1 Introduction

Acid-promoted dissociation studies have been used to compare the relative kinetic inertness of selected metal complexes of many polyamines, especially those of Cu(II) and Zn(II).^{19,51} The dramatically-increased kinetic inertness of Cu(II) and Zn(II) cross-bridged complexes is due to the result of their added cross bridges.^{37(b),40} This enhanced inertness results in dramatically slowed acid-catalyzed dissociation. Addition of dicarboxylate pendant arms further enhances their kinetic inertness. However, kinetic inertness data for Ga(III) and In(III) complexes are rare⁵² and very little is available for their complexes of cross-bridged ligands. It was reported that Ga(NOTA) is stable in 5 M HNO₃ for 6 months, stable in pH 12 for 10 days, while slowly decomposing in pH 13 within weeks.⁵² The half-life of In(NOTA) is about 1 hour in 4M HNO₃.⁵² As for ⁶⁷Ga(tach), it is stable in pH 6 with 10% decomposition in pH 4-5 within 8 days.⁵²

To predict and compare how complexes will survive *in vivo*, these decomplexation half-lives are useful first indicators for predictions. Complexes chosen for these acid decomplexation studies here are as follows: [GaCl₂-CB-Cyclam]Cl,³⁶ [InBr₂-CB-Cyclen]Br,³⁶ [InBr₂-CB-Cyclam]Br,³⁶ [Ga-CB-DO2A]NO₃,³⁷ [In-CB-DO2A]Cl, [In-CB-TE2A]ClO₄, [Zn-CB-DO2A],³⁷ [Zn-CB-TE2A],⁴³ [Cd-CB-DO2A],⁴³ [Cd-CB-TE2A],⁴³ [Hg-CB-DO2A] and [Hg-CB-TE2A].⁴³ Unlike Cu²⁺ complexes, the

It was found that In-CB-Cyclen has a half-life of 1,069 hours ($R^2 > 0.99$) in 0.97 N DCI/D₂O at room temperature (**Figure 3.2**) but only 59(6) minutes ($R^2 > 0.99$) at 90 °C (**Figure 3.3**).

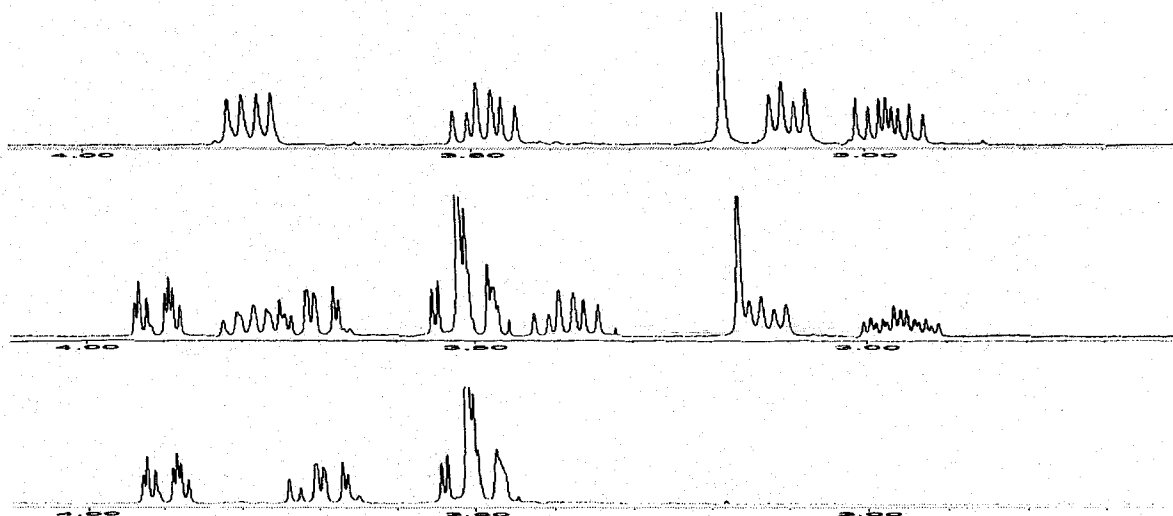


Figure 3.1 ¹H NMR spectrum of (a) [InBr₂-CB-Cyclen]Br in D₂O (top); (b) [InBr₂-CB-Cyclen]Br in 0.97 N DCI/D₂O after 50 % decomplexation (middle); (c) protonated CB-Cyclen in 0.97 N DCI/D₂O (bottom).

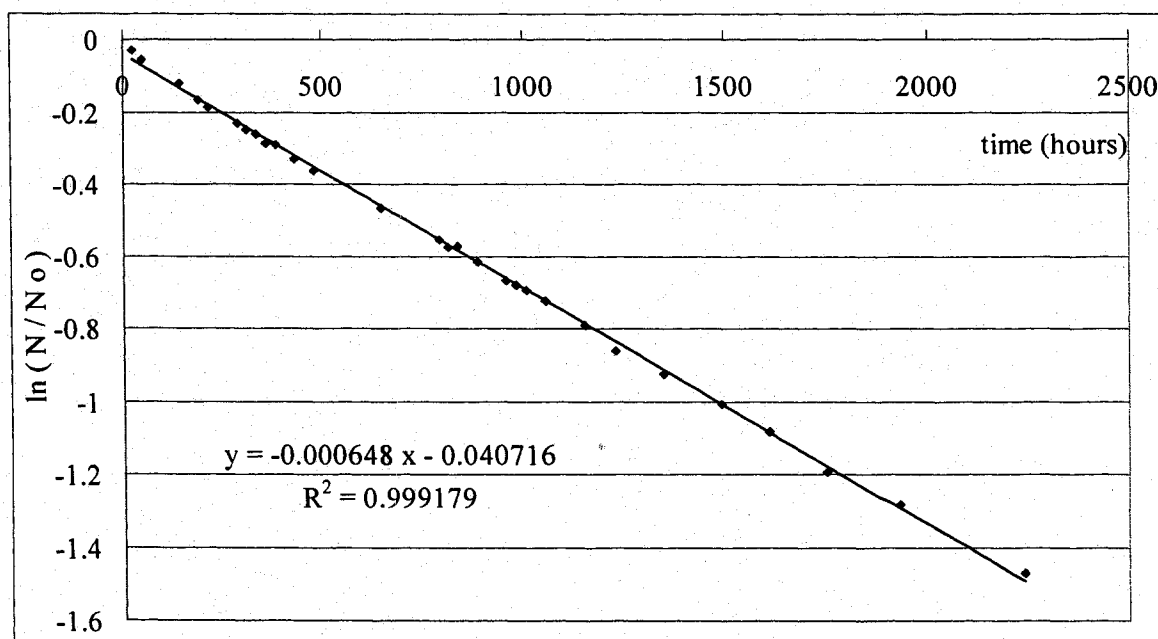


Figure 3.2 A kinetic plot of $\ln(N/N_0)$ (see Experimental Section) vs. time for [InBr₂-CB-Cyclen]Br in 0.97 N DCI/D₂O at room temperature.

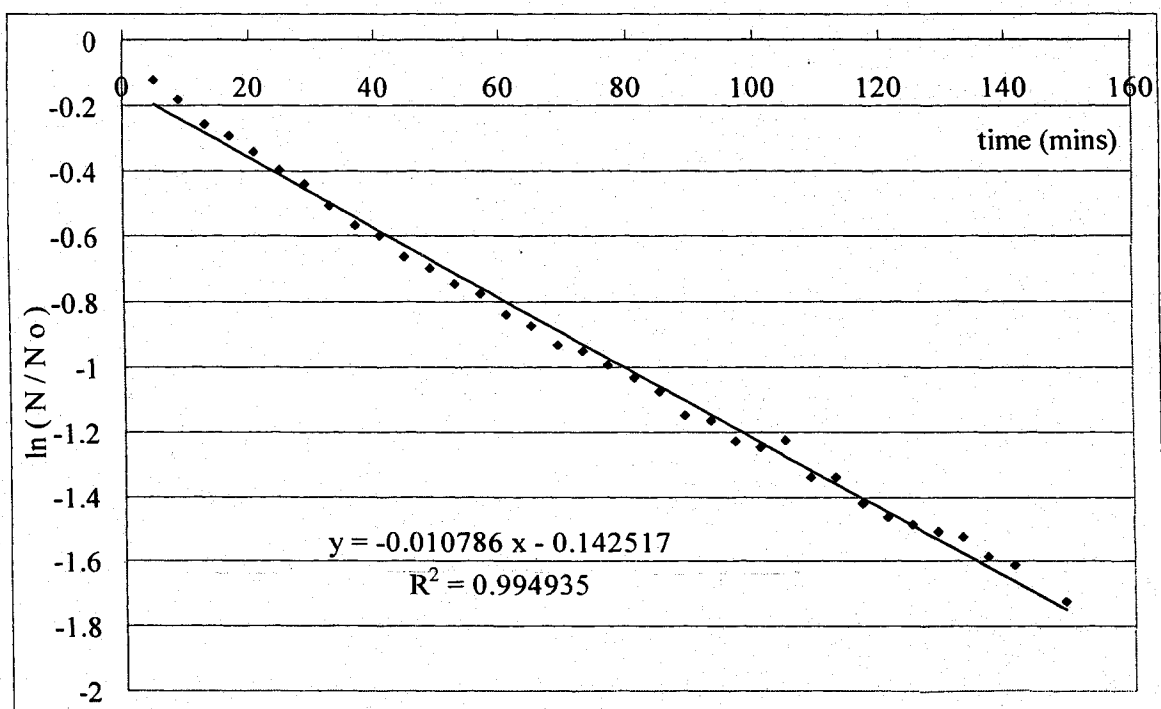


Figure 3.3 A kinetic plot of $\ln(N/N_0)$ vs. time for $[\text{InBr}_2\text{-CB-Cyclen}]\text{Br}$ in 0.97 N $\text{DCl}/\text{D}_2\text{O}$ at 90 °C.

The same peak assignments for the decomposed complex of In-CB-Cyclen were applied in 5.05 N $\text{DCl}/\text{D}_2\text{O}$ since they have the same ^1H NMR spectra as the protonated ligand in 0.97 N $\text{DCl}/\text{D}_2\text{O}$. It was found that In-CB-Cyclen has a half-life of 43.34 hours ($R^2 > 0.99$) in 5.05 N $\text{DCl}/\text{D}_2\text{O}$ at room temperature, while it is almost completely destroyed in less than 5 minutes in 5.05 N $\text{DCl}/\text{D}_2\text{O}$ at 90 °C (**Figure 3.4**).

Unlike the well-resolved ^1H NMR spectrum (**Figure 3.5(a)**) of In-CB-Cyclam in D_2O , the free ligand CB-Cyclam showed broad peaks in 0.97 N $\text{DCl}/\text{D}_2\text{O}$ (**Figure 3.5(c)**). As a result, the decomplexation cannot be quantified by integration due to the broad peaks also shown in **Figure 3.5(b)**. Fortunately, in the ^1H NMR spectra of protonated CB-Cyclam and In-CB-Cyclam in 5.05 N $\text{DCl}/\text{D}_2\text{O}$, the most upfield equatorial and axial

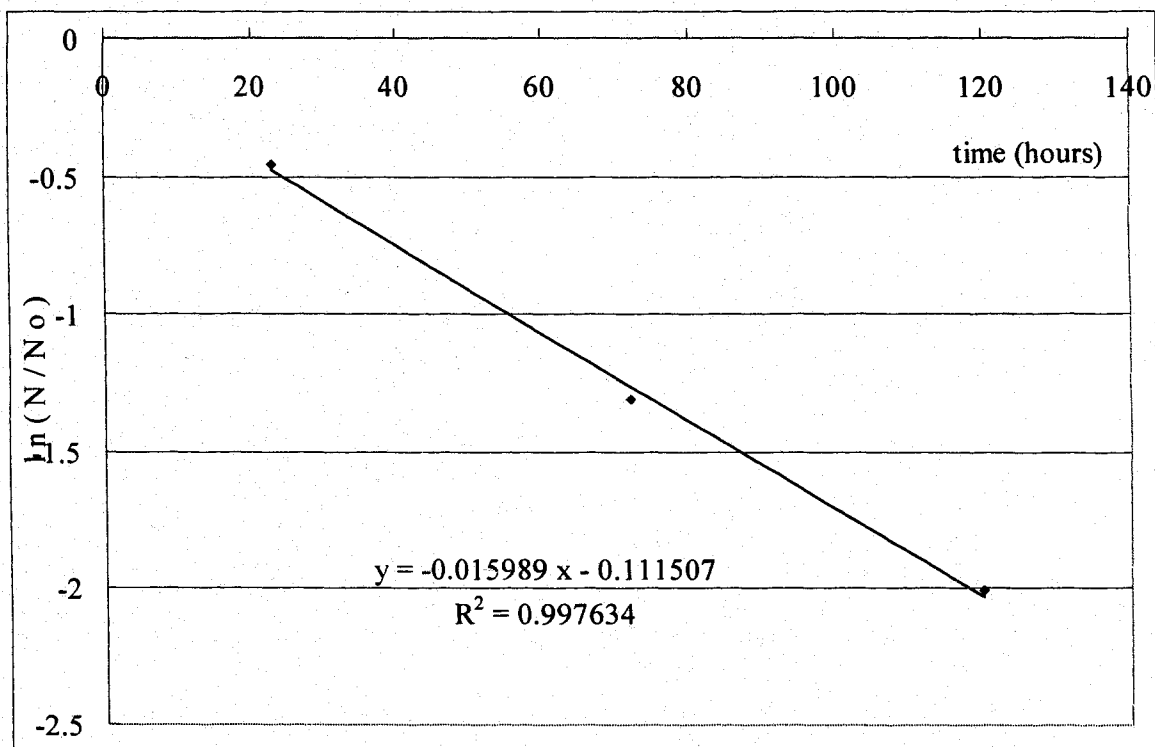


Figure 3.4 A kinetic plot of $\ln(N/N_0)$ vs. time for $[\text{InBr}_2\text{-CB-Cyclen}]\text{Br}$ in 5.05 N DCl/D₂O at room temperature.

protons of the β -methylenes ($\text{CH}_{eq}\text{H}_{ax}$) for In-CB-Cyclam are well-separated, whereas all β -methylene protons are at lower field and overlapping for protonated CB-Cyclam (**Figure 3.6**). In-CB-Cyclam was found to be at least 97% intact after over 3 weeks in 5.05 N DCl/D₂O at room temperature, assuming a ¹H NMR detection limit of 3%. Furthermore, 63.5% of In-CB-Cyclam was decomplexed after 20 hours in 5.05 N DCl/D₂O at 90 °C. The same upfield integration ratio of the residual complex and the protonated ligand was also used for Ga-CB-Cyclam in 5.05 N DCl/D₂O. Ga-CB-Cyclam was found to be at least 97% intact in 5.05 N DCl/D₂O at 90 °C after over 1 month (**Figure 3.7**).

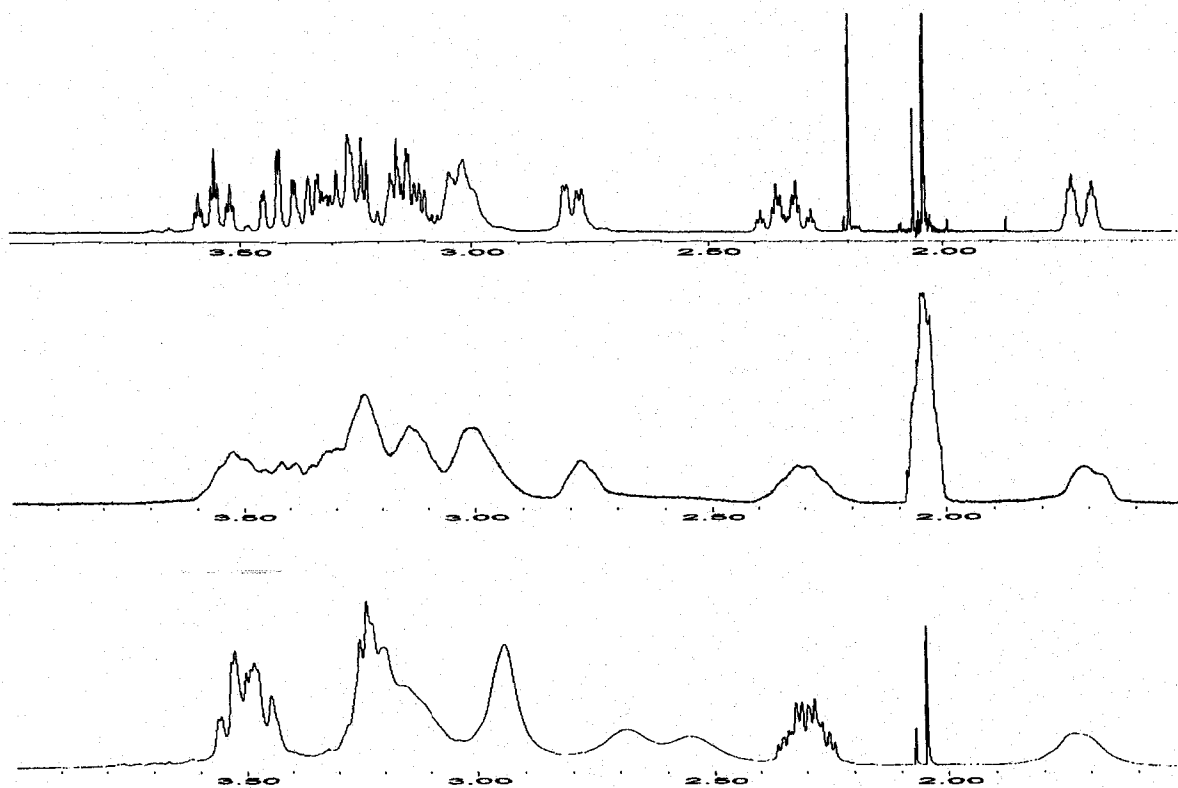


Figure 3.5 ^1H NMR spectrum in 0.97 N DCl/D₂O of (a) [InBr₂-CB-Cyclam]Br after 3 weeks at room temperature (top); (b) [InBr₂-CB-Cyclam]Br at 90°C (middle); (c) protonated CB-cyclam (bottom).

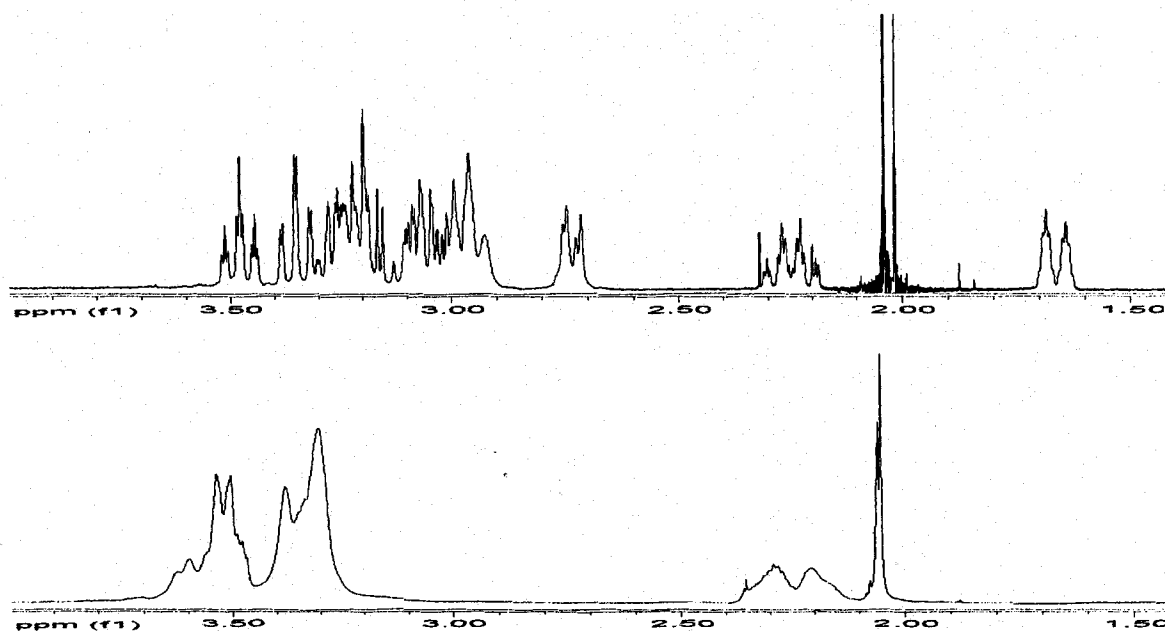


Figure 3.6 ^1H NMR spectrum in 5.05 N DCl/D₂O of (a) [InBr₂-CB-Cyclam]Br after 3 weeks at room temperature (top); (b) protonated CB-cyclam (bottom).

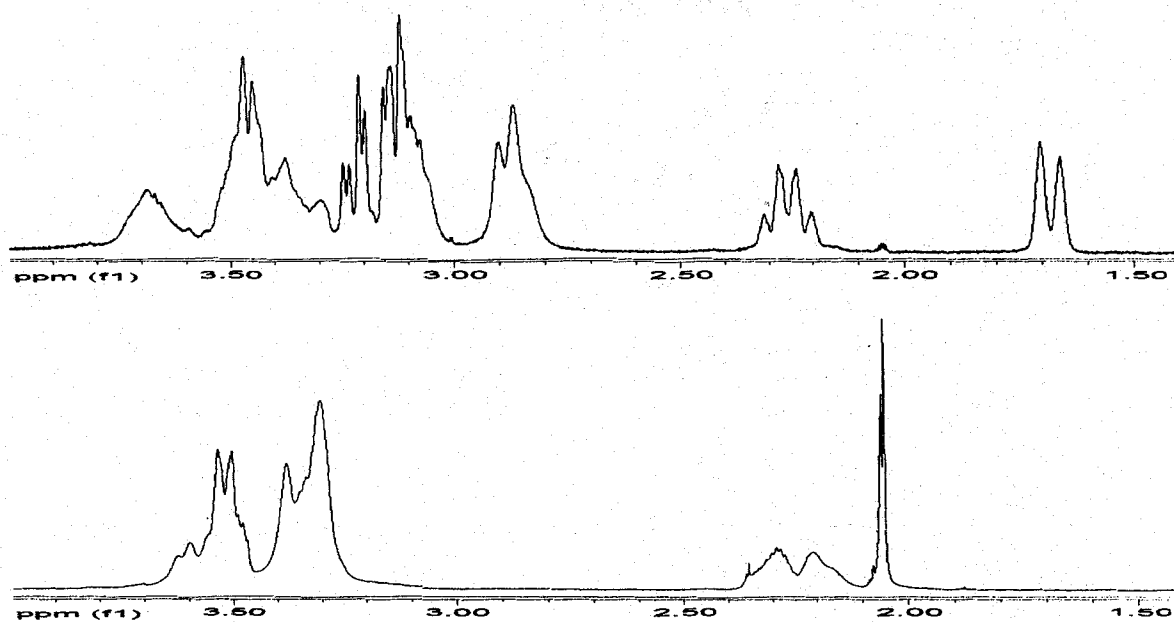


Figure 3.7 ^1H NMR spectrum in 5.05 N DCl/D₂O of (a) [GaBr₂-CB-Cyclam]Br after 1 month at 90 °C (top); (b) protonated CB-cyclam (bottom).

The two added carboxymethyl pendant arms in CB-DO2A are expected to significantly increase the kinetic inertness of its metal complexes. Unlike the singlet resonance for the methylene protons of the CH₂COO arms in the ^1H NMR spectrum for the free ligand CB-DO2A, an AB pattern with an additional long-range W-coupling to the B proton for the [Ga-CB-DO2A]NO₃ complex was observed. There is no dynamic broadening of this pattern up to 87(2) °C.^{37(a)} This AB pattern with a little more complicated split for the C₂-symmetric [Ga-CB-DO2A]NO₃ complex was essentially unchanged in 0.97 N DCl/D₂O at room temperature after 8 months except for a very small singlet at δ 4.17 assignable to the protonated ligand (**Figure 3.8(b)**). Integration of the pendant-arm CH₂ proton resonance versus this small singlet at δ 4.17 indicated about ~1% decomplexation. It is intriguing that this pendant-arm CH₂ proton resonance pattern disappeared after 2 days at 90 °C (**Figure 3.8(c)**). This phenomenon was previously

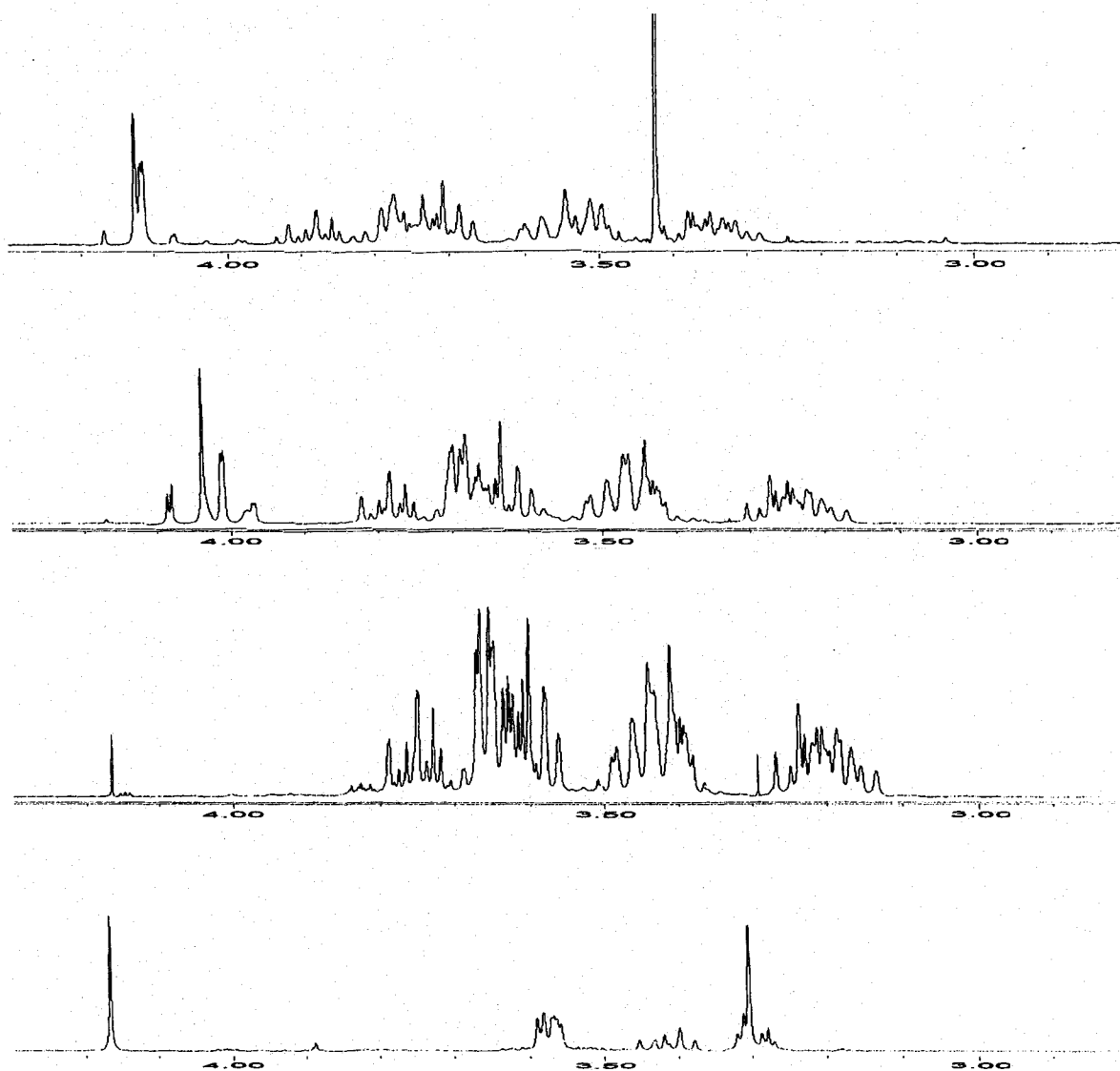


Figure 3.8 ^1H NMR spectra of (a) $[\text{Ga-CB-DO2A}]\text{NO}_3$ in D_2O (top); (b) $[\text{Ga-CB-DO2A}]\text{NO}_3$ in 0.97 N $\text{DCl}/\text{D}_2\text{O}$ at room temperature after 8 months (second from top); (c) $[\text{Ga-CB-DO2A}]\text{NO}_3$ in 0.97 N $\text{DCl}/\text{D}_2\text{O}$ at 90°C after 2 months (third from top); (d) protonated CB-DO2A in 0.97 N $\text{DCl}/\text{D}_2\text{O}$ (bottom).

reported for $[\text{Ga-CB-DO2A}]\text{NO}_3$ in D_2O and explained as a consequence of significant H/D exchange.³⁷ Besides the absence of the pendant-arm CH_2 proton resonance pattern and the appearance of a downfield singlet, perhaps from the protonated ligand, the rest of the resonances are little changed, suggesting that the half-life for $[\text{Ga-CB-DO2A}]\text{NO}_3$ is significantly more than 2 months even in 0.97 N $\text{DCl}/\text{D}_2\text{O}$ at 90°C . (**Figure 3.8(c)**). Note

that the assignment of this small singlet for the protonated ligand may be problematic due to the facile H/D change of the pendant-arm CH₂ protons to CD₂ in the complex which should result in no pendant-arm proton resonance for either the decomplexed and protonated ligand.

A similar assignment in the ¹H NMR spectrum of [In-CB-DO2A]Cl was used as the complete disappearance of the nominal AB pattern of the pendant-arm methylene protons was also observed in 0.97 N DCl/D₂O at 90 °C after 12 days. It was found that there is only about 16.65% decomposition after 34 days by using the integration difference (for complex: 18H between δ 3.14-3.62; 2H between δ 2.94-3.05) of their ¹H NMR spectra, suggesting that the half-life for [In-CB-DO2A]Cl is longer than 34 days in 0.97 N DCl/D₂O at 90 °C.

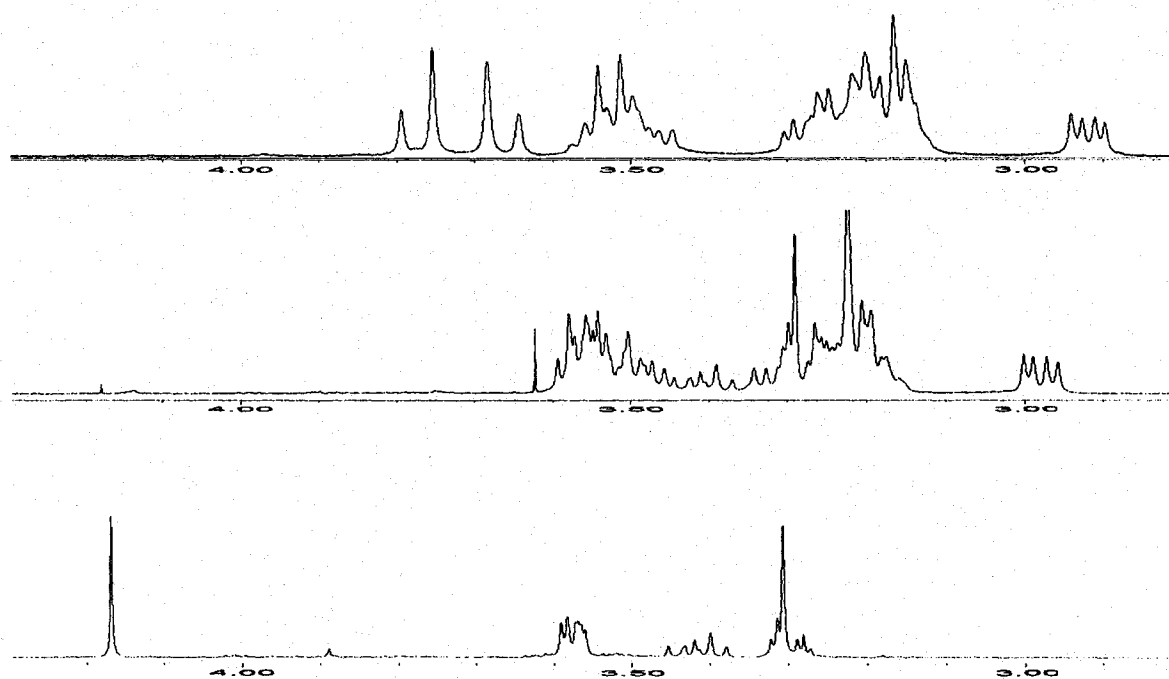


Figure 3.9 ¹H NMR spectrum of (a) [In-CB-DO2A]Cl in D₂O (top); (b) [In-CB-DO2A]Cl in 0.97 N DCl/D₂O at 90 °C after 34 days (middle); (c) protonated CB-DO2A in 0.97 N DCl/D₂O (bottom).

As described above, the disappearance of the nominal AB pattern of the pendant-arm methylene protons was observed for both [Ga-CB-DO2A]NO₃ and [In-CB-DO2A]Cl in D₂O due to H/D exchange over time, suggesting that these protons are acidic to some extent. Consistent with this, this exchange takes longer for [In-CB-DO2A]Cl in a DCl/D₂O solution at 90 °C than for [Ga-CB-DO2A]NO₃ due to the less acidic methylene protons for indium complex. With the AB pattern diminishing over time, two different singlets remained and then completely disappeared, indicating that the two diastereotopic protons on the same arm was exchanged respectively first, then the other (**Figure 3.10**). A series of ¹H NMR spectra of the proposed H/D exchange of the methylene protons on the CH₂COO arms for [In-CB-DO2A]Cl are shown in **Figure 3.11**.

Because [Ga-CB-DO2A]NO₃ and [In-CB-DO2A]Cl are so kinetically inert and have very long half-lives, harsher condition will be necessary to hasten this acid-promoted decomplexation process. Unfortunately, poor solubility of both [Ga-CB-DO2A]NO₃ and [In-CB-DO2A]Cl in 5.05 N DCl/D₂O limited further investigations. In addition, the ¹H NMR spectrum of [In-CB-TE2A]ClO₄ also showed broad peaks in D₂O as well as 0.97 N DCl/D₂O, further inhibiting possible kinetic inertness studies.

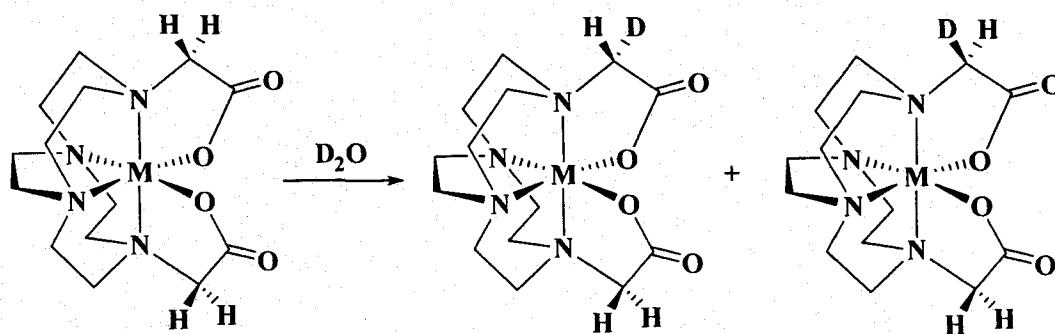


Figure 3.10 H/D exchange for two diastereotopic pendant-arm methylene protons.

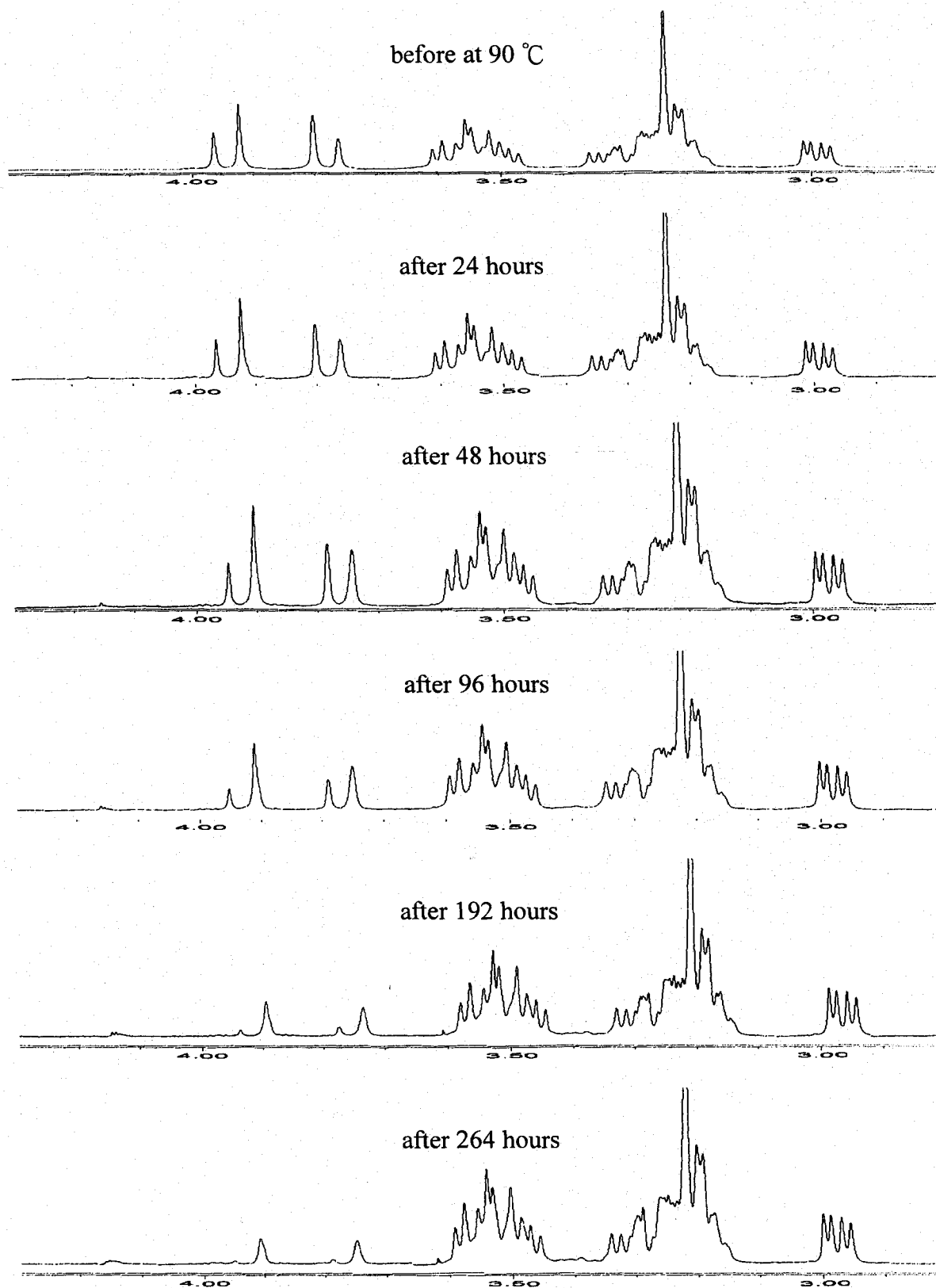


Figure 3.11 H/D exchange of the methylene protons on the CH_2COO arms of $[\text{In-CB-DO}_2\text{A}]\text{Cl}$ in 0.97 N $\text{DCl}/\text{D}_2\text{O}$ at 90 °C over time.

3.2.2 Relative Kinetic Inertness of Zn(II), Cd(II) and Hg(II) Complexes

In order to compare the relative kinetic inertness of Zn(II), Cd(II) and Hg(II) complexes with Ga(III) and In(III) complexes, 0.97 N DCl/D₂O or 5.05 N DCl/D₂O at room temperature or 90 °C were used instead of the pH 5 buffered solution used previously for divalent metal complexes of cross-bridged ligands by Niu.⁴³ The complexes studied include: [Zn-CB-DO2A], [Zn-CB-TE2A], [Cd-CB-DO2A], [Cd-CB-TE2A], [Hg-CB-DO2A] and [Hg-CB-TE2A].

Unlike the AB pattern for the methylene protons of the CH₂COO pendant arms for the C₂ symmetric [Ga-CB-DO2A]NO₃, time-average C_{2v} symmetric Zn-CB-DO2A showed a singlet at δ 3.6 in its ¹H NMR spectrum in D₂O at room temperature.³⁷ The integration of this singlet versus that from protonated CB-DO2A at δ 4.17

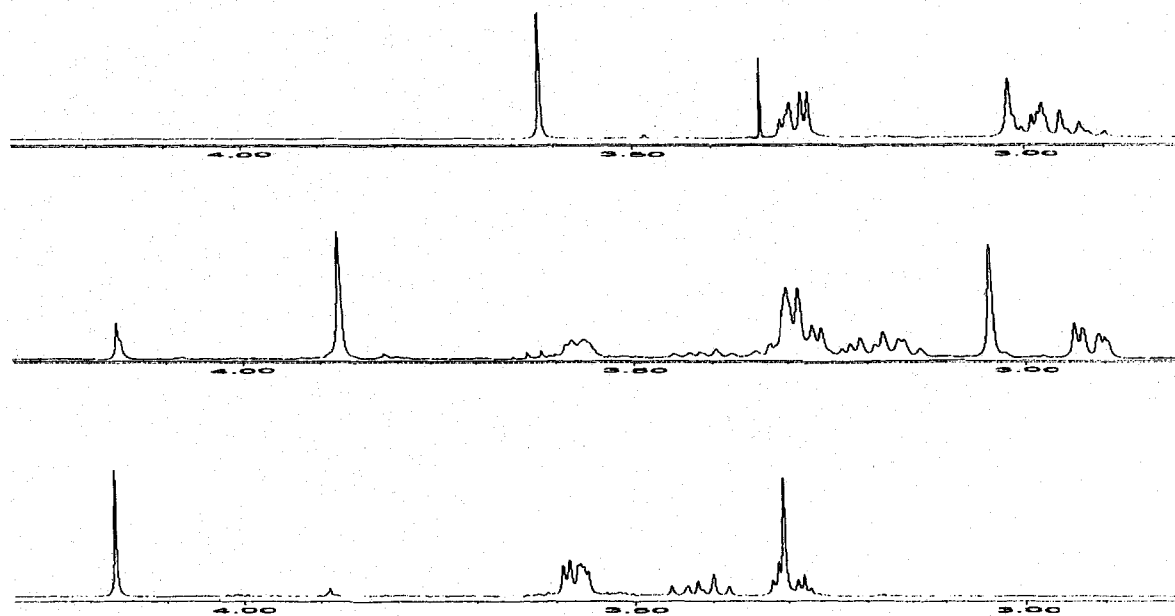


Figure 3.12 ¹H NMR spectra of (a) [Zn-CB-DO2A] in D₂O (top); (b) [Zn-CB-DO2A] in 0.97 N DCl/D₂O at room temperature after 4 minutes (middle); (c) protonated CB-DO2A in 0.97 N DCl/D₂O (bottom). (HOD peak is not shown.)

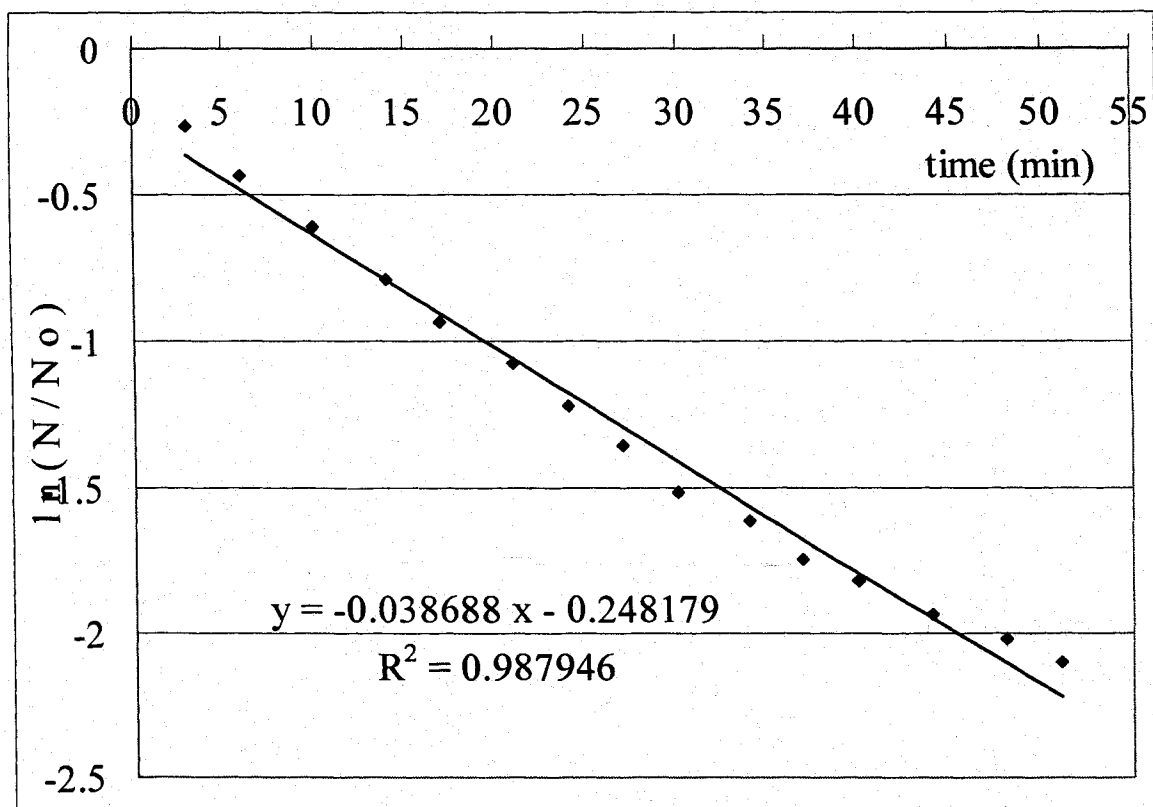


Figure 3.13 A kinetic plot of $\ln(N/N_0)$ vs. time for $[Zn-CB-DO_2A]$ in 0.97 N DCl/D₂O at room temperature.

can be used to monitor this decomplexation process (**Figure 3.12**). Thus, Zn-CB-DO₂A has a half-life of 19(2) minutes ($R^2 > 0.98$, **Figure 3.13**) in 0.97 N DCl/D₂O at room temperature. However, it was completely destroyed within 5 minutes in 5.05 N DCl/D₂O. It is worth mentioning that there is no H/D exchange observed for the pendant-arm methylene protons of Zn-CB-DO₂A probably due to the much less acidic arm-methylene protons for Zn complex and fast complete decomposition in about 90 mins.

By contrast, the Zn-CB-TE₂A complex showed remarkable kinetic inertness towards acid-assisted decomplexation. Unlike Zn-CB-DO₂A, Zn-CB-TE₂A was only slowly decomposed in 0.97 N DCl/D₂O at room temperature with 72% complex remaining even after 71 days (**Figure 3.14**). The most upfield multiplet of a doublet of

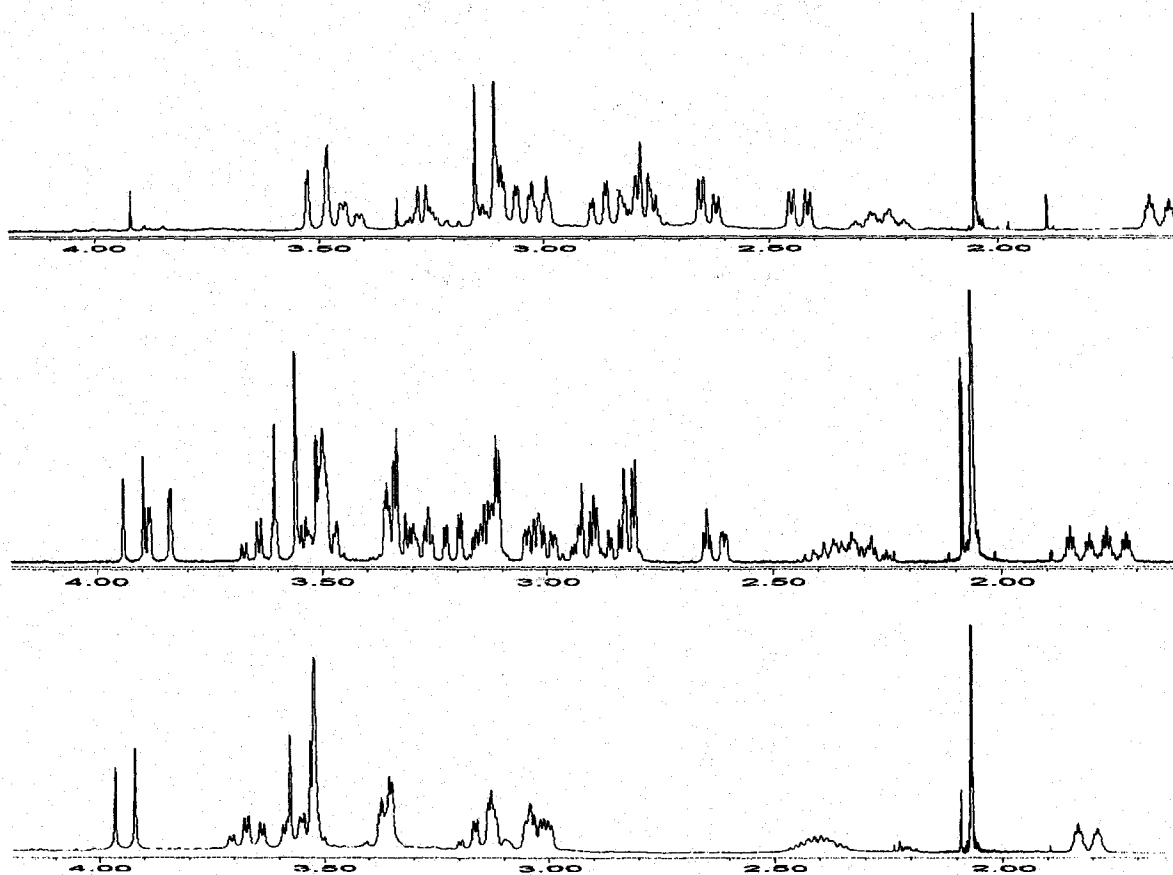


Figure 3.14 ^1H NMR spectra of (a) $[\text{Zn-CB-TE2A}]$ in D_2O (top); (b) $[\text{Zn-CB-TE2A}]$ in 0.97 N $\text{DCl}/\text{D}_2\text{O}$ at room temperature after 71 days (middle); (c) protonated CB-TE2A (bottom) in 0.97 N $\text{DCl}/\text{D}_2\text{O}$.

pentets belonging to the equatorial β -methylene protons can be used to quantify the ratio of residual complex and the decomplexed, protonated ligand. For partly decomplexed solution, two sets of an approximate doublet of pentets in the most upfield region are shown in 0.97 N $\text{DCl}/\text{D}_2\text{O}$. The data yielded a half-life of 49(6) minutes ($R^2 > 0.99$, **Figure 3.15**) at 90 $^\circ\text{C}$. The same assignment for Zn-CB-TE2A was used in 5.05 N $\text{DCl}/\text{D}_2\text{O}$ (**Figure 3.16**). It was found that Zn-CB-TE2A has a half life of 104 hours ($R^2 > 0.99$, **Figure 3.17**) at room temperature. However, it was also essentially completely decomplexed within 5 minutes at 90 $^\circ\text{C}$.

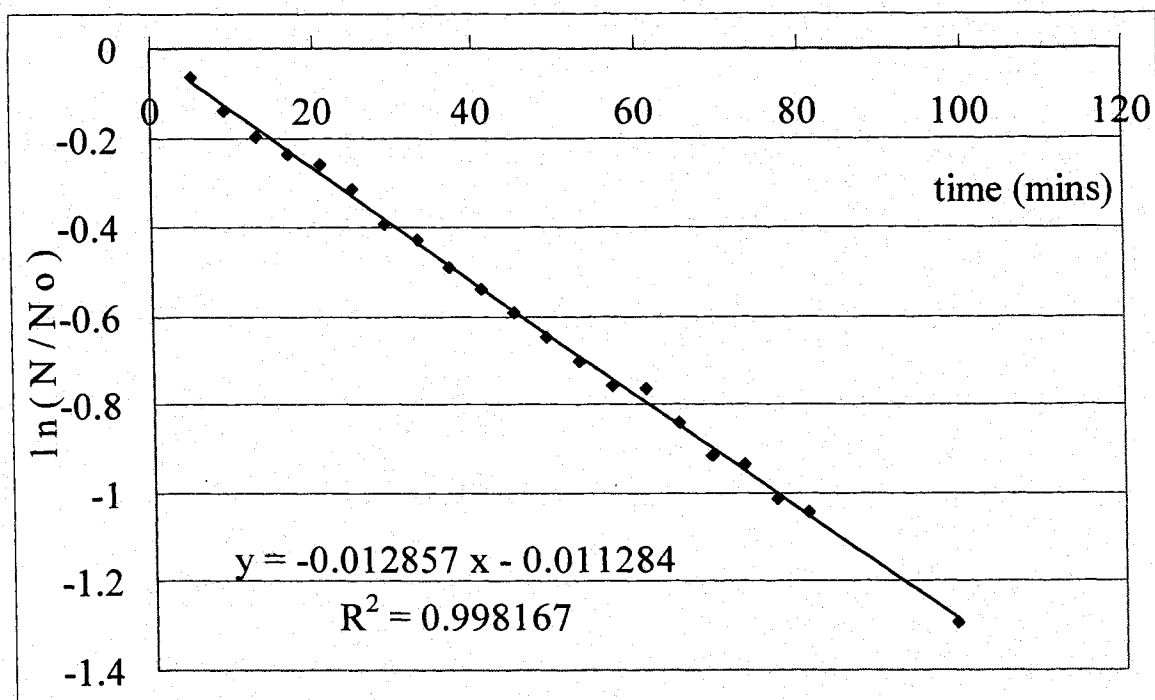


Figure 3.15 A kinetic plot of $\ln(N/N_0)$ vs. time for Zn-CB-TE2A in 0.97 N DCl/D₂O at 90 °C.

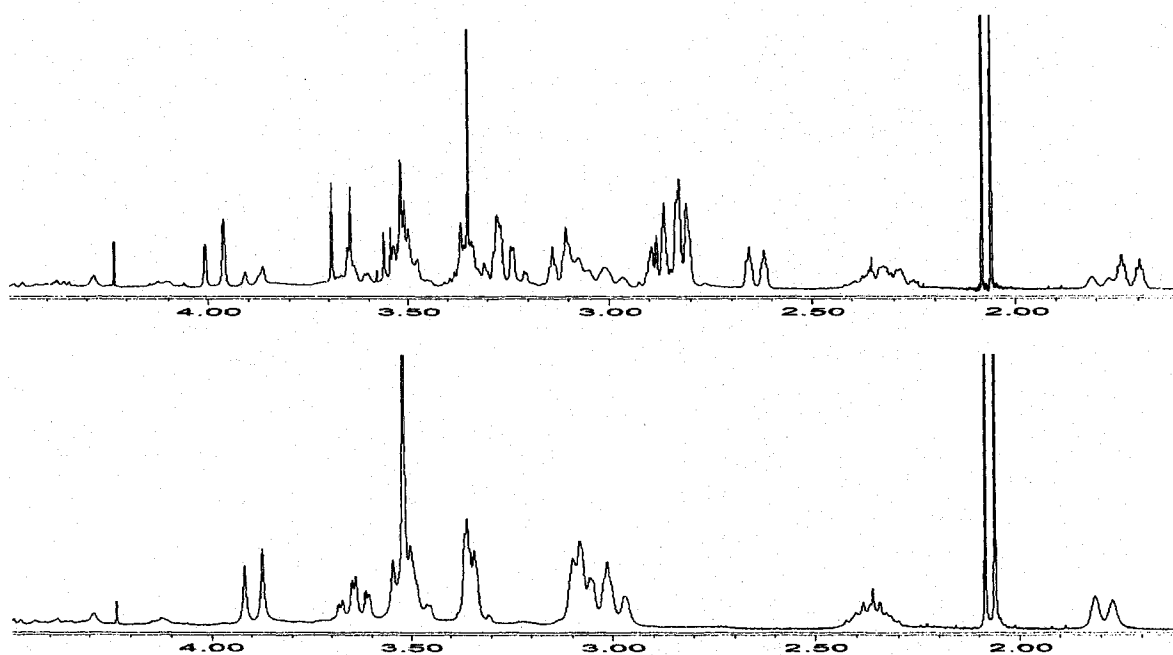


Figure 3.16 ¹H NMR spectra in 5.05 N DCl/D₂O of (a) [Zn-CB-TE2A] (top); (b) protonated CB-TE2A (bottom).

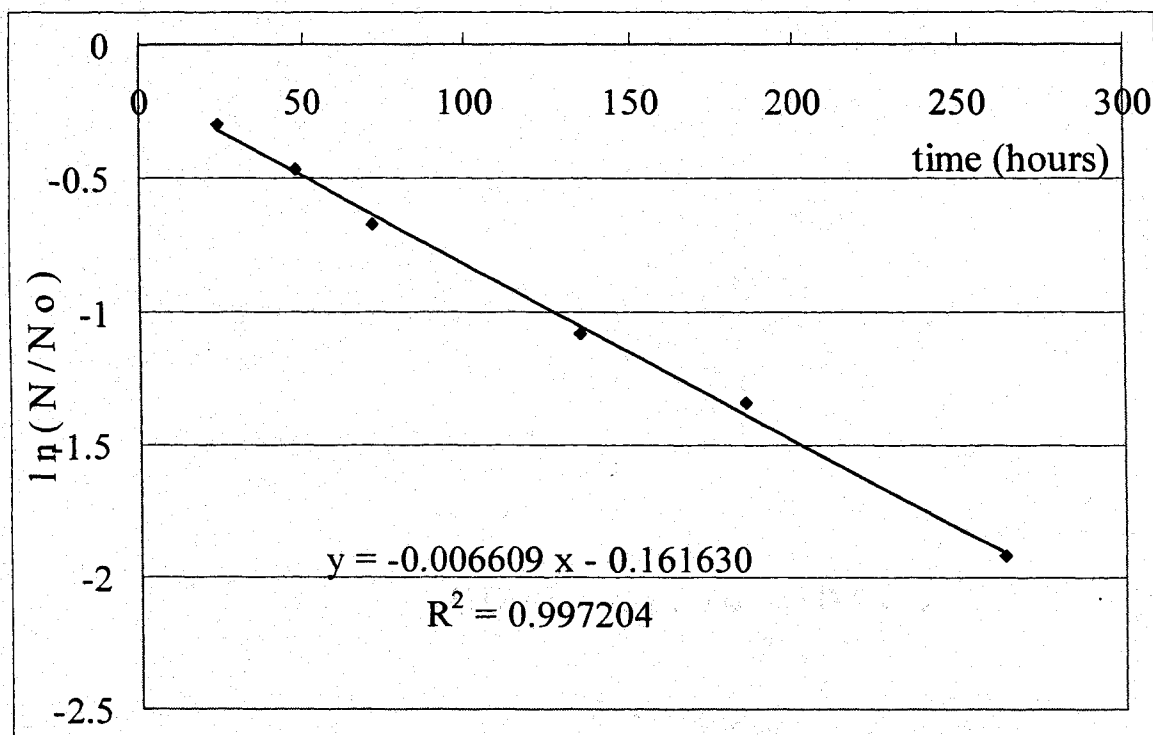


Figure 3.17 A kinetic plot of $\ln(N/N_0)$ vs. time for Zn-CB-TE2A in 5.05 N DCl/D₂O at room temperature.

The ¹H NMR spectrum of Cd-CB-DO2A in D₂O showed satellites around the singlet resonance of the methylene protons from the CH₂COO arms (**Figure 3.18(a)**). Both the disappearance of these satellites and the appearance of a singlet for the protonated ligand at δ 4.17 can be used to monitor this decomplexation process. Cd-CB-DO2A was found to completely decompose within 6 minutes in 0.97 N DCl/D₂O at room temperature (**Figure 3.18**).

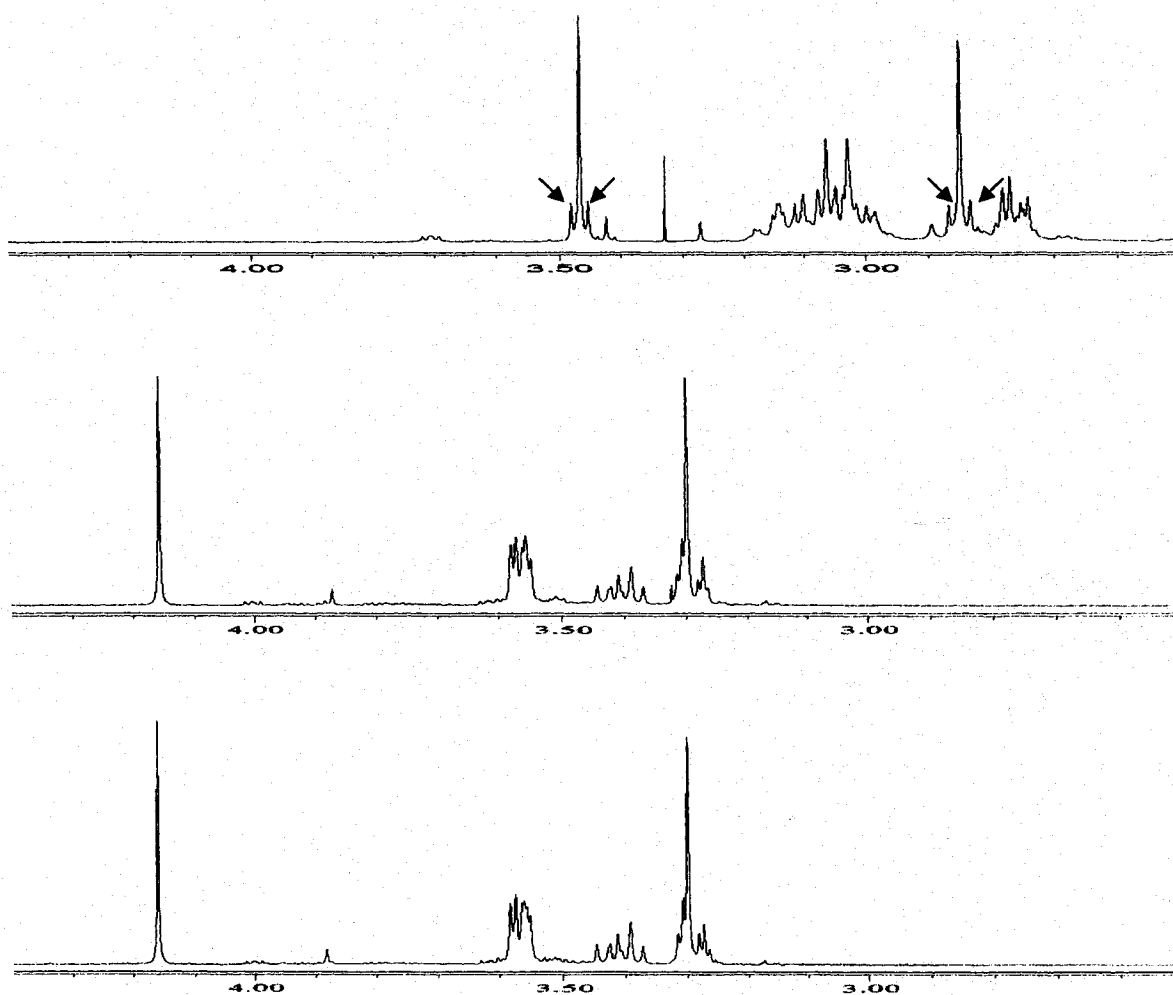


Figure 3.18 ^1H NMR spectrum of (a) Cd-CB-DO2A in D_2O (top); (b) Cd-CB-DO2A in 0.97 N DCl/ D_2O after 6 minutes at room temperature (middle); (c) protonated CB-DO2A in 0.97 N DCl/ D_2O (bottom).

In the ^1H NMR spectrum of Cd-CB-TE2A in 5.05 N DCl/ D_2O , the most upfield multiplet of a doublet of pentets belonging to the equatorial β -methylene protons can be used to monitor the acid decomplexation. It was found that Cd-CB-TE2A was completely decomplexed within 5 minutes at room temperature (**Figure 3.19**).

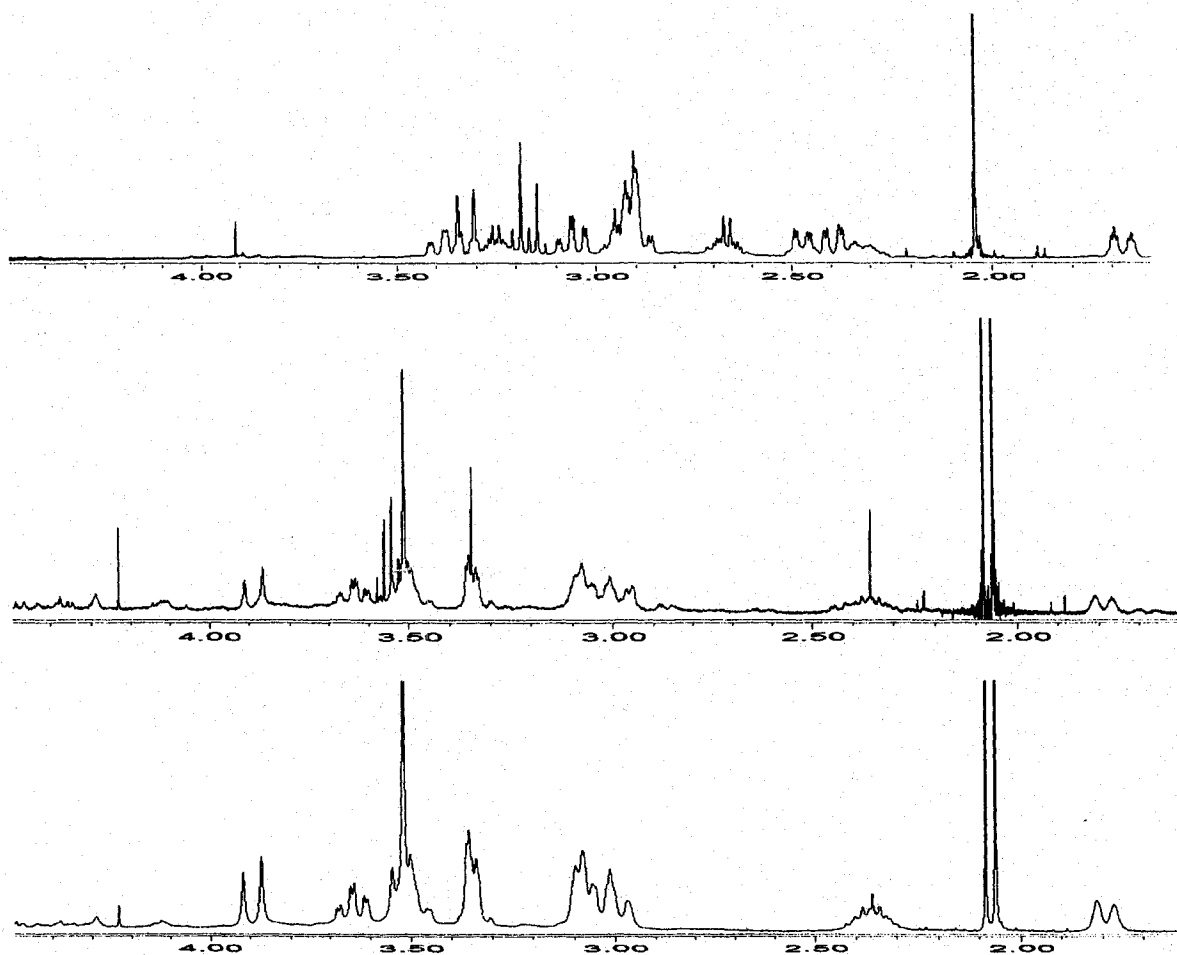


Figure 3.19 ^1H NMR spectra of (a) [Cd-CB-TE2A] in D_2O (top); (b) [Cd-CB-TE2A] in 5.05 N DCl/ D_2O after 5 minutes at room temperature (middle); (c) protonated CB-TE2A in 5.05 N DCl/ D_2O (bottom).

3.2.3 NH/ND Exchange for Ga(III) and In(III) Cross-bridged Complexes

NH/ND exchange was observed at the secondary N-H sites for all Ga(III), In(III), Zn(II), Cd(II) and Hg(II) complexes of cross-bridged cyclam and cyclen in D_2O or CD_3OD (Figure 3.20).^{36,40} The half-lives of this NH/ND exchange for Zn(II), Cd(II) and Hg(II) complexes followed a pseudo-first order process and were previously determined by Niu.⁴³ These exchange rates follow the order: Hg(II) > Cd(II) > Zn(II). Two possible mechanisms were proposed (Figure 3.21).

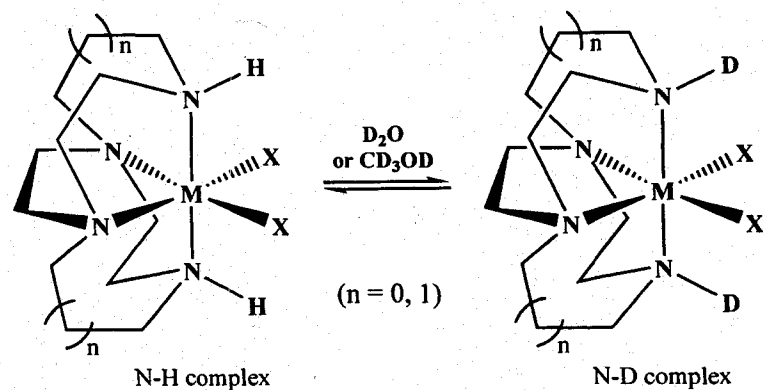


Figure 3.20 NH/ND Exchange in D_2O or CD_3OD .

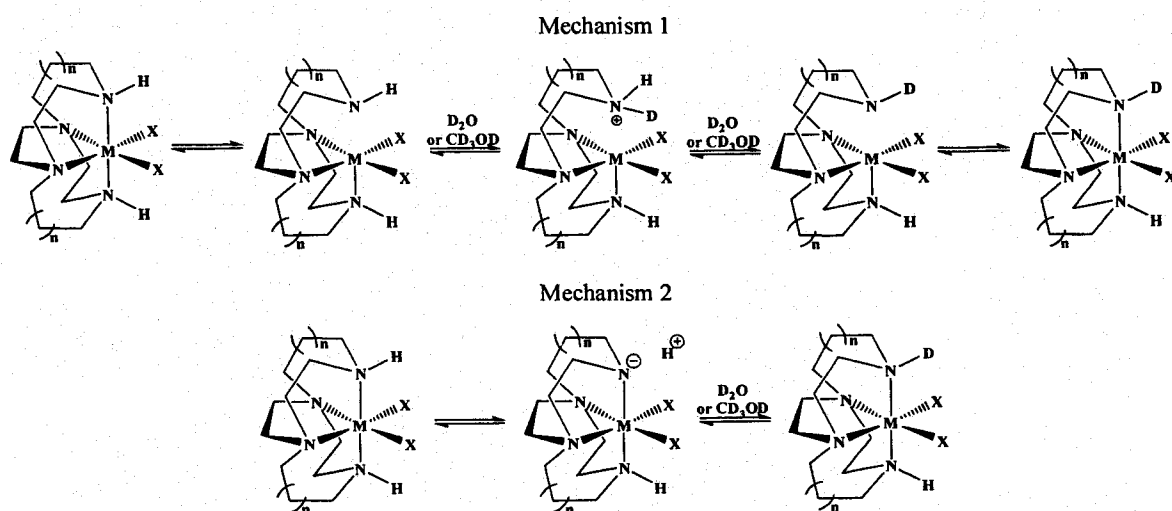


Figure 3.21 Possible mechanisms for NH/ND Exchange in D_2O and CD_3OD .

In Mechanism 1, the more labile complex with its weaker metal-nitrogen bonds will result in the faster exchange. When Mechanism 2 is operating, the strong metal-nitrogen bond and more acidic protons should result in faster exchange. From Niu's NH/ND exchange rates for Zn(II), Cd(II) and Hg(II) complexes of cross-bridged cyclam and cyclen, the exchange rate for the Hg(II) complex was fastest and Mechanism 1 is more consistent with the data.

In order to test the NH/ND exchange rates for gallium(III) and indium(III) complexes, the ^1H NMR spectra of $[\text{GaCl}_2\text{-CB-Cyclam}]\text{Cl}$, $[\text{InBr}_2\text{-CB-Cyclen}]\text{Br}$ and $[\text{InBr}_2\text{-CB-Cyclam}]\text{Br}$ in D_2O were investigated. Broad downfield N-H broad resonances were initially observed in the ^1H NMR spectra in D_2O (Figure 3.22(a) and 3.23(a)). It was found that the NH/ND exchanges of both In-CB-Cyclen and In-CB-Cyclam in D_2O were completed within 4 days, whereas this exchange for Ga-CB-Cyclam was completed

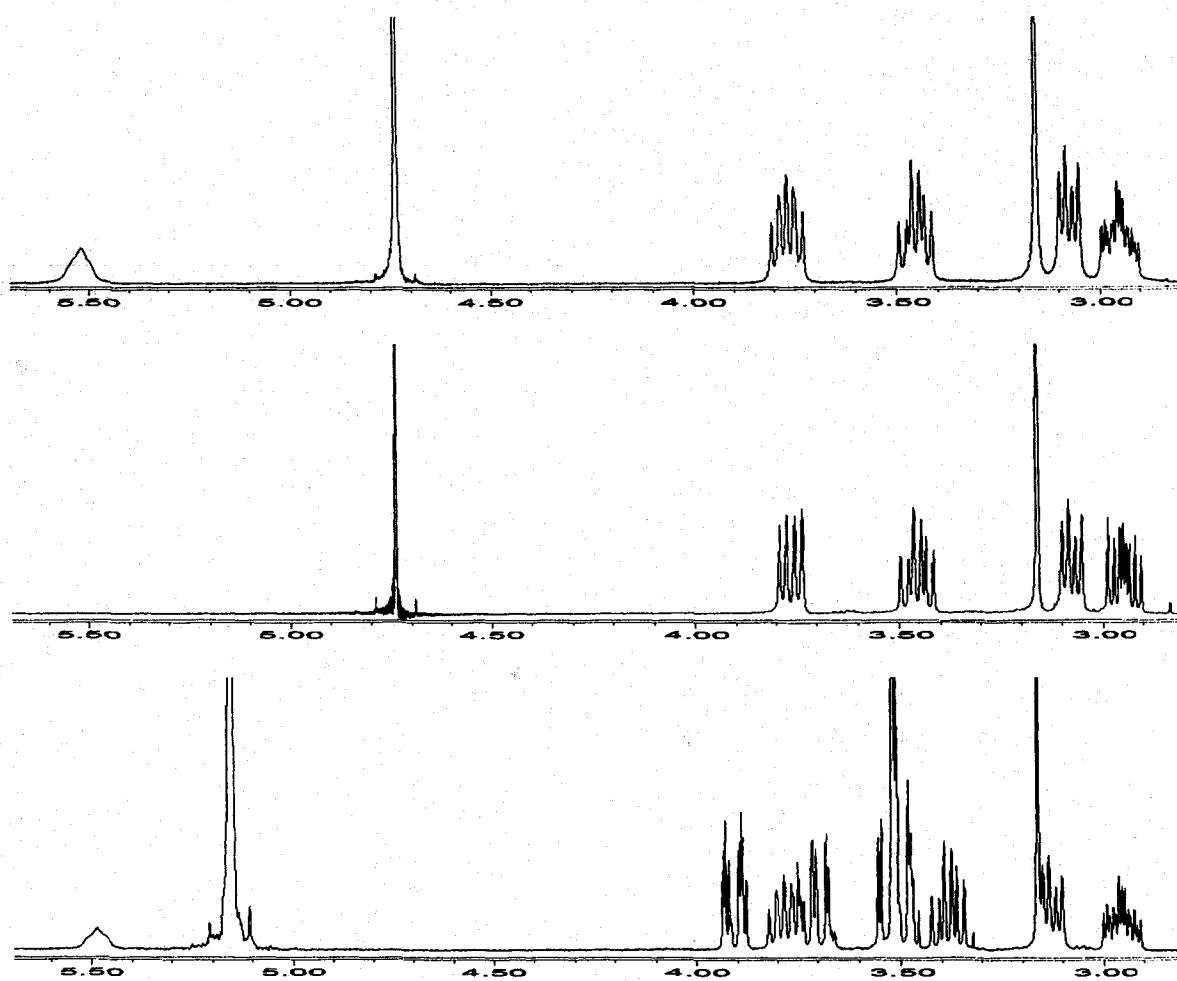


Figure 3.22 ^1H NMR spectrum of $[\text{InBr}_2\text{-CB-Cyclen}]\text{Br}$ at room temperature (a) in D_2O after 5 minutes (top); (b) in D_2O after 4 days (middle); (c) in 0.97 N $\text{DCl}/\text{D}_2\text{O}$ after 43 days (bottom).

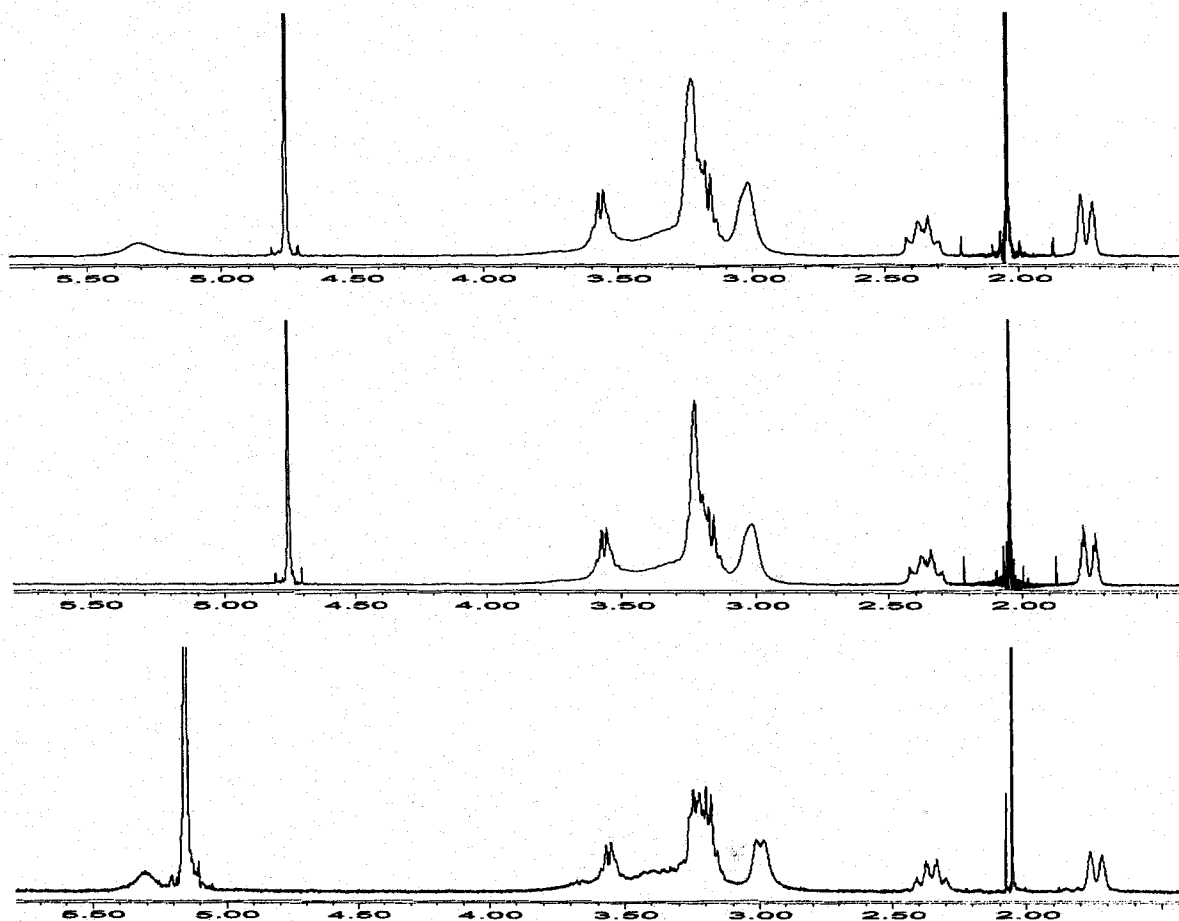


Figure 3.23 ^1H NMR spectrum of Ga-CB-Cyclam at room temperature (a) in D_2O after 5 minutes (top); (b) in D_2O after 1 day (middle); (c) in 0.97 N $\text{DCl}/\text{D}_2\text{O}$ after 16 days (bottom).

in 1 day (**Figure 3.22(b)** and **3.23(b)**). The results show that the NH/ND exchange for $[\text{GaCl}_2\text{-CB-Cyclam}]\text{Cl}$ is faster than for $[\text{InBr}_2\text{-CB-Cyclen}]\text{Br}$ and $[\text{InBr}_2\text{-CB-Cyclam}]\text{Br}$. Thus, the proposed Mechanism 2 (**Figure 3.21**) may be applicable in this case since the stronger interaction between gallium(III) and nitrogen should lead to a weaker nitrogen-hydrogen bond.

Also, in accord with Mechanism 2, when these NH/ND exchange processes are compared to those in acidic D_2O solution, it was found that the NH/ND exchange was much slower in acidic solution than in D_2O for each complex. The broad downfield N-H

proton resonance for In-CB-Cyclen in 0.97 N DCl/D₂O at room temperature was still observed after 43 days (**Figure 3.22(c)**), and after 16 days for Ga-CB-Cyclam (**Figure 3.23(c)**). In addition, as mentioned above in Chapter 2 (2.2.6), 6 equivalents of sodium carbonate exchanged the NH protons completely in 5 minutes, whereas 20 equivalent of sodium acetate did so in several hours, suggesting that base-catalyzed NH/ND exchange is much faster than neutral or acid-catalyzed exchange. A plausible reason for the faster NH/ND exchange in D₂O than in acidic solution is because the N-H protons of these are acidic enough to be deprotonated by D₂O as the base-catalyst. The relative rates of these exchanges thus follow the order: basic condition > neutral condition > acidic condition.

3.3 Summary and Discussion

To describe the fit of a metal cation in a particular ligand cavity, an ideal N_{ax}-M-N_{ax} angle is 180° and the N_{eq}-M-N_{eq} angle is 90° for pseudo-octahedral or square pyramidal geometries (**Figure 3.24**). Metal cation radii for 6-coordinate, octahedral coordination, and the N-M-N angles of selected complexes from X-ray structure data^{36,37,40} are summarized in **Tables 3.1** and **3.2**.

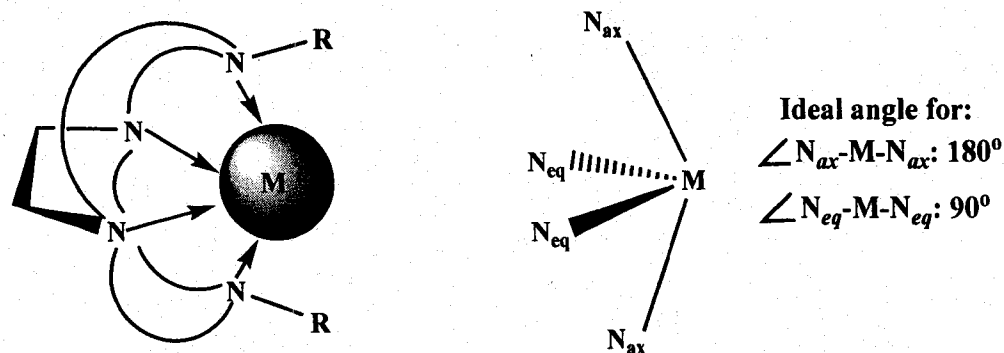


Figure 3.24 (a) Coordination geometry of a metal complex of the cross-bridged ligand. (left); (b) axial and equatorial ideal angles for a metal complex.

Table 3.1 Metal cationic radii for 6-coordinate, octahedral coordination.⁵³

Cu Cu ²⁺ (87pm)	Zn Zn ²⁺ (88pm)	Ga Ga ³⁺ (76pm)
Ag	Cd Cd ²⁺ (109pm)	In In ³⁺ (94pm)
Au	Hg Hg ²⁺ (116pm)	Tl

Table 3.2 X-ray structural data.

complex	$\angle N_{ax}-M-N_{ax}$	$\angle N_{eq}-M-N_{eq}$
Zn-CB-Cyclam ⁴⁰	168.3-173.5	83.4-84.9
Ga-CB-Cyclam ³⁶	169.33	84.17
In-CB-Cyclam ³⁶	164.29	78.89
In-CB-Cyclen ³⁶	143.95	76.78
Zn-CB-DO2A ³⁷	158.36	84.03
Ga-CB-DO2A ³⁷	164.6	86.24

Half-lives are useful indicators for predicting how long the complex will remain intact under forcing decomplexation conditions. The primary error in these half-life calculations is most likely associated with any temperature variation, especially those kinetic experiments performed at room temperature. The half-life data are summarized in **Table 3.3**. It is obvious that the kinetic inertness (**Table 3.3**) of metal complexes in the same group decrease with increasing metal cation size and resulting distorted solid state coordination geometries (**Table 3.1** and **3.2**). Furthermore, Ga(III) and In(III) complexes are more kinetically inert than Zn(II), Cd(II) and Hg(II) complexes even for some with more distorted geometries due to the higher positive charge and resulting stronger interaction between the ligand and metal cation. From the half-life data of the complexes of CB-Cyclam, the kinetic inertness follows the order: Ga-CB-Cyclam >> In-CB-Cyclam > Cu-CB-Cyclam > Zn-CB-Cyclam. In addition, the remarkably increased

kinetic stability from adding two CH₂COO pendant arms was confirmed by the data of In-CB-Cyclen vs. In-CB-DO2A in 1 N DCl/D₂O at 90 °C, Zn-CB-Cyclam vs. Zn-CB-TE2A in 5.05 N DCl/D₂O at RT, as well as other complexes.

Table 3.3 Half-lives of selected metal complexes.

	~ 1 N DCl/D ₂ O at RT	~ 1 N DCl/D ₂ O at 90°C	~ 5 N DCl/D ₂ O at RT	~ 5 N DCl/D ₂ O at 90°C
In-CB-Cyclen	1069 hours	59(6) mins*	43.34 hours	< 5 mins
In-CB-Cyclam	> 3 weeks	-	> 3 weeks	< 20 hours
In-CB-DO2A	-	> 1 month	Poor solubility	
In-CB-TE2A	Broad peaks			
Ga-CB-Cyclam	-	-	-	> 1 month*
Ga-CB-DO2A	> 8 months	> 3 months	Poor solubility	
Zn-CB-DO2A	19(2) mins*	-	< 5 mins	-
Zn-CB-TE2A	> 71 days	49(6) mins*	104 hours	< 5 mins
Cd-CB-DO2A	< 5 mins	-	-	-
Cd-CB-TE2A			< 5 mins	-
Hg-CB-DO2A	< 5 mins	-	-	-
Hg-CB-TE2A			< 5 mins	-
Cu-TETA ^{43,51(e)}			3.5(2) days	4.5(5) mins
Cu-CB-Cyclam ^{43,51(e)}			18.5(7) days	11.8(2) mins
Cu-CB-DO2A ^{43,51(e)}	4.0(1) hour		< 2 mins	
Cu-CB-TE2A ^{43,51(e)}			> 2.5×10 ⁴ hrs	154(6) hours
Zn-CB-Cyclam ^{43,51(e)}			< 3 mins	

* denotes duplicated experiments while the others have only been performed once.

A possible acid-assisted decomplexation mechanism is shown in **Figure 3.25**. The first critical step is the breaking of the metal-nitrogen bond, which depend on how strong the interaction is between metal cation and the nitrogen donor of the ligand. The second step depends on the competition between the proton and the metal cation for the nitrogen

donor. Once mono- or even di-protonation occurs, the subsequent decomplexation may be very fast.

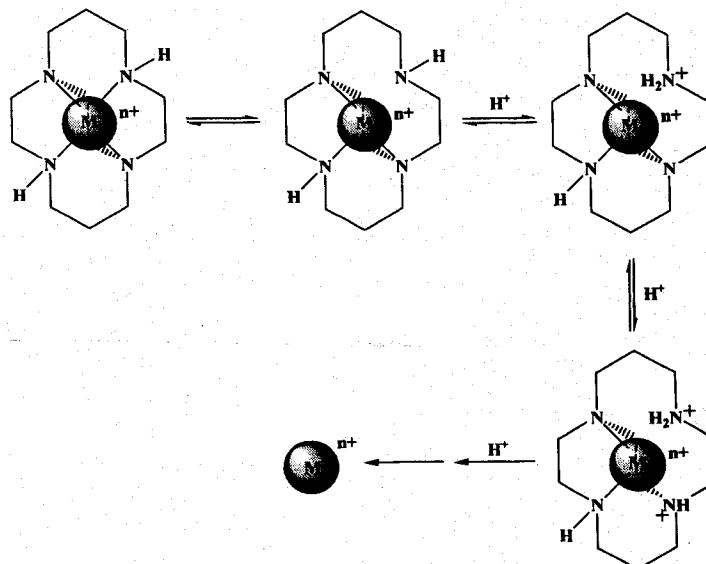


Figure 3.25 Proposed acid-promoted decomplexation mechanism for Cu-CB-Cyclam.

The apparent switch from Mechanism 1 for Zn(II), Cd(II) and Hg(II) complexes in their NH/ND exchange to Mechanism 2 for Ga(III) and In(III) complexes most likely originates from higher charge and Lewis acidity of the group 13 cations.

3.4 Conclusions and Future Work

The metal complexes of cross-bridged tetraazamacrocycles indeed exhibit remarkable kinetic inertness under harsh acidic conditions compared to other complexes of polyamines due to the difficulty of stepwise donor dissociation of these topologically constrained ligands. The combination of a cross-bridged cyclam backbone with two carboxymethyl pendant arms additionally stabilizes the complex. This remarkable kinetic

inertness has correlated well with the improved *in vivo* performance of several copper(II) complexes as potential radio-pharmaceuticals.⁵⁴

It was reported that ⁶⁷Ga(tach) was 10% composition in pH 4-5 within 8 days and In(NOTA) decomposed in pH 0 ~ -0.6 nitric acid within hours.⁵² Compared with ⁶⁷Ga(tach) and In(NOTA), Ga(III) and In(III) complexes of cross-bridged ligands indeed show remarkable kinetic inertness under harsh acidic conditions.

The relative kinetic inertness as gauged from half-lives also correlates with respective solid-state structures of the complexes, especially for metal complexes within the same group. For example, the larger In³⁺ ion does not fit well in cross-bridged cyclam compared to the smaller Ga³⁺ ion as seen in their of N_{ax}-M-N_{ax} and N_{eq}-M-N_{eq} angles (**Table 3.2**). However, despite a poorer fit, In-CB-cyclen even showed higher kinetic inertness than Zn-CB-DO2A. In general, for a given cationic size, the inertness of the complex increases with its charge. In addition, the NH/ND exchange data of Ga(III) and In(III) complexes confirmed that the N-H protons on the metal complexes of the CB-Cyclen and CB-Cyclam are indeed acidic as the exchange rates follow the order: basic > neutral > acidic condition.

To further investigate H/D exchange for the protons of the CH₂COO pendant arms of Ga-CB-DO2A and In-CB-DO2A complexes, more experiments need to be carried out in D₂O at various pH's.

Since many of these preliminary acid-promoted decomplexation studies were just performed once or repeated once, more repeated experiments are needed to ensure their accuracy. Finally, due to significant impurities contained in the Ga-CB-Cyclen sample, there was no kinetic data produced.

3.5 Experimental Section for Kinetic Studies

Complexes for acid decomplexation studies were prepared according to known procedures: $[\text{GaCl}_2\text{-CB-Cyclam}]\text{Cl}$,³⁶ $[\text{InBr}_2\text{-CB-Cyclen}]\text{Br}$,³⁶ $[\text{InBr}_2\text{-CB-Cyclam}]\text{Br}$,³⁶ $[\text{Ga-CB-DO2A}]\text{NO}_3$,³⁷ $[\text{In-CB-DO2A}]\text{Cl}$, $[\text{In-CB-TE2A}]\text{ClO}_4$, $[\text{Zn-CB-DO2A}]$,³⁷ $[\text{Zn-CB-TE2A}]$,⁴³ $[\text{Cd-CB-DO2A}]$,⁴³ $[\text{Cd-CB-TE2A}]$,⁴³ $[\text{Hg-CB-DO2A}]$ and $[\text{Hg-CB-TE2A}]$.⁴³ Proton NMR spectra of these complexes recorded at specific time intervals were used to monitor their decomplexation in acidic D_2O (0.97 M and 5.05 M $\text{DCl}/\text{D}_2\text{O}$) at room temperature and 90 °C. While $[\text{InBr}_2\text{-CB-Cyclen}]\text{Br}$ and $[\text{Zn-CB-TE2A}]$ 90 °C data were directly acquired on the 400 MHz NMR spectrometer (Varian Inova-400), other high-temperature data were collected on batch samples placed in a constant-temperature water-bath. The NMR probe temperature was calibrated using neat ethylene glycol.⁵⁶ Each solution sample was kept in a NMR tube sealed with a cap, Teflon tape and parafilm. Complex concentrations were between 0.027 and 0.037 M. The integration of the decreasing signals for the bound ligand and the increasing signals for the protonated, uncomplexed ligand were used to monitor and quantify the decomplexation. Half-lives were calculated from the slopes of the linear plots ($\ln(N/N_0)$ vs. time) since the decomplexation process can be assumed to be pseudo-first order. (N is the integration of the remaining complex and N_0 is the integration sum of protonated ligand and the remaining complex.) All acid-promoted decomplexations were monitored till at least 75% complex decomposition to ensure accurate results.

CHAPTER IV

EXPERIMENTAL SECTION

General Methods and Materials

Unless indicated otherwise, ^1H and $^{13}\text{C}\{^1\text{H}\}$ NMR spectra were recorded with a Varian Inova-400 spectrometer and referenced against internal TMS. MeCN was used as the secondary internal standard for NMR spectra of D_2O solutions; the methyl resonance was set at δ 2.06 and δ 1.7 for ^1H and $^{13}\text{C}\{^1\text{H}\}$ spectra, respectively. Variable-temperature ^1H and $^{13}\text{C}\{^1\text{H}\}$ NMR spectral studies were carried out with the Varian Inova-400. For high-temperature studies, the probe temperature was calculated from the chemical shift difference between the proton signals of neat ethylene glycol.⁵⁶ IR spectra were recorded as KBr pellets on a Thermo-Nicolet 205 Fourier-Transform spectrometer. Mass spectral data were collected using positive mode on a ThermoFinnigan LCQ-ESI classic mass spectrometer at the Center for Structural Biology, University of New Hampshire. Reactions were run under nitrogen atmosphere with magnetic stirring. Bulk solvent removal was by rotary evaporation under reduced pressure and trace solvent removal from solids was by vacuum pump. All solvents were reagent grade and were dried, when necessary, by accepted procedures.⁵⁷

Unless otherwise noted, all reactions were run in oven-dried glassware and stirred with teflon-coated magnetic stir-bars. Cross-bridged ligands used (**Figure 2.1**) were prepared according to literature procedures.^{31-34,42} All complexes of cross-bridged

tetraazamacrocyclic ligands were prepared according to our published literature procedures: [InBr₂-CB-Cyclam]Br, [GaCl₂-CB-Cyclam]Cl and [Ga-CB-DO2A]NO₃.^{36,37(a)}

[In-CB-DO2A·NaOAc]BPh₄

The same method to prepare [Ga-CB-DO2A]NO₃ developed by Weijun Niu was used.^{37(a)}

To a MeOH solution (8 mL) of H₂-CB-DO2A·4TFA (858 mg, 1.11 mmol) and In(NO₃)₃ hydrate (480 mg, 1.23 mmol) was added the MeOH solution (4 mL) of sodium acetate (1.7 g, 13.04 mmol) in one portion. After 4 days of refluxing, the insoluble solid was centrifuged and decanted off from the supernatant. Addition of a saturated MeOH solution (3 mL) of sodium tetraphenylborate to the supernatant precipitated 616 mg (67 %) of a white crystalline solid. IR (KBr): $\nu_{\text{C=O}}$: 1659.2, 1620.9 cm⁻¹. ¹H NMR (399.75 MHz, CD₃CN) δ 3.57 (s, CH₂COO, 4H), 3.39-3.22 (m, 6H), 3.14-2.90 (m, 12H), 2.82-2.76 (dd, 2H); ¹³C{¹H} NMR (100.52 MHz, CD₃CN) δ 177.71 (CH₂COO), 174.93 (CH₃COO), 65.23, 61.18, 58.54, 57.11, 54.82, 49.43, 47.98, 23.46 (CH₃COO). Anal. Calcd for C₄₀H₄₇N₄O₆InNaB: C, 57.99; H, 5.72; N, 6.76. Found: C, 55.92; H, 5.97; N, 6.41. The FAB⁺ mass spectrum exhibited a major peak at $m/z = 509.08$ for [In-CB-DO2A-NaOAc]⁺ ([C₁₆H₂₇N₄O₆NaIn]⁺).

[In-CB-DO2A]Cl(HCl)₃(NaCl)₂

To a CH₃CN solution (4 mL) of [In-CB-DO2A·NaOAc]BPh₄ (140 mg, 0.17 mmol), a volume of 1 mL of concentrated HCl was added to precipitate 33 mg (42 %) of a white solid. IR (KBr): 1726.8 (ν_{COO}), 1478.3, 1417.5, 1402.9, 1312.6, 1200.5, 1171.1, 1100.5, 1061.5, 1017.9, 881.06, 824.57, 769, 706.77 cm⁻¹. ¹H NMR (399.75 MHz, D₂O) δ 3.74

(AB pattern of CH₂COO, J = 15.9 Hz, 4H), 3.62-3.44 (m, 6H), 3.36-3.12 (m, 12H), 2.98-2.90 (dd, J = 5.46 Hz, 2H); ¹³C{¹H} NMR (100.52 MHz, D₂O) δ 177.46 (CH₂COO), 64.23 (CH₂COO), 61.03, 58.07, 56.98, 53.86, 49.78, 47.83. Anal. Calcd for C₁₄H₂₄N₄O₄In(HCl)₃(NaCl)₂: C, 24.41; H, 3.95; N, 8.13. Found C, 24.48; H, 3.92; N, 8.12. MS (ESI, positive mode): *m/z* = 485.2 for {[In-CB-DO2A]Cl + Na}⁺ ([C₁₄H₂₄N₄O₄InClNa]⁺) and *m/z* = 427.2 for [In-CB-DO2A]⁺ ([C₁₄H₂₄N₄O₄In]⁺).

[InBr₂-Et₂-CB-TE2A]Br·H₂O

To a MeCN solution (40mL) of [InBr₂-CB-Cyclam]Br (562.6 mg, 0.97 mmol) and Na₂CO₃ (1.038 g, 9.8 mmol), ethyl bromoacetate (0.42 mL, 3.79 mmol) was added. This milky mixture was refluxed for 4 days. The insoluble solid was centrifuged and decanted off from the solution. The supernatant was separated and evaporated to dryness to give the crude product. The crude product was washed by diethyl ether (20mL×3) to give 561 mg (77%) of an off-white solid after drying. IR (KBr): 2978.6, 2938.0, 1740 (ν_{C=O}), 1495.9, 1465.5, 1423.5, 1381.6, 1201.6, 1087.0, 1059.7, 1021.7, 985.24 cm⁻¹. ¹H NMR (399.75 MHz, CD₃CN) δ 4.32 (d, 2H, J = 17.34 Hz, NCH_ΔH_XCO₂), 4.16 (q, 4H, COOCH₂), 3.81 (d, 2H, J = 17.54 Hz, NCH_ΔH_XCO₂), 3.64-3.52 (br t, 6H, J = 13.65 Hz), 3.48-3.33 (m, 8H), 3.3-3.18 (m, 2H), 3.0-2.92 (br d, 2H), 2.2.74-2.65 (m, 2H), 2.42-2.28 (~qm, 2H, J ~ 15.4 Hz, CH₂CH_{eq}H_{ax}CH₂), 1.84-1.76 (dm, 2H, J = 17.93 Hz, CH₂CH_{eq}H_{ax}CH₂), 1.25 (t, 6H, COOCH₂CH₃); ¹³C{¹H} NMR (100.52 MHz, CD₃CN) δ 168.46, 62.24 (OCH₂CH₃), 60.04, 57.74 (CH₂COO), 56.22, 54.91, 49.50, 46.70, 23.79 (CH₂CH₂CH₂), 14.41 (OCH₂CH₃). Anal. Calcd for C₂₀H₃₈N₄O₄InBr₃·H₂O: C, 31.15; H,

5.23; N, 7.27. Found: C, 30.78; H, 5.22; N, 6.97. MS (ESI, positive mode): $m/z = 673.2$ for $[\text{InBr}_2\text{-Et}_2\text{-CB-TE2A}]^+$ ($[\text{C}_{20}\text{H}_{38}\text{N}_4\text{O}_4\text{InBr}_2]^+$).

[In-CB-TE2A]ClO₄

To a deionized aqueous solution (10 mL) of $[\text{InBr}_2\text{-Et}_2\text{-CB-TE2A}]\text{Br}$ (223 mg, 0.3 mmol), a volume of 0.57 mL of an aqueous solution of NaOH (1.0441 N) was added to form a clear solution. This was refluxed for 24 hours and then evaporated to dryness to give the crude product. To the ethanol solution (2 mL) of the crude product, a saturated ethanol solution (2 mL) of sodium perchlorate was added to precipitate 128 mg (78 %) of a white solid after drying. IR (KBr): 1643.0, 1635.1, 1626.9, 1144.9, 1089.8 cm^{-1} . ^1H NMR (399.75 MHz, D₂O) δ 4.06-2.88 (broad), 2.66-2.50 (~qm, 2H, $\text{CH}_2\text{CH}_{\text{eq}}\text{H}_{\text{ax}}\text{CH}_2$), 1.96-1.86 (dm, 2H, $\text{CH}_2\text{CH}_{\text{eq}}\text{H}_{\text{ax}}\text{CH}_2$); $^{13}\text{C}\{^1\text{H}\}$ NMR (100.52 MHz, D₂O) δ 176.60, 63.35, 63.31, 58.49, 58.35, 50.80, 50.72, 50.67, 50.61, 50.55, 50.38, 49.93, 49.89, 49.66, 22.60, 22.49.; in D₂O at 85°C: 175.65, 63.84, 59.66, 59.51, 58.42, 52.12, 50.03, 23.00. MS (ESI, positive mode): $m/z = 455.3$ for $[\text{In-CB-TE2A}]^+$ ($[\text{C}_{16}\text{H}_{28}\text{N}_4\text{O}_4\text{In}]^+$).

[Hg-CB-DO2A]

To a MeOH solution (14 mL) of HgCl_2 (161 mg, 0.594 mmol) and CB-DO2A.2TFA (149 mg, 0.27 mmol), a volume of 1.1 mL of an aqueous solution of NaOH (1.0441 N) was added to form a cloudy solution. This mixture was refluxed for 48 hours, and then centrifuged to remove some white insoluble precipitate. Et₂O vapor diffusion into this supernatant yielded 102 mg (74 %) of a white crystalline solid. IR (KBr): 1577.7, 1569.9, 1399.5, 1096.7, 1029.8 cm^{-1} . ^1H NMR (399.75 MHz, D₂O) δ 3.48 (4H, s, CH_2COO ,

^{199}Hg satellite, $J = 30.2$ Hz), 2.92 (4H, s, cross-bridging CH_2CH_2 , ^{199}Hg satellite, $J = 26.0$ Hz); $^{13}\text{C}\{^1\text{H}\}$ NMR (100.52 MHz, D_2O) δ 178.40 (^{199}Hg satellite, $J = 11.7$ Hz), 64.77 (^{199}Hg satellite, $J = 5.4$ Hz), 60.15 (^{199}Hg satellite, $J = 8.9$ Hz), 57.01 (^{199}Hg satellite, $J = 20.7$ Hz), 46.27 (^{199}Hg satellite, $J = 22.9$ Hz).

LIST OF REFERENCES

1. Li, W. P.; Meyer, L. A.; Anderson, C. J. *Top. Curr. Chem.* **2005**, *252*, 179-192.
2. Liu, S. *Chem. Soc. Rev.* **2004**, *33*(7), 445-461.
3. Cutler, C. S.; Lewis, J. S.; Anderson, C. J. *Adv. Drug Delivery Rev.* **1999**, *37*, 189-211.
4. Reichert, D. E.; Lewis, J. S.; Anderson, C. J. *Coord. Chem. Rev.* **1999**, *184*, 3-66.
5. Anderson, C. J.; Welch, M. J. *Chem. Rev.* **1999**, *99*(9), 2219-2234.
6. Yam, V. W.; Lo, K. K. *Coord. Chem. Rev.* **1999**, *184*, 157-240.
7. Jurisson, S.; Berning, D.; Jia, W.; Ma, D. *Chem. Rev.* **1993**, *93*, 1137-1156.
8. Liang, X.; Sadler, P. J. *Chem. Soc. Rev.* **2004**, *33*, 246-266.
9. Parker, D. *Chem. Soc. Rev.* **1990**, *19*, 271-291.
10. Liu, S.; Edwards, D. S. *Bioconjugate Chem.* **2001**, *12*, 7-34.
11. Maecke, H. R.; Hofmann, M.; Haberkorn, U. *J. Nucl. Med.* **2005**, *46*, 1S-7S.
12. Yang, D. J.; Azhdarinia, A.; Kim, E. E. *Current Medical Imaging Reviews*, **2005**, *1*, 25-34.
13. Burgess, J. *Chem. Soc. Rev.* **1996**, *25*(2), 85-91.
14. Wulfsberg, G. *Inorganic Chemistry*, University Science Books, California, 2000.
15. Mingos, D. M. P. *Essentials of Inorganic Chemistry 2*, Oxford University Press, New York, 1998, p. 56.
16. Oberholzer, M. R.; Siegfried, L. C.; Kaden, T. A. *Inorg. Chim. Acta.* **1996**, *246*, 41-45.
17. Liu, S.; Edwards, D. S.; Barrett, J. A. *Bioconjugate Chem.* **1997**, *8*, 621-636.
18. Fichna, J.; Janecka, A. *Bioconjugate Chem.* **2003**, *14*, 3-17.
19. Springborg, J. *Dalton Trans.* **2003**, 1653-1665.

20. Hancock, R. D. *Chem. Rev.* **1989**, *89*, 1875-1914.
21. Busch, D. H. *Chem. Rev.* **1993**, *93*, 847-860.
22. Smith, S. V. *J. Inorg. Biochem.* **2004**, *98*, 1874-1901.
23. Bosnich, B.; Poon, C. K.; Tobe, M. L. *Inorg. Chem.* **1965**, *4*, 1102-1108.
24. Meyer, M.; Dahaoui-Gindrey, V.; Lecomte, C.; Guilard, R. *Coord. Chem. Rev.* **1998**, *178-180*, 1313-1405.
25. Lukes, I.; Kotek, J.; Vojtisek, P.; Hermann, P. *Coord. Chem. Rev.* **2001**, *216-217*, 287-312.
26. Lubal, P.; Kyvala, M.; Hermann, P.; Holubova, J.; Rohovec, J.; Havel, J.; Lukes, I. *Polyhedron*, **2001**, *20*, 47-55.
27. Kothari, K.; Samuel, G.; Banerjee, S.; Unni, P. R.; Sarma, H. D.; Chaudhari, P. R.; Unnikrishnan, T. P.; Pillai, M. R. A. *Nuclear Medicine and Biology*, **2001**, *28*, 709-717.
28. Bu, X. H.; Zhang, Z. H.; An, D. L.; Chen, Y. T.; Shionoya, M.; Kimura, E. *Inorg. Chim. Acta*, **1996**, *249*, 125-130.
29. Heppeler, A.; Froidevaux, S.; Mäcke, H. R.; Jermann, E.; Behe, M.; Powell, P.; Hennig, M. *Chem. Eur. J.* **1999**, *5(7)*, 1974-1981.
30. Liu, S.; He, Z.; Hsieh, W.; Fanwick, P. E. *Inorg. Chem.* **2003**, *42*, 8831-8837.
31. Weisman, G. R.; Rogers, M. E.; Wong, E. H.; Jasinski, J. P.; Paight, E. S. *J. Am. Chem. Soc.* **1990**, *112*, 8604-8605.
32. Weisman, G. R.; Wong, E. H.; Hill, D. C.; Rogers, M. E.; Reed, D. P.; Calabrese, J. C. *Chem. Commun.* **1996**, 947-948.

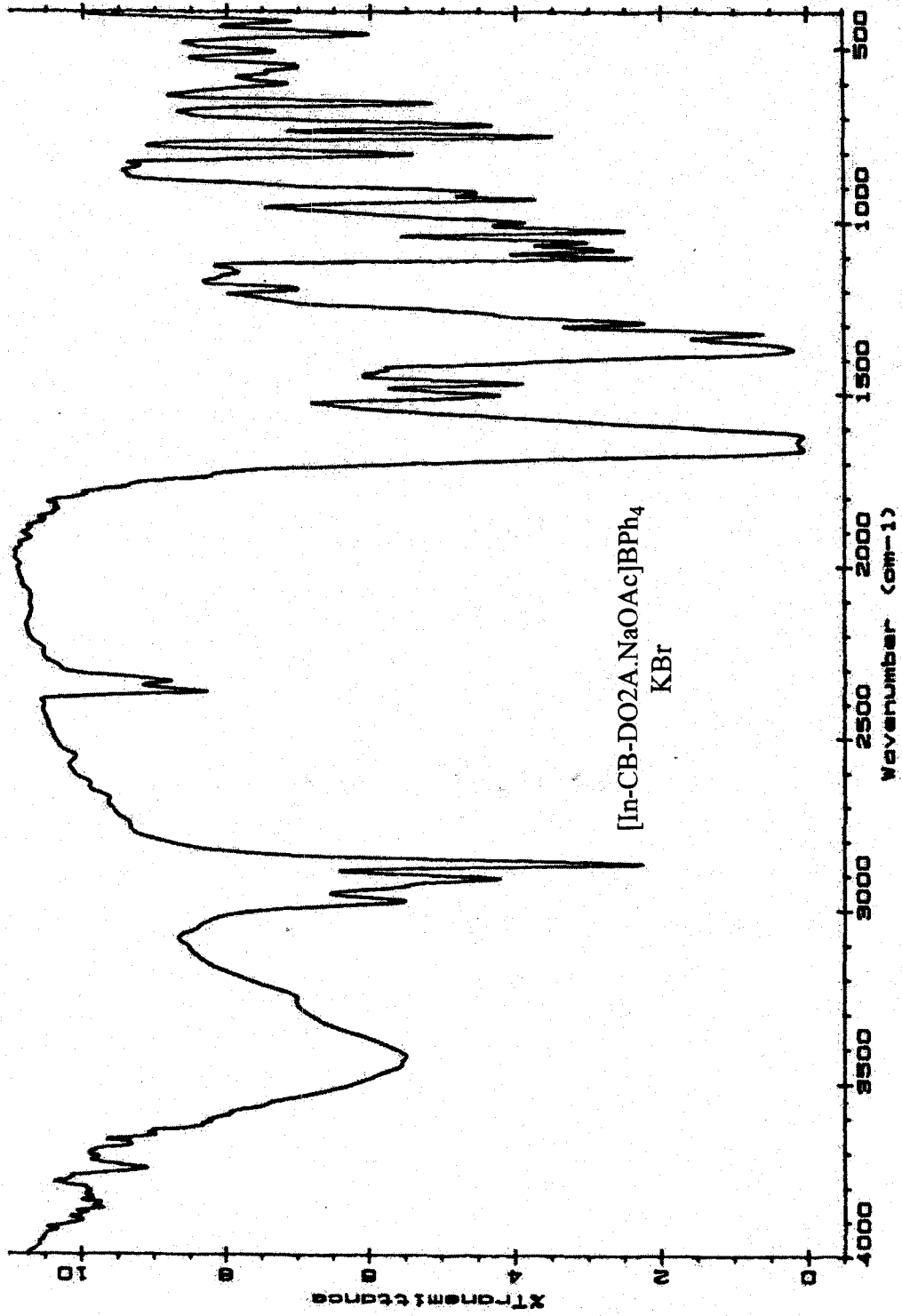
33. Wong, E. H.; Weisman, G. R.; Hill, D. C.; Reed, D. P.; Rogers, M. E.; Condon, J. S.; Fagan, M. A.; Calabrese, J. C.; Lam, K.; Guzei, I. A.; Rheingold, A. L. *J. Am. Chem. Soc.* **2000**, *122*, 10561-10572.
34. Sprague, J. E.; Peng, Y.; Sun, X.; Weisman, G. R.; Wong, E. H.; Achilefu, S.; Anderson, C. J. *Clinical Cancer Research*, **2004**, *10*, 8674-8682.
35. Hubin, T. J.; McCormick, J. M.; Collinson, S. R.; Alcock, N. W.; Busch, D. H. *Chem. Commun.* **1998**, 1675-1676.
36. Niu, W.; Wong, E. H.; Weisman, G. R.; Sommer, R. D.; Rheingold, A. L. *Inorg. Chem. Commun.* **2002**, *5*, 1-4.
37. (a) Niu, W.; Wong, E. H.; Weisman, G. R.; Peng, Y.; Anderson, C. J.; Zakharov, L. N.; Golen, J. A.; Rheingold, A. L. *Eur. J. Inorg. Chem.* **2004**, 3310-3315. (b) Niu, W.; Wong, E. H.; Weisman, G. R.; Peng, Y.; Anderson, C. J.; Zakharov, L. N.; Golen, J. A.; Rheingold, A. L. *Eur. J. Inorg. Chem.* **2006**, 676-677.
38. Niu, W.; Wong, E. H.; Weisman, G. R.; Lam, K.; Rheingold, A. L. *Inorg. Chem. Commun.* **1999**, *2*, 361-363.
39. Niu, W.; Wong, E. H.; Weisman, G. R.; Zakharov, L. N.; Incarvito, C. D.; Rheingold, A. L. *Polyhedron*, **2004**, *23*, 1019-1025.
40. Niu, W.; Wong, E. H.; Weisman, G. R.; Hill, D. C.; Tranchemontagne, D. J.; Lam, K.; Sommer, R. D.; Zakharov, L. N.; Rheingold, A. L. *Dalton Trans.* **2004**, 3536-3547.
41. O'Connor, P.; Berg, D. J.; Twamley, B. *Organometallics* **2005**, *24*, 28-36.
42. Jeffrey S. Condon, M.S. thesis, University of New Hampshire, 2002.
43. Weijun Niu, Ph.D. dissertation, University of New Hampshire, 2003.

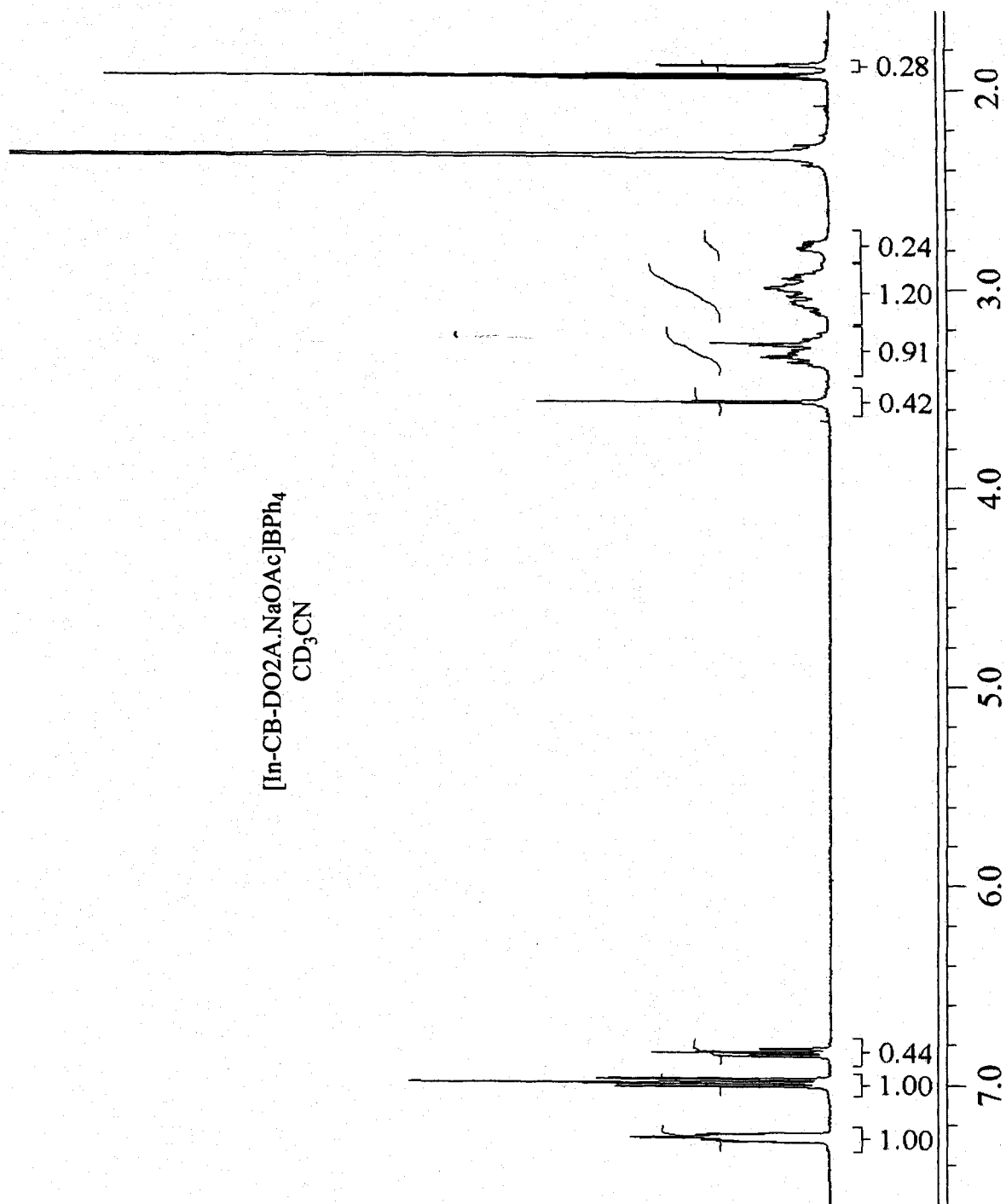
44. (a) Alder, R. W. *J. Am. Chem. Soc.* **2005**, *127*, 7924-7931. (b) Valencic, M.; Does, T. V. D.; V. E. D. *Tetrahedron Lett.* **1998**, *39*, 1625-1628. (c) Greene, A. E.; Luche, M.; Depres, J. *J. Am. Chem. Soc.* **1983**, *105*, 2435-2439.
45. Epple, M.; Kirschnick, H. *Chem. Ber.* **1996**, *129*, 1123-1129.
46. Hao, H.; Sieler, J.; Sicker, D. *J. Nat. Prod.* **2002**, *65*, 466-469.
47. Aliev, A. E.; Elizabe, L.; Kariuki, B. M.; Kirschnick, H.; Thomas, J. M.; Epple, M.; Harris, K. D. M. *Chem. Eur. J.* **2000**, *6*(7), 1120-1126.
48. <http://www.chemcalc.org/>
49. Bebout, D. C.; Stokes, S. W. *Inorg. Chem.* **1999**, *38*, 1126-1133.
50. (a) Matzapetakis, M.; Kourgiantakis, M.; Dakanali, M.; Raptopoulou, C. P.; Terzis, A.; Lakatos, A.; Kiss, T.; Banyai, I.; Iordanidis, L.; Mavromoustakos, T.; Salifoglou, A. *Inorg. Chem.* **2001**, *40*, 1734-1744. (b) Hawkes, G. E.; O'Brien, P.; Salacinski, H.; Motevalli, M.; Abrahams, I. *Eur. J. Inorg. Chem.* **2001**, 1005-1011. (c) O'Brien, P.; Salacinski, H.; Motevalli, M. *J. Am. Chem. Soc.* **1997**, *119*, 12695-12696.
51. (a) Hubin, T. J.; Alcock, N. W.; Morton, M. D.; Busch, D. H. *Inorg. Chim. Acta*, **2003**, *348*, 33-40. (b) Siegfried, L.; Kaden, T. A. *Dalton Trans.* **2005**, 3079-3082. (c) Woodin, K. S.; Heroux, K. J.; Boswell, C. A.; Wong, E. H.; Weisman, G. R.; Niu, W.; Tomellini, S. A.; Anderson, C. J.; Zakharov, L. N.; Rheingold, A. L. *Eur. J. Inorg. Chem.* **2005**, 4829-4833.
52. (a) Broan, C. J.; Cox, J. P. L.; Craig, A. S.; Katakya, R.; Parker, D.; Harrison, A.; Randall, A. M.; Ferguson, G. *J. Chem. Soc. Perkin Trans. 2* **1991**, 87-99. (b) Dadachova, E.; Park, C.; Eberly, N.; Ma, D.; Paik, C. H.; Brechbiel, M. W. *Nucl. Med. and Biol.* **2001**, *28*, 695-701. (c) Clarke, E.; Martell, A. E. *Inorg. Chim. Acta*, **1991**, *190*, 37-46.

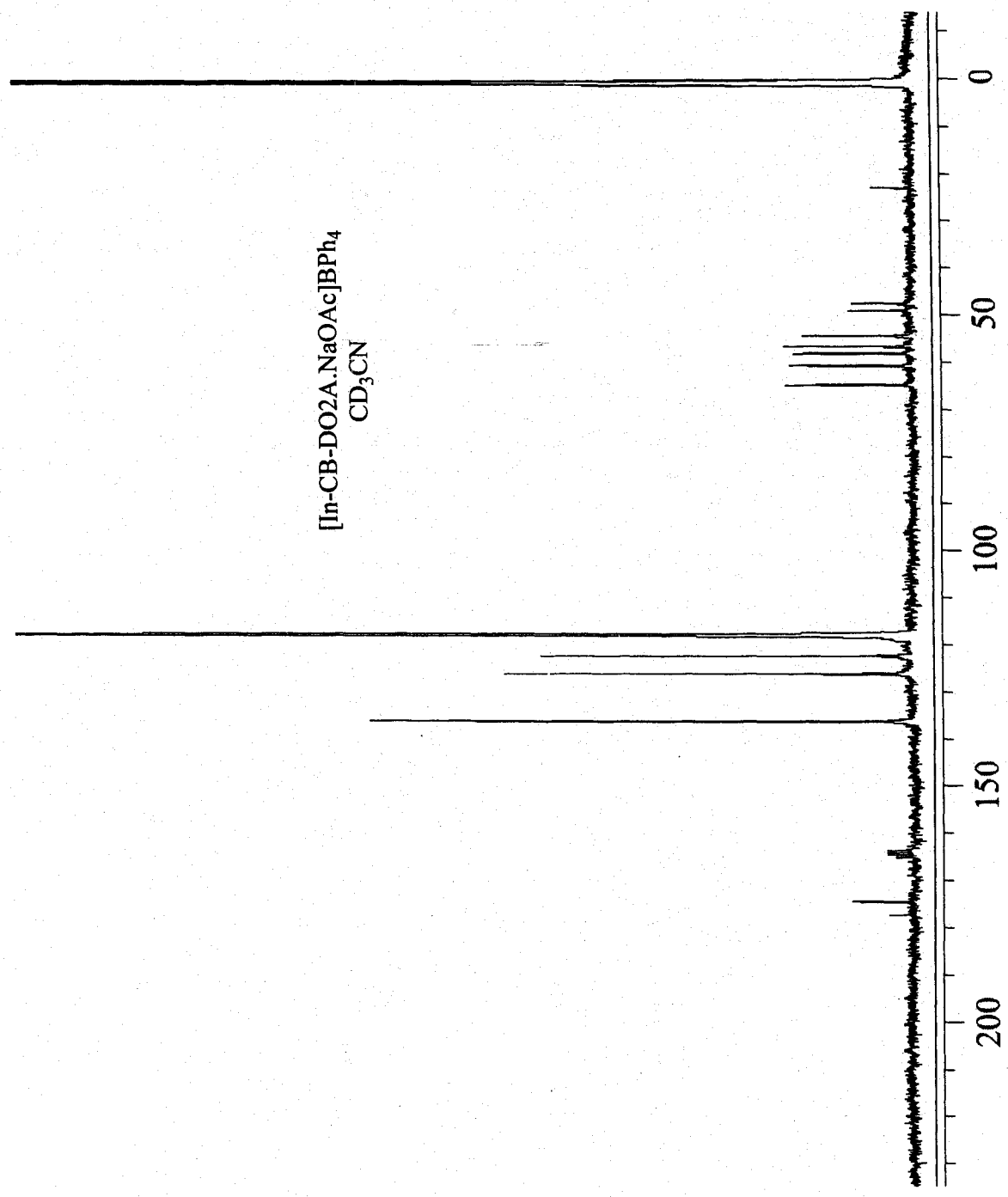
53. <http://www.webelements.com/>
54. Sun, X.; Wuest, M.; Weisman, G. R.; Wong, E. H.; Reed, D. P.; Boswell, C. A.; Motekaitis, R.; Martell, A. E.; Welch, M. J.; Anderson, C. J. *J. Med. Chem.* **2002**, *45*, 469-477.
55. Constable, E. C. *Coordination Chemistry of Macrocyclic Compounds*, 1999, p. 63.
56. Claridge, T. D. W. *High-Resolution NMR Techniques in Organic Chemistry*, Elsevier Science, California, 1999, p. 104.
57. Perrin, D. D.; Amarego, W. L. F.; Perrin, D. R. *Purification of Laboratory Chemicals*, 2nd ed., Pergamon Press, New York, 1980.

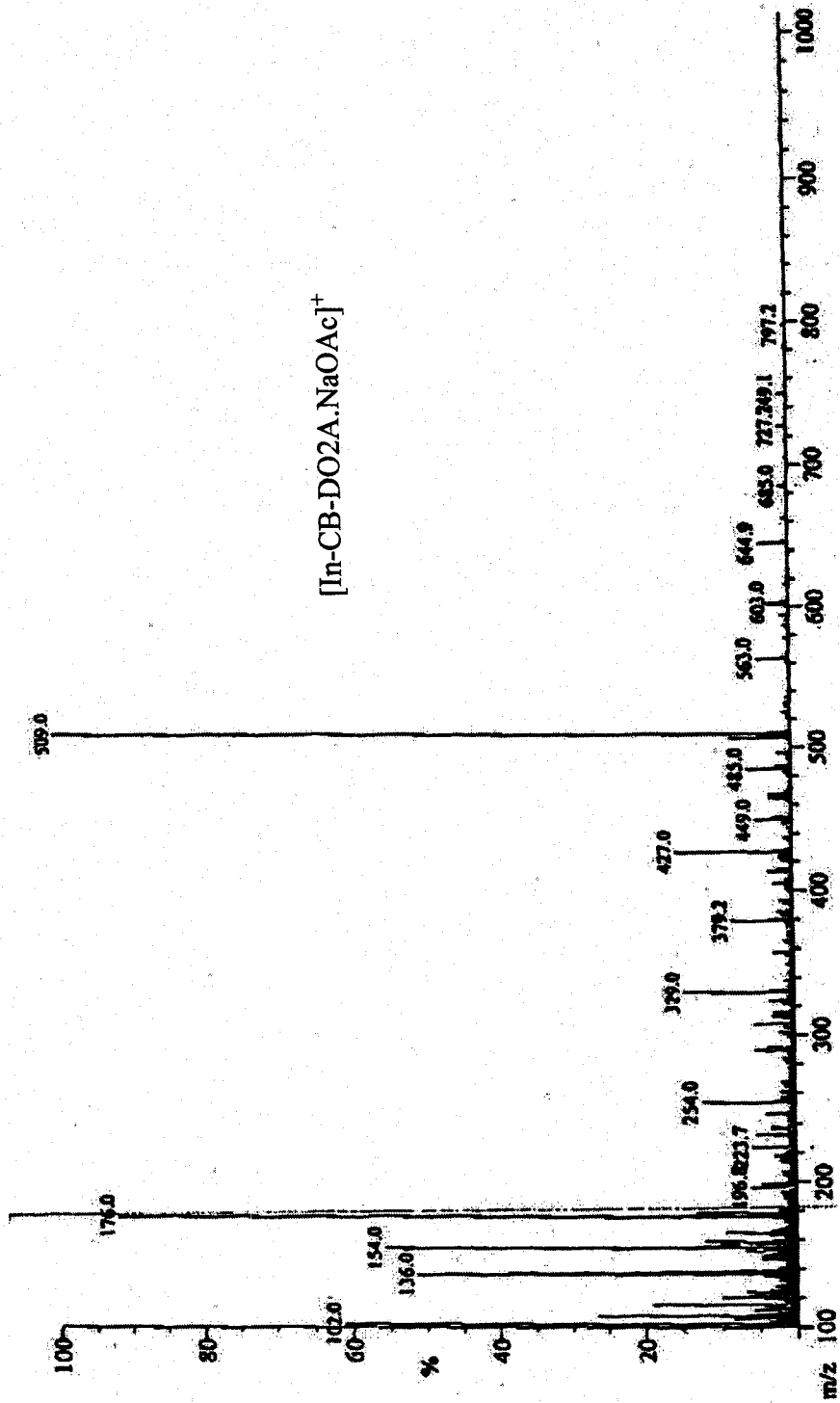
APPENDIX

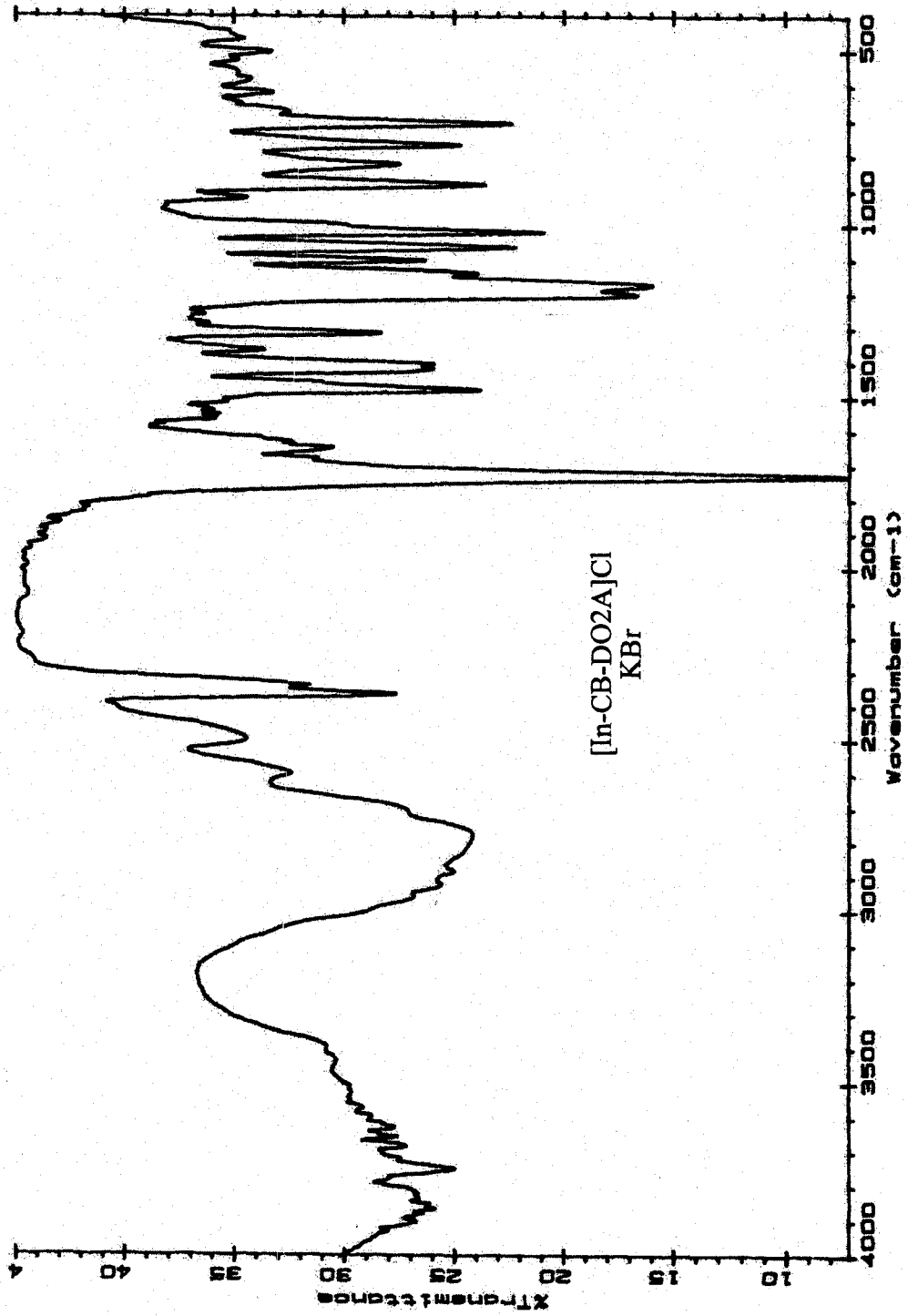
SPECTRA

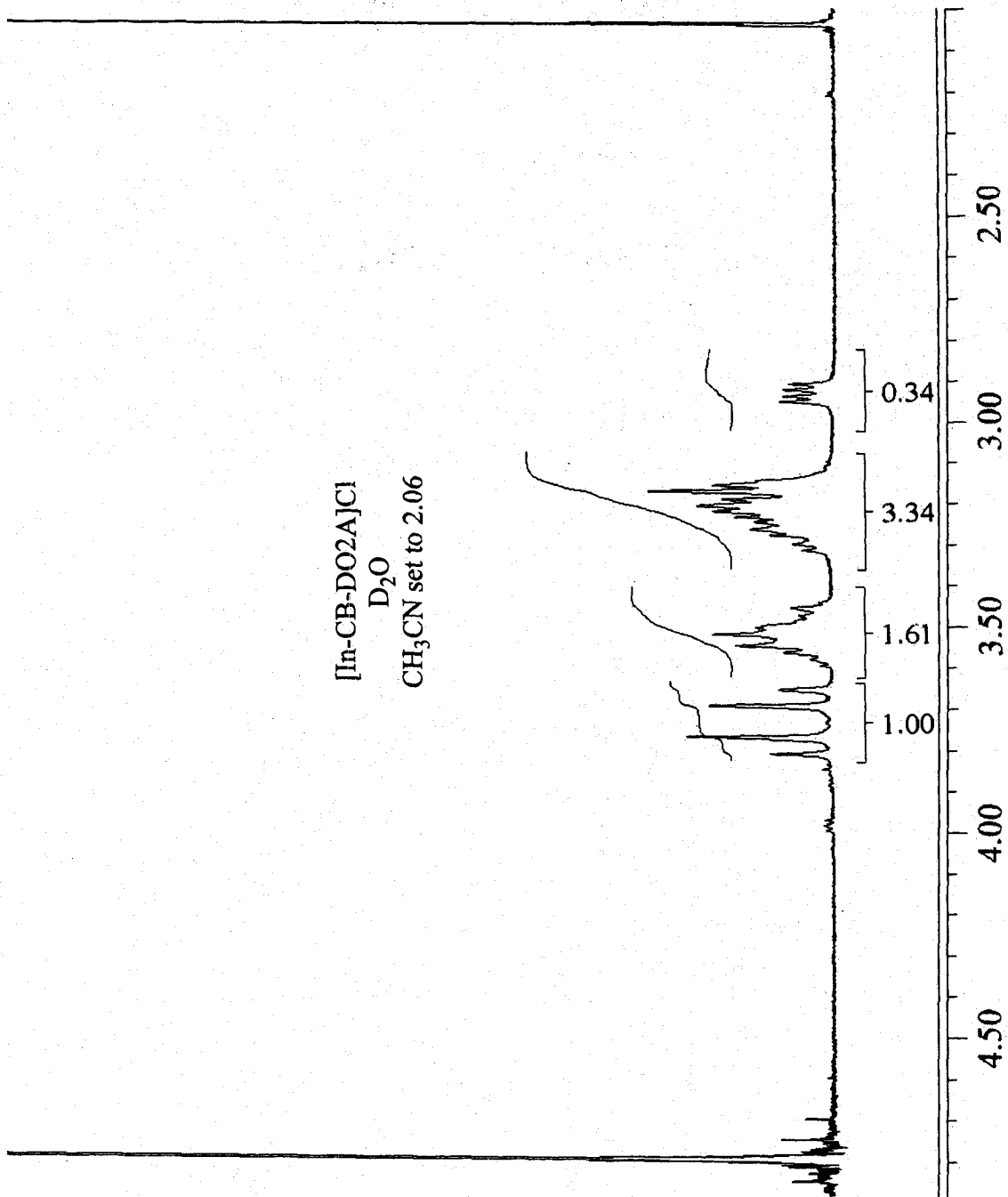




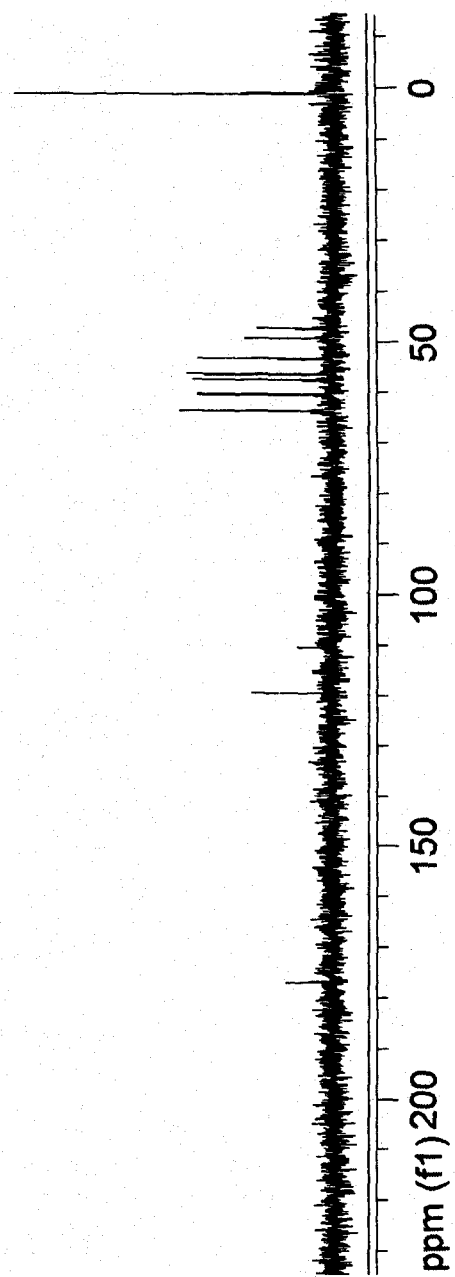


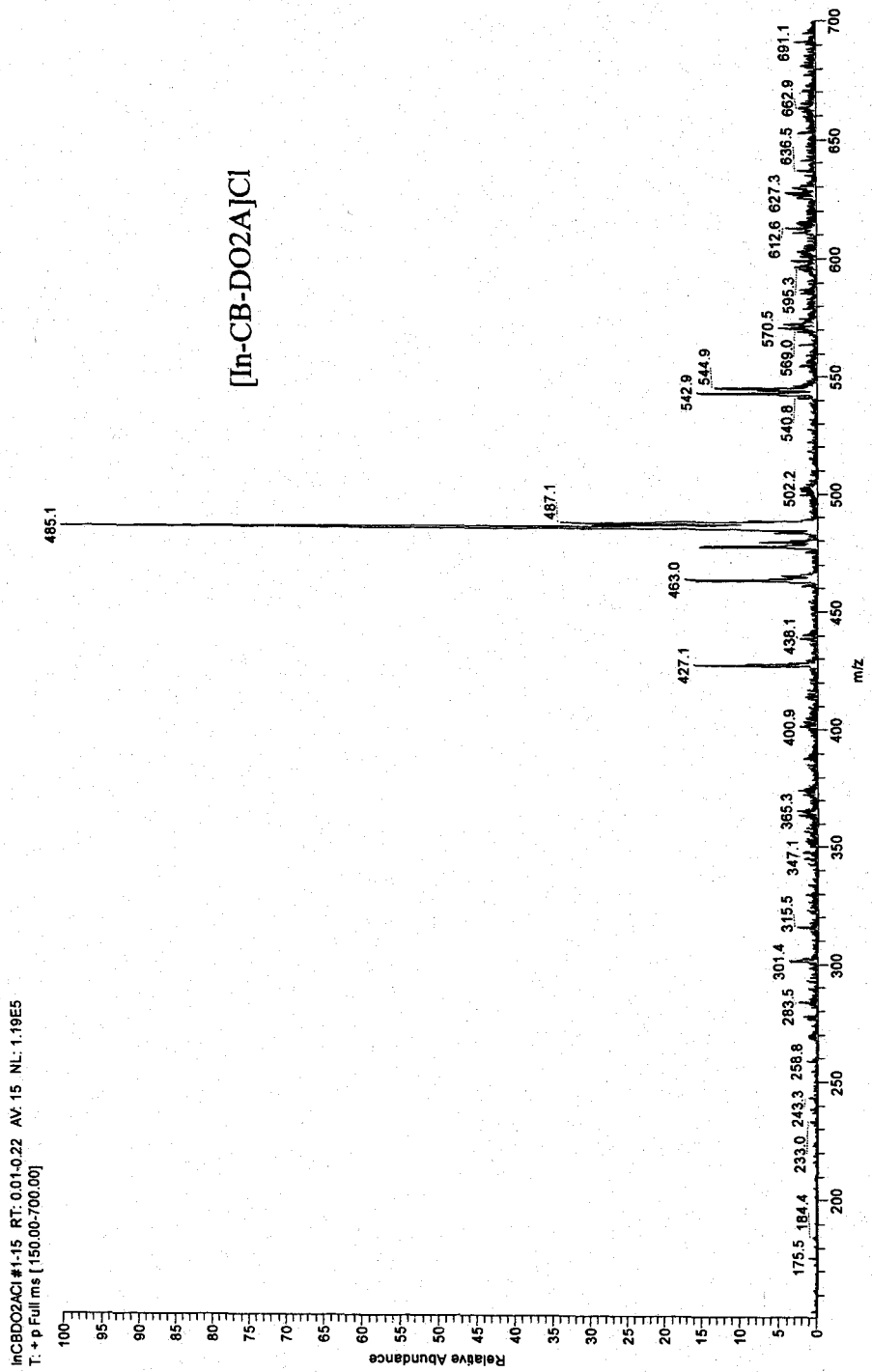


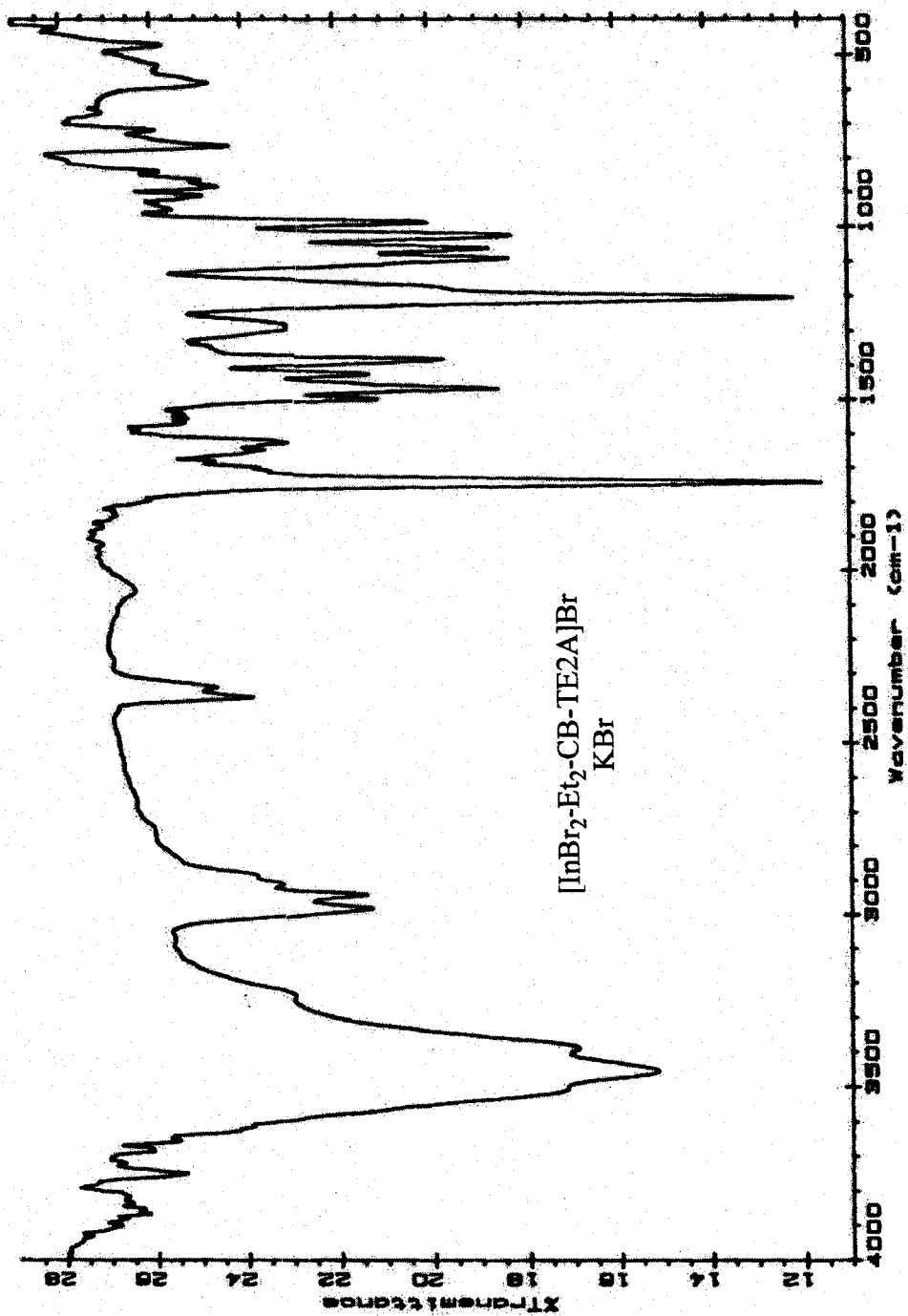


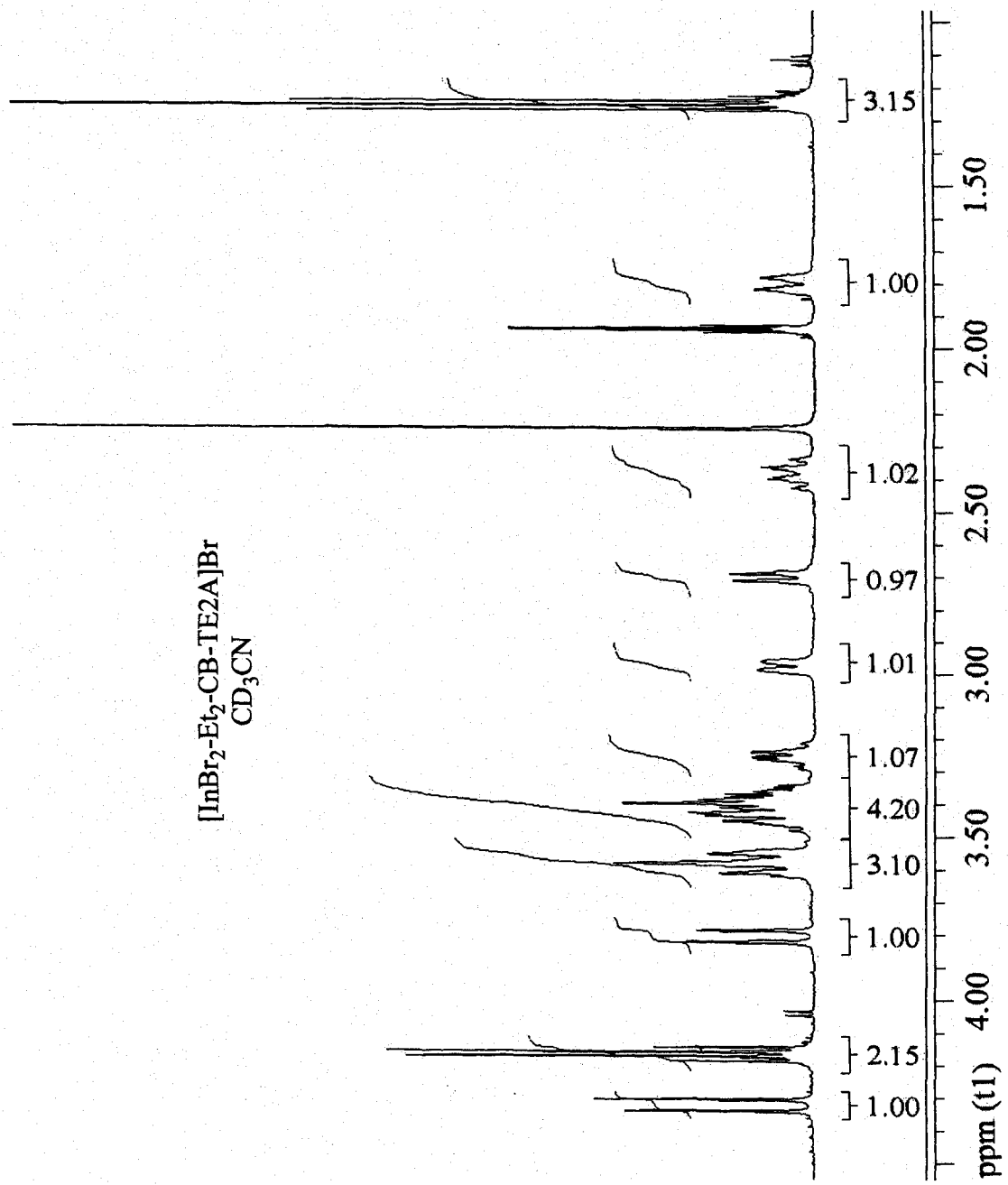


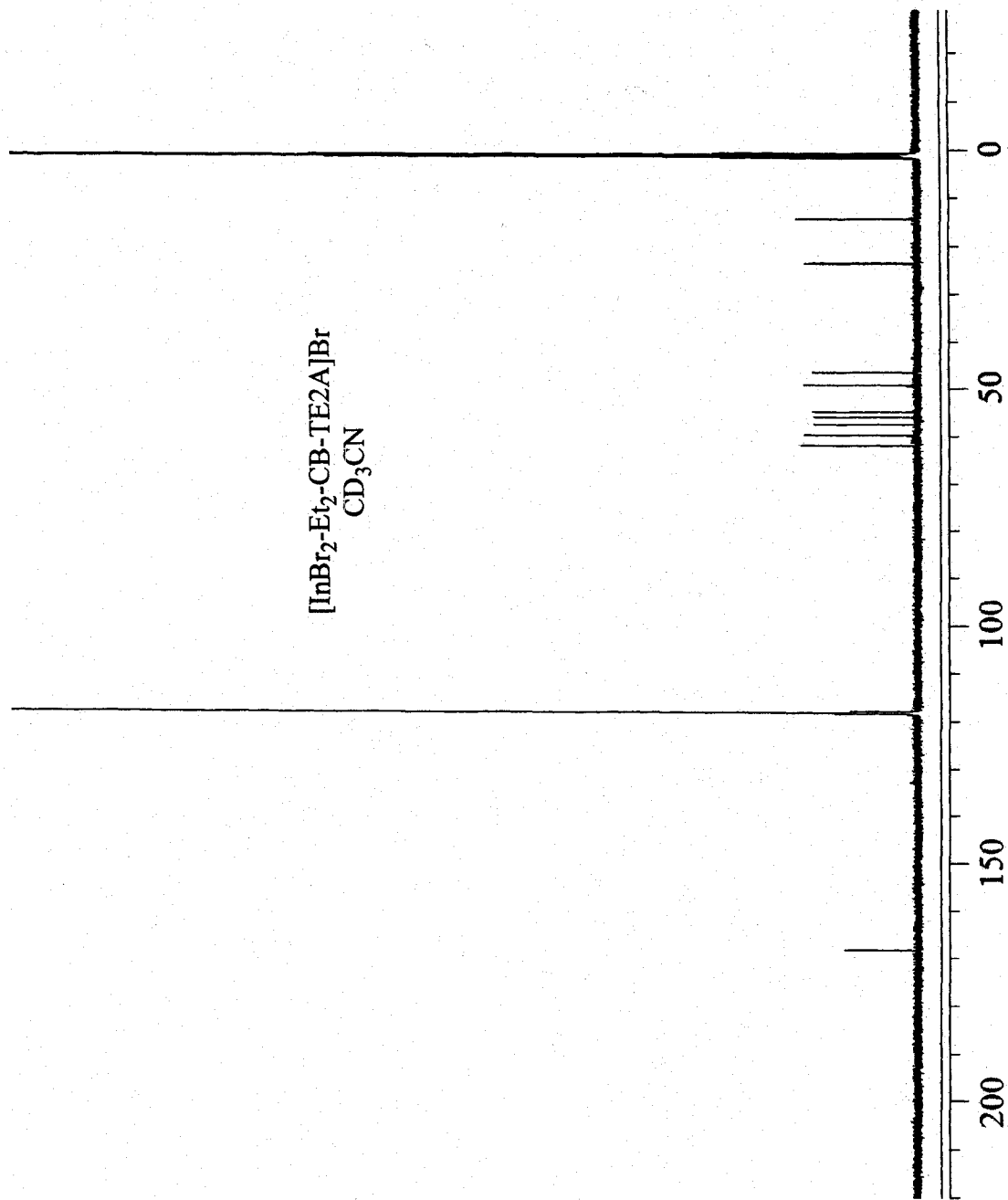
[In-CB-DO2A]Cl
D₂O
CH₃CN set to 1.7

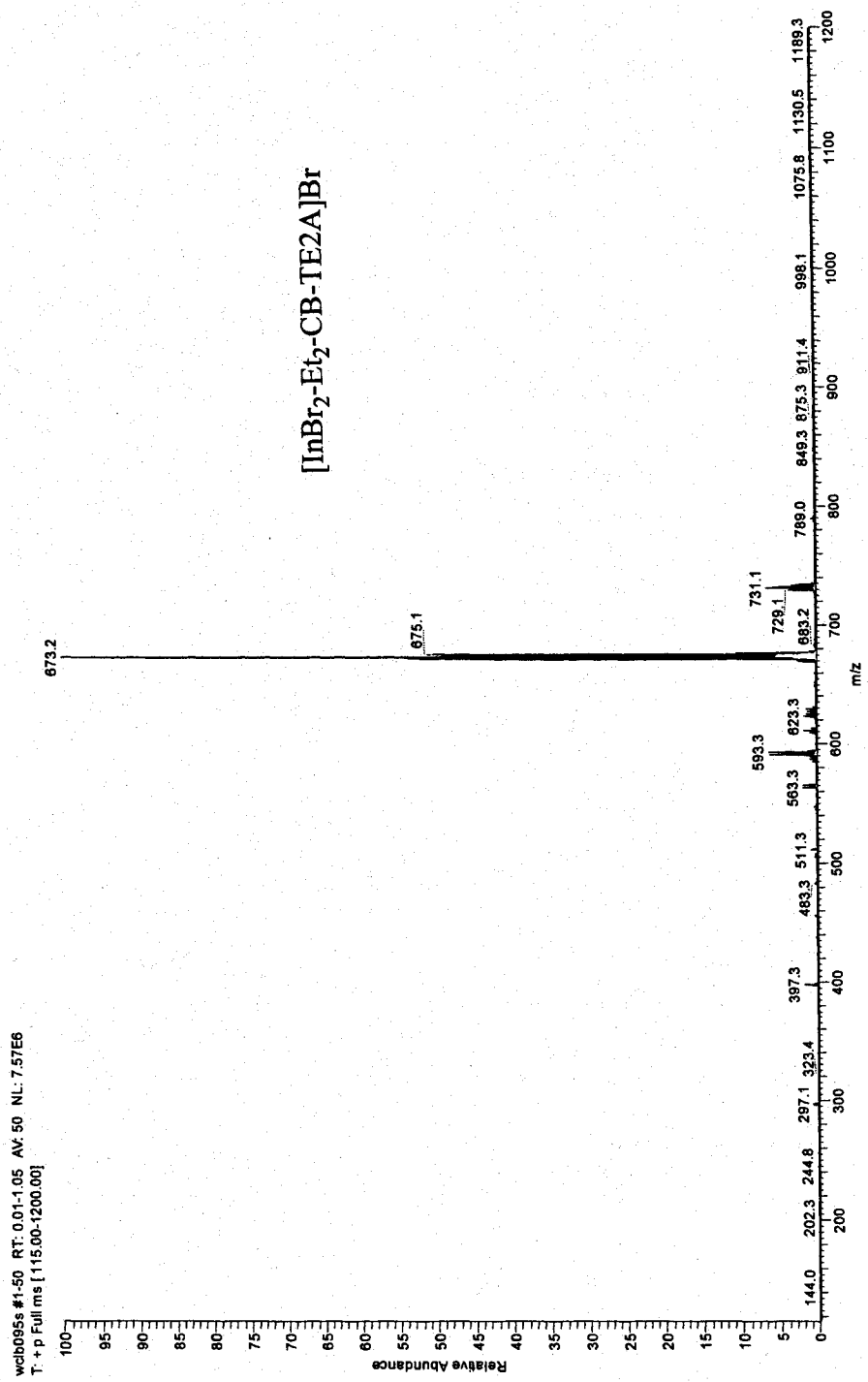


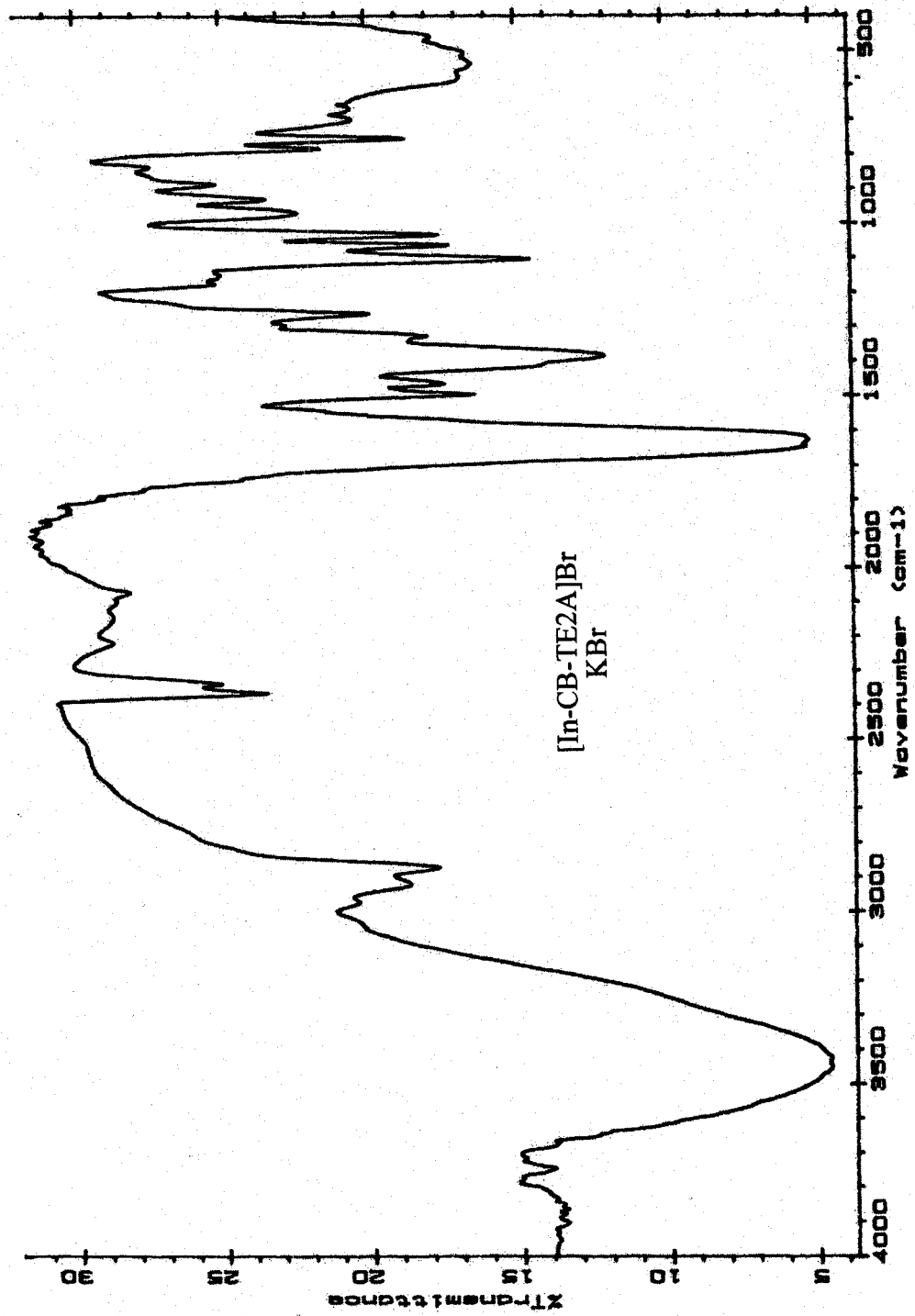


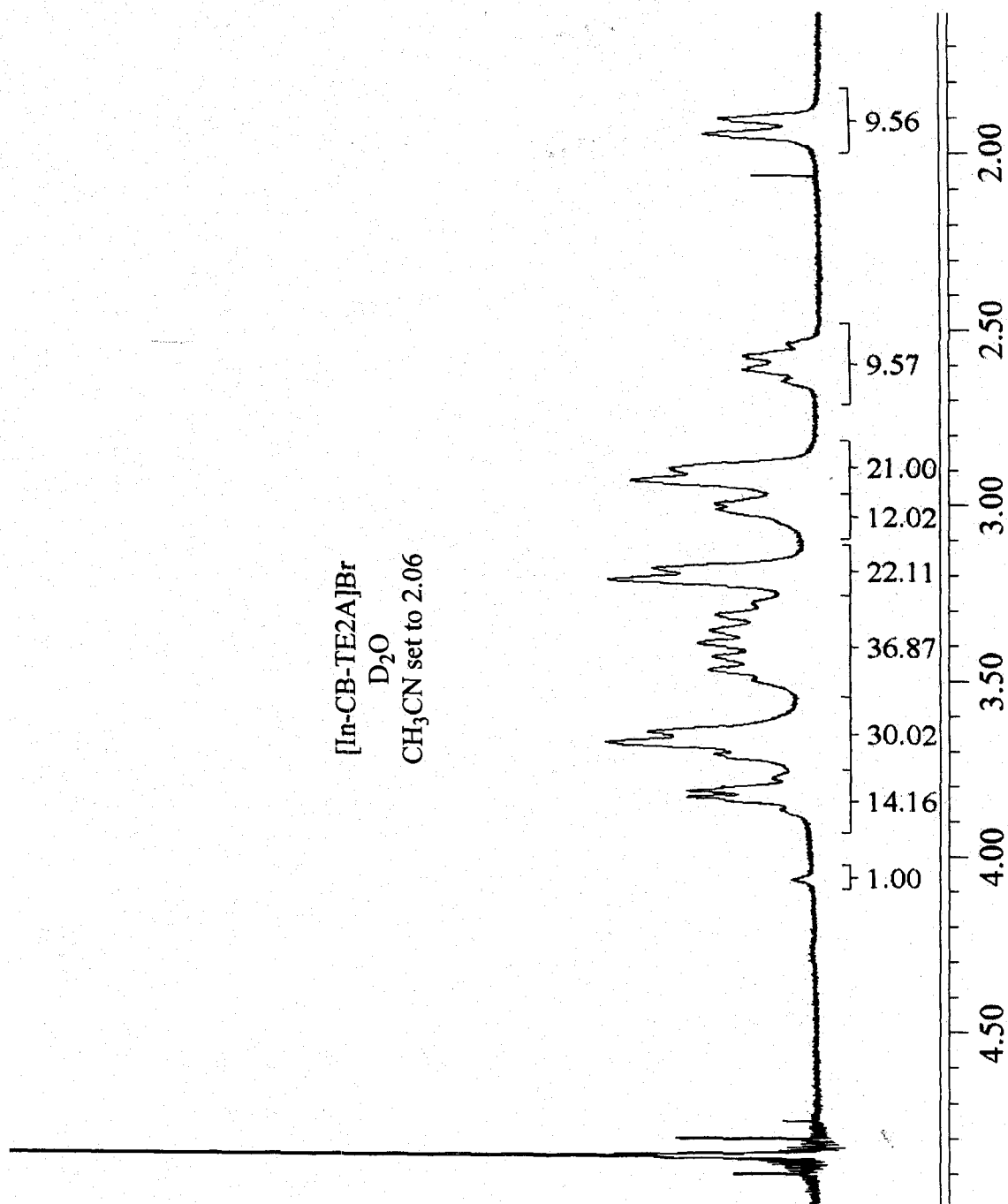












[In-CB-TE2A]Br
D₂O
CH₃CN set to 1.7

